Doctoral Thesis

Vision-based Force Compliance Control Method for Motion Navigation in Haptic Bilateral Control System

ハプティックバイラテラル制御システムにおける
運動誘導のための画像に基づく力コンプライアンス制御手法

Muhammad Herman Bin Jamaluddin
(ムハンマド　ヘルマン　ビン　ジャマルディン)

Department of Physics, Electrical and Computer Engineering
Graduate School of Engineering
Yokohama National University

Supervisor: Professor Dr. Atsuo Kawamura
Co-Supervisor: Associate Professor Dr. Tomoyuki Shimono

March, 2015

Vision-based Force Compliance Control Method for Motion Navigation in Haptic Bilateral Control System

by

Muhammad Herman Bin Jamaluddin

Dissertation submitted to the
Graduate School of Engineering of the Yokohama National University
in partial fulfillment of the requirements for the degree of

Doctor of Engineering
in
Electrical and Computer Engineering

Supervisor: Professor Dr. Atsuo Kawamura
Co-Supervisor: Associate Professor Dr. Tomoyuki Shimono

Department of Physics, Electrical and Computer Engineering
Graduate School of Engineering
Yokohama National University

Yokohama, Japan
March, 2015

Advisory Committee:
Atsuo Kawamura, Chair
Yasutaka Fujimoto
Tsutomu Oyama
Takao Tsuji
Tomoyuki Shimono

Printed in Japan

Abstract

The integration of high transparent bilateral control system and vision-based navigation system is important for the development of safe and secure teleoperation technology. To realize this, it is necessary to be able to handle the object's motion tracking elements that form this invention. The advent of real-time image guidance in the haptic environment has led to the development of the latest technologies. One of the important parts to be considered is how the object can be tracked.

This study proposes a force-based compliance control method utilizing visual information that can be integrated with a haptic system for motion navigation tasks. The force generated on the basis of useful image information of the tracked object is utilized to provide a response to the bilateral control system. An eye-to-hand approach is used to magnify the information from the vision sensor. The control strategy, image processing method, and integration techniques are elaborated upon in detail. To prove the utility of the proposed method, the study is conducted to find the effect of the generated force by the different scaling of the object's size. Experiments were conducted using different distances between the camera and object to validate the proposed integration method. The effectiveness of the proposed method was evaluated through a comparison with the conventional bilateral control method. The intention is also be given to the robustness of the navigation technique. As for the motion navigation task, the integration of bilateral control of a master-slave system with the vision-based force compliance controller will have some modelling error. The disturbance of the modelling error that occurs in the integration of the system will be compensated by the implementation of vision-based disturbance observer (VDOB). The concept of control structure between the integration of bilateral manipulator, vision-based force compliance controller and the vision-based disturbance observer is described. Experiments were conducted to compare the result of without and with the proposed integration method. From the experimental results, the robustness of the proposed system are confirmed. The study also be focussed on the object coordinate orientational effect to the proposed virtual force navigation method. Thus, this study provides a solution for solving the object's rotational effect during the navigation process by the haptic bilateral control system. During object's navigation, the virtual force is generated and affected to the manipulator's horizontal trajectory movement. The study on the different rotational angle of an object's trajectory which reflects to different movement direction of produced force are observed.

Acknowledgements

ALHAMDULILLAH. This dissertation would not have been possible without the assistance, help and guidance from several individuals who directly or indirectly contributed in the preparation and completion of my Ph.D. study.

First and foremost, my utmost gratitude to Associate Professor Dr. Tomoyuki Shimono, who has guided me for years in my research. His sincerity and encouragement will always be remembered. Associate Professor Tomoyuki Shimono has been my inspiration as I overcome all the obstacles in the completion of this research work.

Secondly, I would like to express my sincere gratitude to all panel Professors, Atsuo Kawamura, Yasutaka Fujimoto, Tsutomu Oyama and Takao Tsuji for giving comments, ideas and recommendations to improve my research topic.

Next, my gratitude goes to several teammates who helped me a lot such as, Dr. Naoki Motoi, Dr. Takahiro Nozaki and Nobuyuki Togashi. Also to my good companions, Dr. Zaki, Dr. Fariz, Dr. Aliza, Dr. Saifulza and Hafiz who always been around for discussions and as good listeners when I have problems.

Not to forget to the scholarship and allowance providers, Universiti Teknikal Malaysia Melaka (UTeM), Ministry of Education Malaysia (MoE) and Global COE (Centers of Excellence) Program of Japan. Without the funding, it is impossible for the author to complete his study in Yokohama National University.

I would also want to thank my lovely wife, Nor Baishirah binti Yaakob and my beloved children, Dhiya Zulaikha binti Muhammad Herman, Muhammad Danial Zulqarnain bin Muhammad Herman and Muhammad Danish Ziqri bin Muhammad Herman for their understanding and love during the past few years. Their support and encouragement was in the end what made this dissertation possible. Last, but not least, million thanks to my parents, Hj Jamaluddin bin Shahrom and Hjh Norliah binti Hj Abu Bakar, also to all my sisters and brothers, for their prayers that contributed to my success.

Muhammad Herman bin Jamaluddin
November, 2014

I dedicate this dissertation to my family members;

to Ayah, Mama, Shira, Dhiya, Danial, Danish, Kak Nor, Abg Imy,
Ira, Idah, Aini, Ely, Lias, Haiqal, Shereen, Yana and Amalina...

Contents

List of Figures

List of Tables

Page

Chapter 1

Introduction

1.1 Background

In this chapter, I will review some related works in haptic system, implementation of disturbance observer (DOB), application of reaction force observer (RFOB) and bilateral control system, correspondingly. Next, it will continue by the review on the vision-based system, the visual navigation, image processing techniques and visual force control, respectively.

1.1.1 Haptics for Human Support

Haptic feedback offers the potential to increase the quality and capability of human–machine interactions, as well as the ability to skillfully manipulate objects by exploiting the sense of touch [1]. It also can be used to sense a physical environment at a remote site in order to overcome spatial or scale barriers in telemanipulation [2]. There a many methods in the development of motion control for robotic devices in order to realize the haptic sensation. The literature on the haptic development method is very extensive. Several control and integration techniques have been presented to cope with real-time haptic telemanipulation system. Hachisu *et al.* had done the investigation about the integration of pseudo-haptic feedback with vibratory feedback [3]. Thus, they proposed two novel approaches that combine pseudo-haptic feedback with visual and tactile vibrations. The other researcher had implemented the Kalman active observers technique to control a robotic manipulator with haptic device [4]. Haptic devices can representing real behavior of objects in virtual space. It can be done by gathering the correct frictional information of that object and one of the solution is by implementing the vision-aided system [5, 6].

The virtual reality [7] is one of the example of haptic vision system. Kenji *et al.* proposed the detection of finger touch using transparent flexible sheet by using the vision-based system [8]. The indentation of the contact point is measured and represented as the haptic cue in the display system. The application of vision-based haptic also can be applied for the development of robotic finger [9]. The camera can be placed at each tip of the robot finger and act like a force sensor based on the deformation of its markers. Well-positioned of the sensor may provide better sensory information [10]. Thus, the system can distinguish between different types of materials, i.e., solid, soft and amorphous, from the 3D reconstruction of the tip finger's membrane contact area [11].

Haptic also being reported can be used in microrobotics applications [12, 13]. Even for the small scale object manipulation task, the tiny gripper can effectively provide the haptic feedback. For the living micro biological cell injection application, Mehdi *et al.* proposed the 3D human-machine user's interface in order to allow real-time realistic visual and haptic control strategies [14,15]. This technique later can also be applied for the telerobotic surgical system [16] and integrated EMG-based medical system [17].

As haptic application getting much interest, some researchers had conducted the study to develop a system for the disabled people. Akhter *et al.* applied a smartphone-based haptic–vision system to help the blind to 'see' through touch [18]. While, Lisa *et al.* focussed on aiding the non-sighted art makers people [19] to support their art and design task. Not only for the human aided system, the haptic research also be applied for the basketball robot which can balance the ball on a plate [20]. The system was imposed to the six degrees of freedom serial industrial robot based on pure haptic information. In 2013, Agravante and his team developed the human-humanoid joint haptic technology to support the table carrying task [21]. This research's goal is to incorporate the vision into human-humanoid haptic joint actions control and planning.

For the application of perceiving the object stiffness, the pure information must be gathered from the haptic feedback. Thus, in medical application, it can permit surgeons to distinguish the softness of tissues [22]. This can be supported by providing the visual feedback. By the way, the correct viewing angle (VA) [23] is important to give correct apparent of visual deformation of objects. The study was conducted and resulted that the VA should never be greater than 15° to eliminate perceptual illusions. All in all, the visual informations of the target object and

its haptic cues are depends upon each other in order to offer precise senses in perceiving object stiffness.

1.1.2 Implementation of Disturbance Observer Method

Controlling the robots in contact with the environment is an important problem in industry applications. The robots are subject to interaction forces whenever they perform task involving motion that is constrainted by environment [24]. It is commonly known that information of a force sensor provides much noise. In order to solve the instability of force control, a disturbance observer (DOB) technique can be implemented instead of the force sensor. Thus, it can reduce the number of sensor uses on a robot yet producing better motion control feedback.

The disturbance observer method was proposed by Ohnishi *et al.* in early 80's [25]. The DOB can estimates external disturbances and system uncertainties [26], e.g., friction, inertia variation and etc., automatically. Year by year, various study had been conducted to improve the design of DOB method [27–31]. In earlier stage, the DOB was designed by the second-order derivatives of the position response, which is sensed by a position encoder, to attain the acceleration information. However, the bandwidth is limited due to the derivatives noise [32]. To solve the problem, Katsura *et al.* developed a novel structure of a disturbance observer which uses an acceleration sensor to enlarge the bandwidth [33]. Other types of DOB technique were reported earlier to be combined with other control methods such as fuzzy state control [34], sliding-mode control [35] and PID control [36].

As the popularity of DOB technique become increase, many application were developed which based on the concept of disturbance compensation. One of the famous applications is be applied for the manipulator motion control. In April 2000, Satoshi *et al.* was proposed a redundant manipulator control method using the disturbance observer with no inverse dynamics. The proposed strategy can realize acceleration control and second derivative of force control in task space [37], which realizes robust [38] and precise control of manipulators [39, 40]. Not only for robotic manipulator applications, the concept of DOB also reported being used in the missile seeker application [41]. This study applied the filtering of base motion disturbance estimation method from the sight line rate for homing guidance of missiles. In May 2008, Natori *et al.* developed the time-delay compensator in network communication line by using the communication disturbance observer concept [42].

For the application to the speed control of a motor, a new multiple-input-multiple-output (MIMO) fuzzy disturbance observer based method was applied [43]. This method was proposed by Kim *et al.* to achieve the good tracking performance of a permanence magnet (PM) synchronous motor. In tiny motor application, Lee *et al.* proposed the state space disturbance observer method for robust fast seek control of a hard disk drive positioning servo track writer [44, 45]. Since the rotation of the motor is based on the magnetic influence, Thomas *et al.* developed the nonlinear decoupled disturbance observer method to estimate and suppress static offset and synchronous vibration in rotating shaft with magnetic bearings application [46]. As a result, the proposed design provides a simple precision motion control strategy that can give accurate positioning over the bearing air gap of manipulator system.

The DOB not only support for the linear system, but it also can be extended to provide a solution in disturbance compensation of a nonlinear system. Several research were conducted to prove the concept. In August 2000, Wen-Hen Chen *et al.* proposed the nonlinear disturbance observer based control method [47] to be applied in the control problem of a nonlinear system [48]. Later, in April 2011, Mohammadi and his team developed the disturbance observer-based control of nonlinear haptic teleoperation systems. The control scheme is able to decrease the adverse effects of the disturbance on the stability and transparency of the teleoperation system [49]. Next, in August 2013, Mou Chen and Shuzhi Sam Ge proposed the direct adaptive neural network control method for a class of uncertain nonaffine nonlinear systems with unknown nonsymmetric input saturation [50]. By the results, it shows that the disturbance observer based control method had illustrated the effectiveness of the proposed adaptive control techniques.

1.1.3 Utilization of Reaction Force Observer Method

Control of the contact between robot and environment has been one of the most popular research problems in robotics. Force control is crucial to realize to realize a contact motion, yet poor stability and low performance of force control systems are the main challenging issues to realize aforesaid applications [51]. In order to tackle this issue, the extended method of disturbance observer concept was developed to estimate the reaction force of the system without use of force sensor [52, 53]. This method called as the reaction force observer (RFOB). The DOB can be coupled with RFOB [54] to give the proper position and force feedback control. There are many way to design the effective RFOB. Smith *et al.* proposed two neural-network-based force/torque

observers that do not require a system dynamic model [55]. While, Phuong *et al.* developed the FPGA-based high performance force control system for the development of friction-free and noise-free force observation system [56]. For the teleoperation systems, a model-independent force observer based system was developed by Farid *et al.* for hand force estimation [57].

The technique of estimated force or torque observer can be applied in various application. In the medical field, it can be used for the rehabilitation [58] and surgical robot instrument system [59]. This method can handle the lack of feedback of tactile sensation of master-slave "da-Vinci" surgical robot system [60]. For the flexible arm manipulator system, the method of reaction force observer has promises better feedback. Izumikawa *et al.* proposed the RFOB technique for the vibration suppression control of a one line flexible arm robot [61]. While, Katsura *et al.* developed the force servoing method to suppress torsional vibration of two-mass resonant flexible manipulator system [62]. They also considered the bandwidth of force sensing since it is very important for contact motion control [63].

The development of reaction force observer also reported be used in the mobile applications. In power-assisted mobile vehicle (PAMV) wheelchair system, the implementation of torque estimation can provide appropriate assisted force [64]. In order to stabilize the vehicle motion, independent in-wheel motor control and active steering control are treated. To achieve that, Kanghyun *et al.* proposed the motion stabilization of electric vehicles based on active front steering control [65]. In June 2006, Ohishi *et al.* developed the robust tracking servo system for the optical disk recording system with the implementation of feedforward controller based on the prediction of the tracking error [66]. This system which considering the disturbance force has resulted robust tracking control that keeps the tracking error smaller compared to the conventional method. Other than that, the RFOB technique also can be used for the force estimation of piezoelectric actuator [67] and electrohydraulic actuator [68].

For the application of force estimation in the field of motor drives, Hwang *et al.* has proposed an active ripple-reproduction scheme for an linear hybrid stepping motor (LHSM) [69]. The proposal was based on a position-dependent nonlinear model developed through an elaborate reluctance network analysis. In April 2010, Mitsantisuk *et al.* developed the force control technique of human-robot interaction method using twin direct drive motor system which considering the RFOB [70]. In the field of injection molding machine, the RFOB were reported to be used to develop the robust sensorless pressure control system [71] and sensorless force control

considering torsion phenomenon [72].

1.1.4 Bilateral Motion Control System

A bilateral control is a control system for teleoperation with haptic feedback. In the bilateral control system, position and/or force information of both master and slave robots is transmitted bidirectionally between the two robots [73, 74]. The bilateral control are based on the concept of reproducibility and operationality. Reproducibility shows degree of reproduction of the environmental impedance in master robot. While operationality shows degree of operation force which human operator feels obstacle force beside environmental impedance [75]. Recently there are many many research consider on its design methodology. Mitsantisuk *et al.* proposed the estimation of action/reaction forces for the bilateral control manipulator by using the Kalman filter method. Here, the authors used two types of observer which are a Kalman-filter-based state observer and a Kalman-filter-based disturbance observer [76, 77]. One of the important factor in designing the bilateral control parameter is a frequency-domain damping effect [78]. It can be designed by using the high pass filter (HPF) method in order to increase the performance and stability of the acceleration-based bilateral control (ABC) system. To maintain the stability of the bilateral system, Amir *et al.* proposed the robust stability analysis method based on the notions of wave variables and scattering parameters [79]. The authors had designed a powerful 3D geometrical graphical method to enhance the 2D method of the system. By the result, the proposed method promising a better compromise between stability and performance of two bilateral control architectures. As the degree of freedom of the master–slave robots can be extended, thus the control design can be enhanced from bilateral control into the multilateral control scheme [80].

To help human operators perform tasks more efficiently and comfortably from the remote site, the concept of bilateral teleoperator control system can be applied. A lot of consideration need to be accounted to make the designed system works perfectly. Dongjun *et al.* had proposed a passive bilateral teleoperation control method for a pair of n-degree-of-freedom nonlinear robotic systems. The control laws ensures energetic passivity of the closed-loop teleoperator with power scaling, coordinates motions and installs useful task-specific dynamics for inertia scaling, motion guidance and obstacle avoidance in master–slave system [81]. A teleoperation transparency (fidelity) is the extent of telepresence of the remote environment available to the

user through the master–slave system. In December 2007, Mahdi *et al.* had conducted the research to study the high-fidelity of the bilateral teleoperation systems and its effect on the multimodal haptics [82]. Next, Chang *et al.* proposed a telepresence index for bilateral teleoperation, which can be used both for the performance evaluation of bilateral control architectures and for design purposes [83]. In the research, telepresence index has been compared favorably with the other indices in term of clarity, convenience and accuracy, thereby demonstrating its superiority. For the nonlinear teleoperation system, Quyen *et al.* had conducted a study on a bilateral control of nonlinear pneumatic actuators for achieving high-performance control of the mass flow rate [84]. By the experimental results, it shows that good teleoperation transparency is achieved despite all the obstacles such as discrete input and nonlinear behavior of the pneumatic-actuated teleoperation system.

As the bilateral system can be controlled remotely by the teleoperation system, the time delay between the master–slave controller seriously deteriorates its performance and stability [85]. Thus, many research have been conducted that consider this effect. To achieve more vivid haptic transmission in the bilateral teleoperated system, Dapeng *et al.* performed a study on haptic system which rely on the wireless communication under varying delay [86]. The consideration of time-delayed output feedback research also had been conducted by John *et al.*. In his study, he used second-order sliding mode unknown input observers for estimating the external forces, neglecting the need for both velocity and force sensors for bilateral teleoperation of nonlinear manipulators [87]. While Franken *et al.* used a two-layer approach combining passivity and transparency of time-delayed bilateral telemanipulation system [88]. Even the time delay is the important parameters to be considered in the teleoperation of bilateral system [89–93], by implementation of certain technique can avoid the unnecessary delay effect.

The bilateral control system can be applied with the scaling technique. Scaling is usually applied for a master–slave robot system with different sizes. Thus, a concept of macro-master and micro-slave can be realized to extend human ability in delicate tasks such as robotic surgeries. Many examples of this scaled bilateral manipulation system research have been studied. Mizoguchi *et al.* implemented the scaling of bilateral control system for their study on stiffness transmission by using the gyrator element integration [94]. The proposed method integrates the gyrator element in the F matrix to convert transparency scaling ratio during contact motion. The concept of scaled bilateral system not only support the single or one degree-of freedom

(DOF) system, but also can be extended into the multi-DOF manipulation system [95]. By this implemented system, Sakaino *et al.* proved that this concept can provides stable and precise responses and it is applicable for actual robot systems, which necessary for advanced and sophisticated medical operations.

1.1.5 Advancement of Vision-based System

Nowadays, the vision-based technologies are increasingly used in many area. It leads to many new applications such as video surveillance, person identification, motion capture for entertainment industry or medical purposes but also tools and systems, where the user can interface a device e.g. gesture recognition, human–machine interaction or interactive web-based commercial applications [96]. In industrial processes field example, the vision-based system can be represented by the virtual reality concept. Virtual prototyping consists in replacing physical prototypes by virtual mock-ups in order to increase productivity and shorten design, development, engineering and training times on industrial product [97]. The use of the vision-based system in daily life also can improve the quality of human life. To enable lectures using graphical illustration, students who are blind should be able to read the instruction, listen and to fuse both information streams in real time. Thus, Fang *et al.* had developed a real-time vision-based tracking system together with haptic gloves to help students who have visual impairments [98]. The developed system is able to provide direction in conjuction with speech and fingertip reading.

An useful information from the vision system can be captured to be used in many applicable visual analysis. For tracking trajectories application, a movement-flow based visual servoing system was proposed by Pomares *et a l.*. The system fusing the visual and force information of an object by using a three-dimensional (3-D) image space in unstructured environments [99]. By considering the human skin's surface traction fields, Kamiyama *et al.* had performed a research to study about the impact of force in developing the depth information trough color in vision-based sensory system for real-time measurement [100]. Here, it show that all the information of the visual data is possible to be translated to generate another useful application.

Vision system have been reported uses in robotic area. In December 2013, Raffaella Carloni and his fellow researchers had implemented the obstacle-avoidance techniques for unmanned aerial vehicles (UAV). This method can overcome the problem of nonfunctional global posi-

tioning system (GPS) of the UAV when flying indoors in an unknown and unstructured environment [101]. In another similar UAVs application, Ha *et al.* had proposed the vision-based teleoperation method to control the speed and movement's capability of the paired unmanned ground vehicle (UGV) [102]. This system later be integrated with the haptic device [103] allowing a human user to (haptically) teleoperate the UAV and UGV coordination. For the planar robots servoing system, Emmanuel *et al.* proposed the image-based position-force control for constrained planar robots subject to complex friction. In that research, a new formal solution is presented for the problem of the uncalibrated image-based robot force control under the parametric uncertainties without the singularities in the camera orientation angle [104].

An image information can be manipulated to generate the force guidance for the mobile application. In November 2007 at San Diego, the concept of vision-based force guidance have been applied for a teleoperative mobile robot manipulation system. This research was conducted by Chung *et al.* [105] to study the effectiveness of guidance forces in a haptic system to enable ease-of-use for human operators performing common manipulation activities of daily tasks. While Bartolini *et al.* used the virtual force approach to study the vulnerabilities of mobile sensor deployment [106]. The concept of virtual-force-based control method was also applied by Chong Liu and Jie Wu in order to study the geometric routing protocol in mobile ad hoc networks (MANETS) [107]. For the power assisted wheelchair application, an interactive control method by implementation of vision-based reaction force observer was proposed by Oda *et al.*. In the proposed approach, both encoder-based and vision-based reaction force observer are designed for obtaining the virtual force due to the environmental change in the field of view [108].

1.1.6 Perspective of Visual Navigation Technique

Tracking the movement of objects by a vision system in real-time is an important problem. It has been addressed by researchers in a number of different fields including target tracking, surveillance, automated guidance systems, inspection and monitoring [109]. Thus, the real-time tracking system is necessary for the creation of intelligent robotic systems.

There are many research discussing about the visual servoing method. Simas *et al.* had proposed the visual tracking technique which based on 3D probabilistic reconstruction. This proposal executes the markerless visual tracking observing the environment through a model based in a volumetric reconstruction technique [110]. Further, Harlan *et al.* had developed the

visual navigation approach for a mobile devices [111]. The study presents the integration of an improved camera pose recovery method into a landmark-based visual navigation system for mobile devices. In March 2012, Bonin-Font *et al.* proposed the inverse perspective transformation (IPT) technique for concurrent visual navigation and localisation [112]. In their method, they used the IPT-based image feature classification criterions for an obstacle detection and avoidance purposes of a Pioneer 3DX robot. For the hand gesture detection and recognition study, the real time application of visual servoing approach was proposed by Nagaraj N Bhat. He developed this technique to prove that the fast process of hand gesture recognition and direction control can be developed for human computer interaction [113]. To improve the detection process during teleoperated navigation, Rong Lie *et al.* had proposed the integration of visual navigation and auditory feedback. This study provides evidence that auditory displays have the potential to improve user performance and system safety for "end-to-end" teleoperation tasks under unfavorable conditions [114]. Next, for the moving object tracking method, Akira *et al.* introduced the visual servoing technique based on real-time distance identification of a 6 DOF manipulator. As a result, the system shows that the camera can track the moving object perfectly by identifying distance real-time and calculating pseudo inverse matrix [115].

The camera can be used as a vision sensor for the navigation system. There are many types of camera available to be used and one of it is omnidirectional camera. Omnidirectional camera can provide 360° view in a single image. The uses of this type of camera in visual servoing was reported by Ming *et al.*. In his research, he develop the visual homing approaches to enable a mobile robot to a reference position using only visual information of an uncalibrated omnidirectional camera [116]. By the same camera, Gaspar *et al.* also developed the vision-based navigation and environmental representation of a mobile robot in indoor environments [117]. In stead of the omnidirectional type camera, the stereo vision technique of normal camera also can be implemented. In 2007, Li Ge and Zhao Jie had proposed a real-time stereo visual servoing approach for grasping of moving object [118]. The study introduced a visual tracking control method based on template matching and stereo matching method to solve problems of slow servoing speed and low oriented precision at invariable periods of object tracking.

The visual navigation method has been reported to be used for an industrial robot application. In 1999, Sung-Hyun *et al.* has proposed the real-time control of an industrial robot by using an image-based visual servoing approach. This method overcomes several problems in

visual servoing with the monocular vision system [119]. Later, in November 2002, Han Liu and his team had introduced a position-based approach to visual servoing and pose estimation for an unknown target of robot manipulator works to reach the object. This study was based on the genetic algorithm method [120]. Not only for the industrial manipulator robot, the servoing technique also can be applied to be used by the humanoid robots. This is proved by the research conducted by Hwang *et al.*. In his research, he study the comparison between two visual navigation strategies for kicking to virtual target point of humanoid robots [121]. For further reducing the total processing time of the system, he uses a single board computer with webcam.

The development of mobile navigation system can also applying the vision-based servoing technique. In September 1988, Ishikawa et al. had conducted a study on the visual navigation of an autonomous vehicle by using the white line recognition. In their approach, the automatic unmanned vehicle (AUV) follows a white guide line on a flat ground floor sensing through a forward looking camera [122]. Andrea *et al.* had conducted a study to validate a framework for avoiding moving obstacles during visual navigation with a wheeled mobile robot [123]. By conducting the real outdoor experiments, the proposed method show that the robot behavior is safer, smoother and faster when the obstacle velocities are considered. As for flying object navigation system, Salazar *et al.* proposed a real-time stereo visual servoing control method for an UAV that have eight-rotors. By this implementation, the system can estimate the UAV's 3D position yet allowing to control the orientation and position of flying robot [124].

1.1.7 Overview of an Image Processing Techniques

The literature of image processing offers a variety of well-established methods, both linear and nonlinear, for filtering monochrome or gray-level images [125]. Color image filtering, on the other hand, has started receiving attention only in recent years [126–129]. The implementation of visual navigation method in a vision based system must be went through some image filtering or processing techniques [130]. Thus, understanding of its processing pipeline or step may be a good starting point to fully comprehend the signal processing perspective [131].

One of the popular steps is the detection of edges in color images. Andreas *et al.* was mentioned that edge detection is one of the most important tasks in image processing and scene analysis systems [132]. From their finding, color edge operators are able to detect more edges than gray-level edge operators. Thus, additional features can be obtained in color images that

may not detected in gray-level images [133]. Another popular method is an image binarization technique. Krishna *et al.* had conducted the study on clustering based method of an image binarization process in palm leaf manuscripts [134]. This method was used to extract the foreground data from palm leaf manuscript images. With existing thresholding approaches, the proposed method achieves better accuracy. In binarization process, the image contrast will bring a big impact to the final result. Therefore, the contrast enhancement of an image can be done by using the color and depth histograms [135]. Moreover, the color, texture and shape detection are also important process in image processing technique. Kavitha *et al.* had conducted the research on object based image retrieval from database using mentioned combined features. The results show significant improvement over the existing systems [136].

The image processing technique can be applied in the vision-based human-computer interaction (HCI) especially to detect the skin color. In August 2003, Chen *et al.* proposed a simple and fast method for face detection to dynamically define region-of-interest (ROI) in real time application. He developed this method on his study on ROI video coding based on H.263+ with robust skin-solor detection technique [137]. In 2011, Liu *et al.* had conducted a study on the real-time skin color detection under rapidly changing illumination conditions [138]. In the study, face detection is employed to online sample skin colors and a dynamic thresholding technique is used to update the skin color model under Bayesian decision framework. This method can perfectly detect illumination changes of the skin color.

1.1.8 Superiority of Visual Force Control System

Most applications of advanced robotics, and particularly hazardous environment robotics, require to provide robot manipulators with the ability of working in environments with unknown location and geometry. Thus, external sensory information has to be integrated in the manipulator control [139]. One of the solutions is by implementing the visual force control method that can be integrated to the manipulator system. The development criterion of this method is applied in many perspective such as the positioning of visual sensor, a suitable application and so on. That criterion should be considered to confirm the superiority of the developed visual force control system.

The technique of vision-based force control can be applied in different method of visual sensor location. One of the method is called as the Eye-in-Hand (EIH), which the vision sensor

is being attach together on the manipulator or robotic hand. In 2007, Hiroyuki Kawai *et al.* had conducted the study on the development of the visual force feedback system with the eye-in-hand configuration [140]. The vision and force control were applied to horizontal/vertical direction for the environment which is thought as a frictionless, elastically compliant plane. In other related study, Pomares *et al.* had proposed a technique on the implementation of the EIH method to the manipulator system which also encompasses the information from a laser. Then, a visual servoing approach was defined to track trajectories and to detect surface changes of the target object [141]. The visual information not only gathered from the charge-coupled device (CCD) types camera, but also can be obtained from the stereo head-mounted display (HMD) as a study conducted by Williams *et al.*. They had developed the system to study the effects of bisensory force feedback on teleoperator performance of a drill task under four different force display conditions [142].

Besides EIH, the other method is called as the Eye-to-Hand (ETH), which the camera or the vision sensor is located not on the manipulator, but in one static place. The camera can view the servoing object and also the tip of the manipulator system from that static location. In September 2008, Maciej Staniak *et al.* had proposed the parallel visual-force control system which based on the eye-to-hand configuration [143]. The research presented an alternative solution in which the grasping operation is aided by force control which accommodates positional inaccuracies. In same year, other study had been conducted to show that the 3D visual feedback system has the passivity which allows them to prove the stability of the developed system [144]. The ETH method is very popular in the application of the micro-manipulation control system. Haibo Huang *et al.* had conducted a research on the visual force control of 3D cell injection system [145]. There, the injection force was calibrated in a cell injection task to derive the relationship between the force and the cell deformation.

In other aspect of controlling method, Ch. S. Kim *et al.* had proposed the fuzzy logic control of a robotic manipulator which based on visual servoing [146,147]. They provided an alternative way to solve the control of the dynamics of the manipulation system. The fuzzy logic was used to detect easily situation of action mapping for the manipulation task at hand of the robot by the visual force information generated from the vision sensor. In May 1999, Akio Namiki had conducted the study on the high speed grasping using visual and force feedback. From the study, the authors used the information from the 1000Hz camera system and compared the generated

force by the calculated visual force with the estimated force of the manipulator's gripper [148]. The high speed camera will provide a huge number of captured image frame in a second. Thus, the sensory-motor fusion system which based on the 1ms cycle time was successfully developed. In June 2014, the study on the designing of a new flexible controller for humanoid robot that considers the interaction of visual and force control system [149] had been implemented. This study was conducted by Gan Ma *et al.*. Moreover, the usefulness of the visual force control system is proved by its implementation in the area of medical application. Wensheng Hou *et al.* proposed a visual force-feedback system that suitable for neuroscience experiment [150]. In that system, the force output produced by participants can be detected and recorded in real time, while force output was visually displayed as a feedback cue to the participants simultaneously. Yet, the produced force feedback system was MRI compatible and can be used for the clinical application studies.

1.2 Motivation

Although many researchers have ventures into the application of haptic system, but the integration of the devices with the vision-based system for navigation purpose is still lack. Most of the developed vision–haptic system were based on the virtual reality feedback. Thus, it will not give the real representation of the manipulated haptic environment. Therefore, the study can be focussed on the development of real-time camera vision-feedback to monitor live image of the servoing objects.

There are many object servoing techniques have been developed before. Most of the techniques are based on the position control and acceleration control. There are a few researchers who apply it in the form of force control. But, many of them have applied for the application of controlling a motion of mobile manipulator such as automatic unmanned vehicle (AUV), power-assisted wheelchair and mobile robot. On that account, the integration of the object servoing technique to the haptic bilateral master–slave manipulator system should be given preference in order to find the originality.

The effectiveness of the implementation of disturbance observer (DOB) and reaction force observer (RFOB) have been proven in order to develop a robust acceleration based motion control. Its capabilities that can be applied in many field, is undeniabled. Hence, the consideration of applying the DOB and RFOB technique in the designed system, should be given priority.

The focussed can also be given on the integration method of developed force controller to those observer. Hereinafter, the motion control of bilateral haptic system for object servoing purposes can be assisted by the generated force of integrated observer based methodology.

1.3 Research Objective

The direction in the development and implementation of this research are based on several objective. A number of research objectives have been planned as the main goal to be realized. The main objectives of this study are listed as below:

1. To design a vision-based system that can be integrated with the haptic system for motion navigation. It will includes the suitable controller and image processing approach that can be used for object tracking method in the bilateral system for horizontal movement. The concept of bilateral master–slave manipulator system can be applied together with the disturbance observer and reaction observer technique.

2. To investigate the utility of the designed method by the scaling effect of the object size. The different of distance between the camera and the same navigated object can produces the different scaling effect. The designed controller should be able to handle this effect.

3. To evaluate the performance of the proposed method by implementing the error or noise suppression technique in the integrated vision–haptic system.

4. To analyse the ability of the designed controller to track the object by taking object coordinate orientational effect into account. As for the one focus area of the object surface, the self-rotation of the object may generate the object rotational effect to the navigation system. The proposed method should be able to follow the rotation of the object so that the focussed area can be navigated effectively.

1.4 Thesis Outline

The organization of this thesis can be described as follows. Chapter 2 explains the basic concept of bilateral control methods of a master–slave manipulator system. Chapter 3 describes the advent of proposed Vision-based Force Compliance control method and its integration with the haptic bilateral control system. Next, Chapter 4 discusses the scaling effect on the generated

virtual force by the vision-based force compliance controller. Further, Chapter 5 investigates the proposed system's performance by implementing the vision-based disturbance observer technique. Moreover, Chapter 6 presents the object's coordinate behavior which consider the rotational control approaches. Lastly, Chapter 7 summarizes the conclusion and contribution of the research.

Chapter 2

Bilateral Motion Control

In the previous chapter, I have explained the relevant previous studies that have been conducted by researchers associated with the topic to be discussed.

In this chapter, I will explain the basic knowledge of the bilateral control. This is crucial in the realization of haptics motion control in order to move two motors simultaneously. At the same time, through the concept of the master–slave system, the stiffness of the target object at slave environment can be felt by the master manipulator rigidly.

I will begin by describing the explanations of basic theory of disturbance observer (DOB) and reaction force observer (RFOB). Then move to the original concept of master–slave bilateral control system and its basic theory.

2.1 Disturbance Observer

This section describes robust acceleration control based on disturbance observer [85, 151]. Parameters for the system are shown as in Table 2.1.

In actual motion control, disturbance force F^{dis} is exerted on a robot. Disturbance Observer (DOB) estimates disturbance force F^{dis} and gives compensating current I^{cmp} for robust motion control. The block diagram of DOB is shown in Figure 2.1. The components of F^{dis} are described as follows:

$$F^{dis} = F^{ext} + F^{int} + F^{fric} + (M - M_n)s^2X^{res} + (K_{tn} - K_t)I_a^{ref}. \tag{2.1}$$

Disturbance force F^{dis} also includes the force caused by modelling error of nominal mass M_n and nominal thrust coefficient K_{tn}. Interactive force F^{int} includes Coriolis term, centrifugal term and gravity term. As a result, the disturbance force F^{dis} is estimated through the low

Table 2.1: Parameters for the DOB system

Parameters	**Discription**
M	Mass
X	Position
K_t	Force coefficient
I_a	Motor current
F^{dis}	Disturbance Force
F^{ext}	External Force
F^{int}	Interactive Force
F^{fric}	Friction Force
I^{cmp}	Compensation Current
$\widehat{\ }$	Estimated Value
C_p	Position Controller
C_f	Force Controller
K_p	Position Gain
K_v	Velocity Gain
K_f	Force Gain
g_{dis}	Cutoff frequency of DOB
Z_e	Impedance of environment
$(superscript)cmd$	Command value
$(superscript)cmp$	Compensation value
$(superscript)ref$	Reference value
$(superscript)res$	Response value
$(superscript)n$	Nominal value
$(superscript)m$	Master system
$(superscript)s$	Slave system

pass filter (LPF) as follows:

$$F^{dis} = \frac{g_{dis}}{s + g_{dis}} F^{dis}. \tag{2.2}$$

The equivalent system of Figure 2.1 is shown in Figure 2.2. It shows that the disturbance force F^{dis} is input to the system through the high pass filter (HPF) by the compensation of DOB. If g_{dis} is large enough, the disturbance force F^{dis} hardly affects the system. Then, Figure 2.2 changes to Figure 2.3. Plant model is described as $1/s^2$. To achieve robust acceleration control, it is absolutely necessary condition that g_{dis} should be large enough.

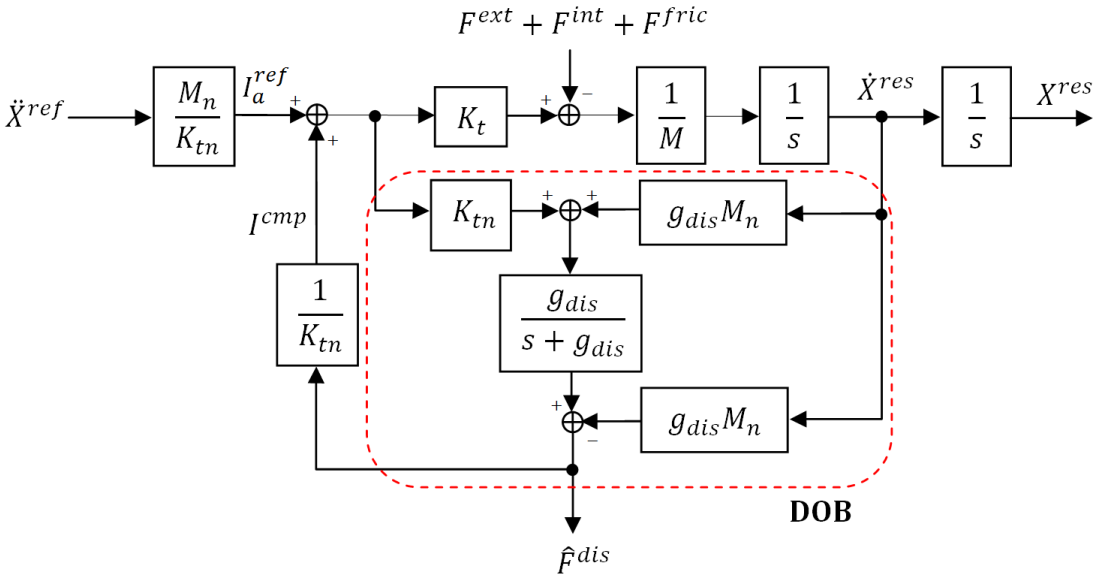

Figure 2.1: Disturbance compensation by DOB

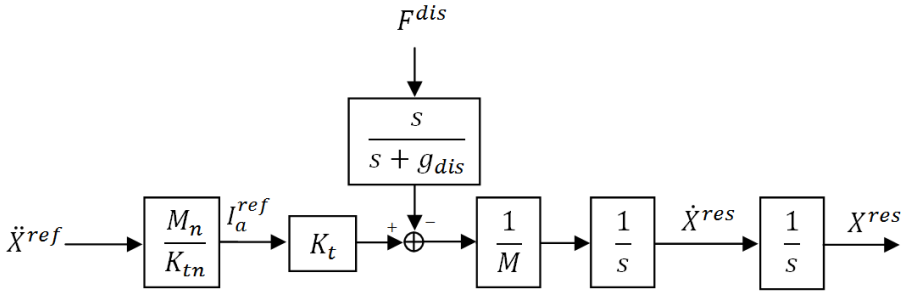

Figure 2.2: Robust acceleration control

2.1.1 Acceleration Based Position Control

Robust motion control is achieved by using the DOB. The block diagram of a position control system based on acceleration control is shown in Figure 2.4. C_p is a position controller where

$$C_p(s) = K_p + sK_v. \tag{2.3}$$

Position response is described as follows:

$$x^{res} = \frac{C_p}{s^2}(x^{cmd} - x^{res}). \tag{2.4}$$

Equation 2.7 is transformed as follows:

$$\begin{aligned} \frac{x^{res}}{x^{cmd}} &= \frac{C_p}{s^2 + C_p} \\ &= \frac{sK_v + K_p}{s^2 + sK_v + K_p} \end{aligned}$$

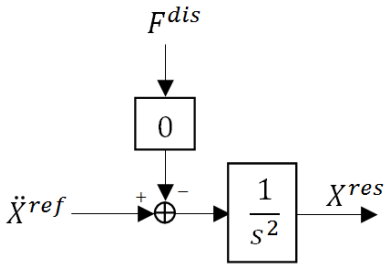

Figure 2.3: Ideal robust acceleration control

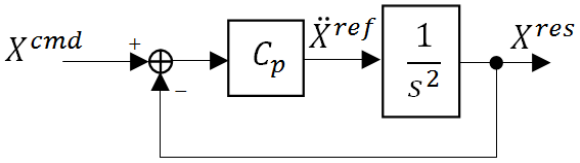

Figure 2.4: Acceleration based position control

$$= \frac{2\zeta\omega_n s + \omega_n^2}{s^2 + 2\zeta\omega_n s + \omega_n^2}. \tag{2.5}$$

The damping ratio ζ can set at 1.0 to achieve a critical damping effect. While, natural angular frequency $\omega_n = \sqrt{K_p}$ or $\frac{1}{2}K_v$.

2.2 Reaction Force Observer

DOB is utilized for not only estimation of disturbance force but also estimation of reaction force. Reaction force observer (RFOB) can estimate wider band force information than a force sensor [153]. However, it requires identification of friction force F^{fric} and interactive force F^{int} such as the gravity term, in advance. The block diagram of RFOB is shown in Figure 2.5. If the identification of parameters are perfect, estimated external force F^{ext} is calculated as follows.

$$\hat{F}^{ext} = \frac{g_{dis}}{s + g_{dis}} F^{ext}. \tag{2.6}$$

The cutoff frequency of RFOB is same with that of DOB.

2.2.1 Acceleration Based Force Control

The block diagram of a force control system based on acceleration control is shown in Figure 2.6. C_f is force controller where

$$C_f = K_f. \tag{2.7}$$

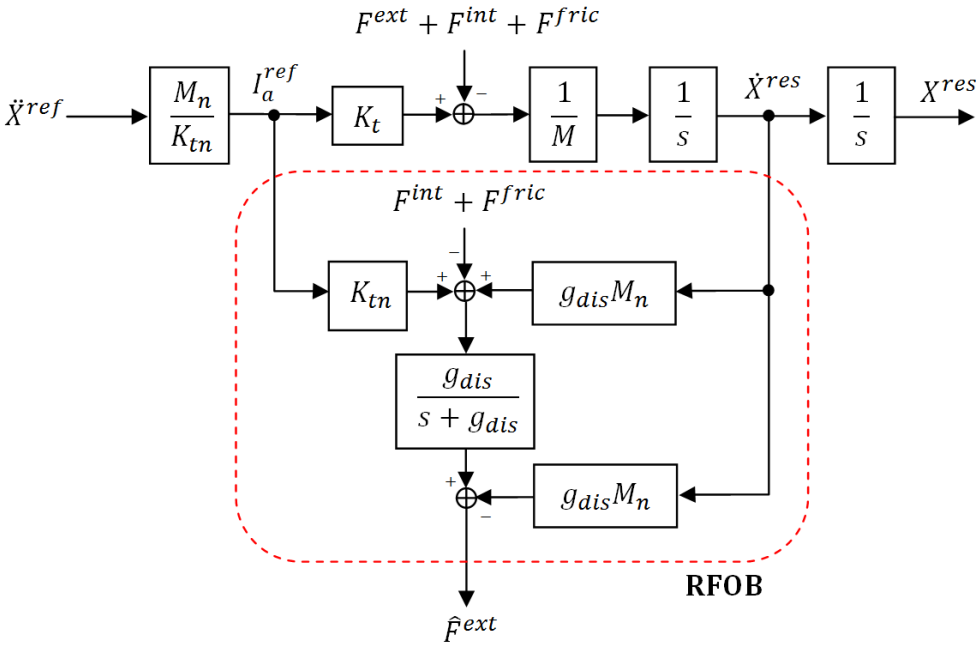

Figure 2.5: Reaction force estimation by RFOB

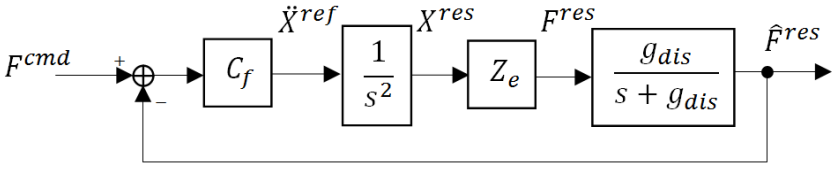

Figure 2.6: Acceleration based force control

Estimated force response is described as follows:

$$\hat{F}^{res} = \frac{C_f Z_e g_{dis}}{s^2(s + g_{dis})}(F^{cmd} - \hat{F}^{res}). \tag{2.8}$$

Equation 2.8 is transformed as follows:

$$\frac{\hat{F}^{res}}{F^{cmd}} = \frac{1}{\frac{s^2(s + g_{dis})}{C_f Z_e g_{dis}} + 1}. \tag{2.9}$$

2.3 Bilateral Master–Slave Control System

A haptic environment can be realized by using the bilateral control of a master and slave system. A force sensation that occurs in the slave environment can be perceived on the master's control side and vice versa. To enable the operator to accurately perceive a force sensation, both the

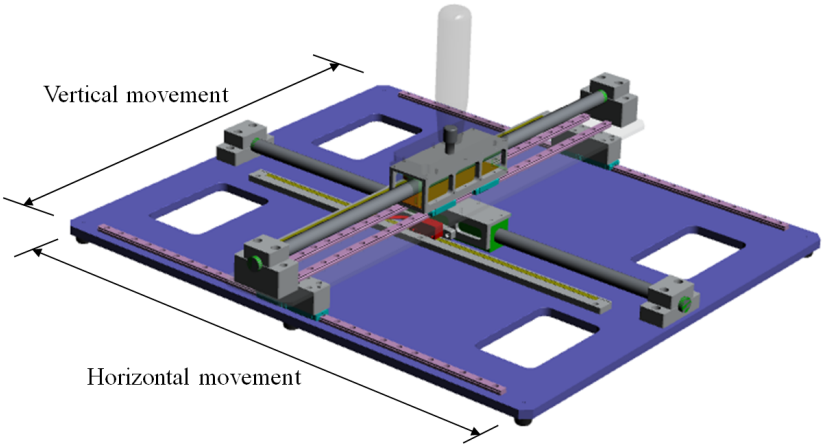

Figure 2.7: CAD illustration of X-Y table

force and position feedback should be transferred bidirectionally. In this study, two X-Y tables are used to realize the bilateral motion system. An X-Y table is depicted in Figure 2.7.

The bilateral control concept uses the total acceleration $\ddot{x}_{dif}$ in the differential mode and the total force F_{com} in the common mode [152] on both the master and slave systems, where

$$\begin{aligned} \ddot{x}_{dif} &= \ddot{x}_m - \ddot{x}_s \\ &= 0 \end{aligned} \tag{2.10}$$

$$\begin{aligned} F_{com} &= F_m + F_s \\ &= 0. \end{aligned} \tag{2.11}$$

Moreover, it can be rearranged into the matrix form as,

$$\begin{bmatrix} \ddot{x}_{dif} \\ \ddot{x}_{com} \end{bmatrix} = \begin{bmatrix} 1 & -1 \\ 1 & 1 \end{bmatrix} \begin{bmatrix} \ddot{x}_m \\ \ddot{x}_s \end{bmatrix} \tag{2.12}$$

or can be integrated with Hadamard transformation matrix as,

$$\begin{bmatrix} \ddot{x}_{dif} \\ \ddot{x}_{com} \end{bmatrix} = \mathbf{H} \begin{bmatrix} \ddot{x}_m \\ \ddot{x}_s \end{bmatrix} \tag{2.13}$$

where,

$$\mathbf{H} = \begin{bmatrix} 1 & -1 \\ 1 & 1 \end{bmatrix}. \tag{2.14}$$

To satisfy this control requirement, the differential mode and common mode are respectively position-controlled and force-controlled using a disturbance observer (DOB) [153] and reaction

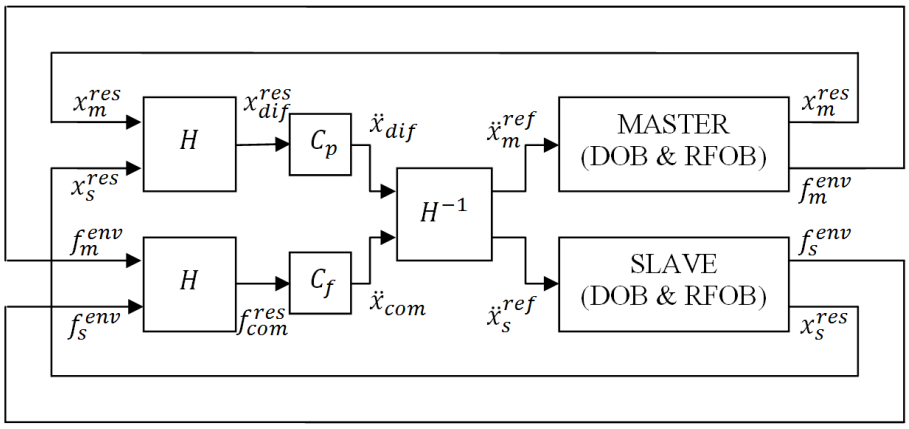

Figure 2.8: Block diagram of bilateral control for master and slave system

force observer (RFOB) [151], respectively. In the differential mode, the position controller C_p can be described as

$$\ddot{x}_{dif}^{ref} = C_p(s)(x_s^{res} - x_m^{res}) \tag{2.15}$$

and in the common mode, the force controller C_f can be described as

$$\ddot{x}_{com}^{ref} = C_f(f_s^{ext} + f_m^{ext}) \tag{2.16}$$

where C_p and C_f as described in Equation 2.6 and 2.7 correspondingly. Here, K_{p}, K_{v}, and K_{f} are the position, velocity, and force coefficients, respectively. Figure 2.8 shows the detail of bilateral control system's block diagram.

In this control method, low pass filters (LPF) are implemented in the proportional-derivative (PD) controller of C_p to prevent noise and chattering. These LPFs can be described as follows:

$$\mathrm{LPF} = \frac{g}{s+g} \tag{2.17}$$

where g is the cut-off frequency. Their position coefficient K_{p} and velocity coefficient K_{v} are set based on the natural frequency ω_n to demonstrate the critical damping ratio effect, as shown below:

$$K_{\mathrm{p}} = (\omega_n)^2 \tag{2.18}$$

$$K_{\mathrm{v}} = 2\omega_n. \tag{2.19}$$

2.4 Summary

In this chapter, the original basic concept of disturbance observer (DOB) and reaction force observer (RFOB) has been defined. Next, the realization of bilateral master–slave control system also has been described. By implementing the DOB and RFOB in the bilateral system, a robust motion control can be achieved.

Chapter 3

Vision-based Force Compliance Control Method

In the previous chapter, I have described the basic knowledge of the disturbance observer (DOB), reaction force observer (RFOB) and bilateral motion control which can be considered as a conventional method in haptic system.

In this chapter, I will explain about the proposed tracking control method which based on the vision-based force compliance controller. This technique is important in order to manipulate one object under the master–slave environment but at the same time the object is moving. Thus, by the implementation of vision-based servoing method and integrates it with the bilateral control system, the robust vision-aided master–slave motion control can be realized.

The chapter will begin by the overview of the overall proposed system. Next, I will describe about the vision-based navigation technique. Then, the description of the basic concept of vision-based force tracking control will be derived. After that, I will elaborate about how to integrate it with the bilateral master–slave control system.

3.1 Introduction

In recent years, there have been great expectations surrounding the development of sophisticated robot technology that can directly support human activities. A human-support robot should be able to adapt to a human environment. A visual sensing technique is a good candidate for integration with a robot system for such environmental adaptation [154].

There have been many studies on the integration of visual sensing techniques with robot systems. One of the most popular research topics is visual servoing. Visual servoing is effective

not only for the robust tracking of a target object [155, 156] but also for effective robot motion control [157, 158]. However, the pure position-feedback-based visual servoing is not suitable for human–robot interaction. This is because the robot motion based on it is not compliant with the reaction force generated by the physical interaction with the environment, including a human. Compliance with the reaction force is necessary to realize safe interaction with the environment [159]. Thus, the development of a force-feedback-based approach that utilizes visual information is essential to realize safe physical interaction [160].

As for a human support robot, the master–slave robot system has recently attracted much attention. A bilaterally controlled master–slave robot can realize haptic interactions between the human, robot, and environment. The conventional research on bilateral control systems has mainly focused on the realization of haptic communication. The introduction of a visual sensing technique to a bilateral control system will dramatically improve the interactive function. Indeed, visual information can improve the perception [161] and recognition [2]. Moreover, visual information can improve the manual manipulation from the viewpoint of motion navigation. Thus, vision-based navigation should be based on the force-feedback approach to avoid significantly disturbing the physical interaction. However, few studies have been conducted on the integration between compliant motion navigation based on visual information and a bilateral control system.

The intention to undertake a robust sensational feeling of actual environment and its feedback especially in the bilateral haptic system had triggered a new phenomenon in the field of haptics research. There are several ways to realize that inspiration and one of the techniques is by performing the visual force compliance control feedback to the bilateral haptic system. Figure 3.1 shows the complete combination diagram of vision system and its integration with the bilateral master-slave haptic system indicated in this research.

3.2 Vision-based System

The development of this research was integrated with the visual data as the important part to be studied. The appropriate image processing's data of the dedicated object will be computed and used as a coordinate trajectory for the system. If the vision system detects some changes in term of object's movement, it will send that data (treated as position error) to the bilateral system's controller and resulted the generation of visual force, which will be further explained

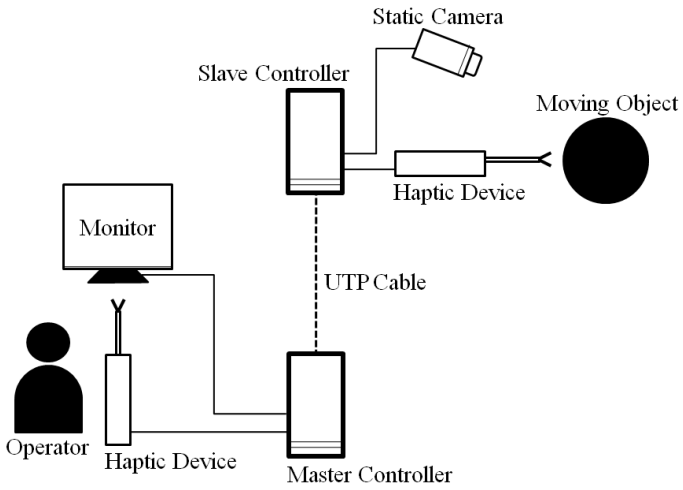

Figure 3.1: Bilateral haptic system with visual force compliance control.

in the next section of this chapter.

In this study, the object coordinate recognition is performed by using single camera technique with single coordinate identification. The vision sensor or camera is mounted static above the object (facing down). Even though it is not attached together with the haptic device but it can render pixel error of the horizontal and vertical axes on its image plane. To simplify the object detection, a marker is attached to the object surface. There are several type of marker that can be used either rectangular type [162] or line type. In this study, a 2-cm blue line is used as an object marker, as shown in Figure 3.2. In the image plane, the coordinate is extracted from a single pixel of the object marker. The coordinate extraction method uses several image-processing techniques.

The image-processing program had been developed using the OpenCV software to detect and track the marker on the object. There are four main processes which are colour detection, image binarization, corner detection and centroid identification. The software is designed to trace only the blue colour with the pixel intensity from 0 to 255. Next, the detected blue color of the object marker will be filtered using the image binarization process. In the binarization process, the detected blue pixel will be assigned as '1' that represents white and the others with '0', that represents black. Thus, only the object marker can be seen on the screen with white pixels. Then, a corner detection process is performed to find the left-most and right-most coordinates of the marker. The centroid of the object marker can be identified using this process. The average of the coordinates will be calculated to find the center point, which will later be

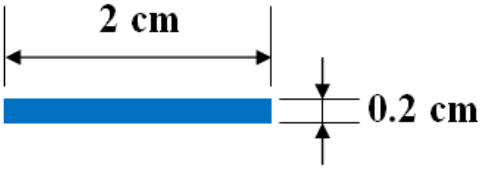

Figure 3.2: Blue line marker on the moving object

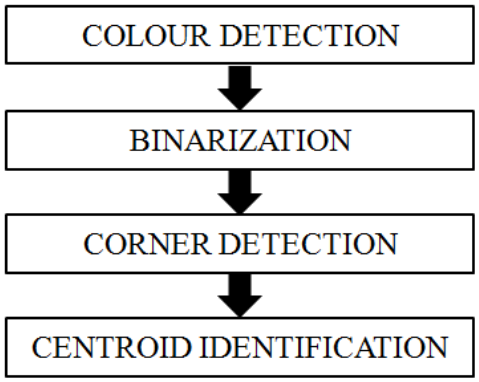

Figure 3.3: Image processing flow diagram

used as the object's reference coordinate for the whole system. The centroid point will be in the form of one single pixel and every change in the pixel value is cited as position error. It will be sent to the system controller as a position command for the horizontal or vertical movement of the haptic device with 1 kHz of sampling time. Although the transfered data is in the form of x and y coordinates, only the horizontal movement will be considered in this research. Figure 3.3 shows the image processing flow diagram as for the identification of the object's coordinate. While Figure 3.4 shows the visualization of imaging process for detecting the blue line.

The camera is located about 10cm from the marked object. Since the captured object information is in pixel value, it need to be converted into the real measurement value (in SI unit). The different in camera's distance will results different size of the original object's marker image [163]. To solve this, the image scale needs to be identified. So, the scaling factor of the image size (between two corner horizontally) can be stated as,

$$\text{Scaling factor, } s_x = \frac{\text{Actual length (m)}}{\text{Number of pixel}}. \tag{3.1}$$

The camera is mounted on an adjustable camera stand that allows it to be raised to different heights. This is also known as the camera distance magnification process. The height of the

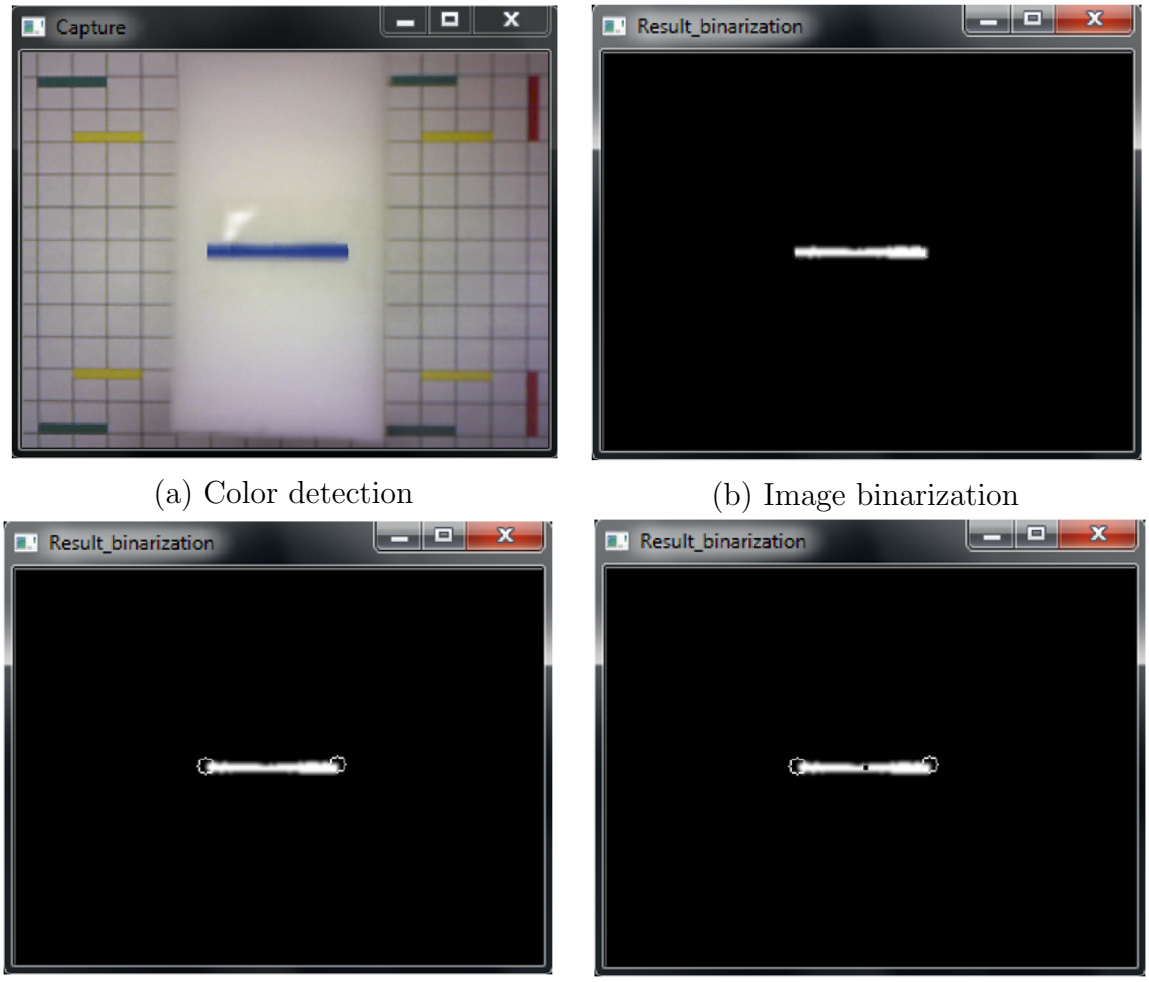

(a) Color detection (b) Image binarization

(c) Corner detection (d) Centroid identification

Figure 3.4: Visualization of image-processing techniques flow

camera is justified as the distance d between the camera and the object surface. The magnification process will affect the generation of virtual force and it will be discussed in the next chapter. Figure 3.5 shows the positions of the camera, object, and manipulator, along with the coordinate frame.

3.3 Force-Based Compliance Control Method Utilizing Visual Information

The movement of an object from one position to another can be modeled as depicted in Figure 3.6. On an image plane, a pixel's coordinates can be referred to as P(p_x, p_y). In this study, only changes in an object's location along the horizontal axis are considered, which only affect

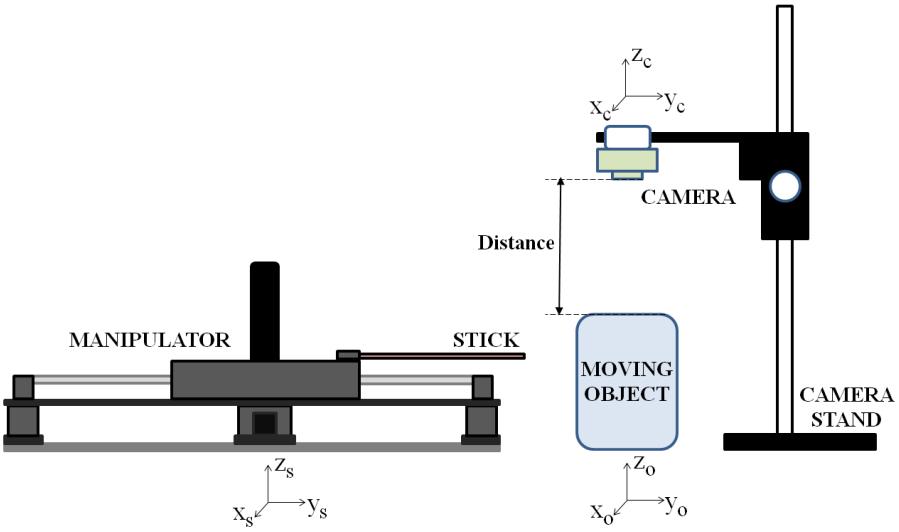

Figure 3.5: Camera–object distance measurement and its coordinate frame

the values of p_x. The location of a moving object can be detected by using a camera, which has been elaborated in the previous section. Thus, the mechanical model of one moving object along the horizontal axis of the image plane can be described as

$$M\ddot{p}_x^{res} + K(p_x^{res} - p_x^{initial}) + D(\dot{p}_x^{res} - \dot{p}_x^{initial}) = 0 \tag{3.2}$$

where M is the virtual object's mass, whereas K and D are the virtual spring and virtual damper coefficients, respectively. The term $p_x^{initial}$ is the initial position of the object, and p_x^{res} is the current object's position in the image plane (pixel value).

Then, (3.2) can be restructured as the proportional derivative (PD) position controller shown in (3.3):

$$\begin{aligned} \ddot{p}_x^{res} &= \frac{1}{M}\{K(p_x^{initial} - p_x^{res}) + D(\dot{p}_x^{initial} - \dot{p}_x^{res})\} \\ &= \frac{K}{M}(p_x^{initial} - p_x^{res}) + \frac{D}{M}(\dot{p}_x^{initial} - \dot{p}_x^{res}) \\ &= K_{\mathrm{pv}}(p_x^{initial} - p_x^{res}) + K_{\mathrm{vv}}(\dot{p}_x^{initial} - \dot{p}_x^{res}). \end{aligned} \tag{3.3}$$

where K_{pv} is a virtual position coefficient, and K_{vv} is a virtual velocity coefficient.

As a result of the movement, the system will generate a virtual responsive force F_x^{res} as the feedback of the spring and damper in order to move back to its original position. This can be defined as

$$F_x^{res} = M\ddot{p}_x^{res}. \tag{3.4}$$

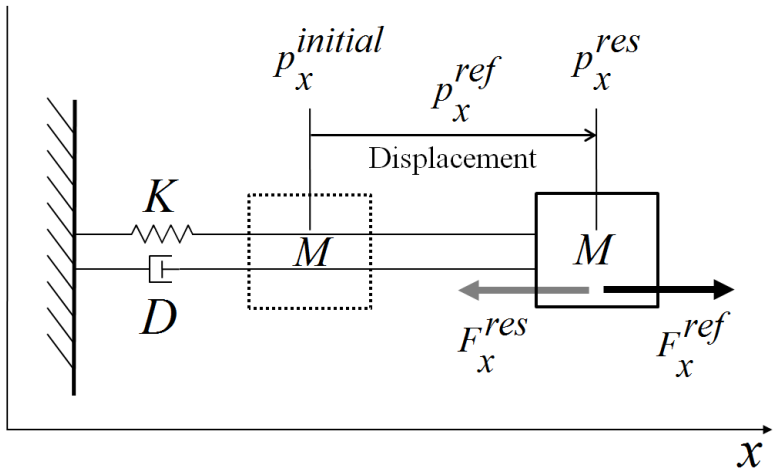

Figure 3.6: Modeling concept of force-based compliance control

Further, this force will be used as a manipulator's reference force for navigation purposes. Because the object moves to the right on the horizontal axis of the image plane, the manipulator's reference force F_x^{ref} will be in the negative direction of F_x^{res}. Hence,

$$F_x^{ref} = -F_x^{res} \tag{3.5}$$

and for the same virtual object's mass, M, it leads to

$$\begin{aligned} \ddot{p}_x^{ref} &= -\ddot{p}_x^{res} \\ &= -[K_{\text{pv}}(p_x^{initial} - p_x^{res}) + K_{\text{vv}}(\dot{p}_x^{initial} - \dot{p}_x^{res})] \\ &= K_{\text{pv}}(p_x^{res} - p_x^{initial}) + K_{\text{vv}}(\dot{p}_x^{res} - \dot{p}_x^{initial}). \end{aligned} \tag{3.6}$$

Let

$$p_x^{ref} = p_x^{res} - p_x^{initial}. \tag{3.7}$$

Then, (3.6) can be simplified to

$$\ddot{p}_x^{ref} = K_{\text{pv}} p_x^{ref} + K_{\text{vv}} \dot{p}_x^{ref}. \tag{3.8}$$

Finally, the virtual force generated from the visual information in the image plane can be described as

$$\begin{aligned} F_x^{ref} &= M\ddot{p}_x^{ref} \\ &= M(K_{\text{pv}} p_x^{ref} + K_{\text{vv}} \dot{p}_x^{ref}). \end{aligned} \tag{3.9}$$

If (3.1) is considered, the resulting movement for the manipulator's reference x_{img}^{ref} can be written as

$$\begin{aligned} x_{img}^{ref} &= S_x(p_x^{ref}) \\ &= S_x(p_x^{res} - p_x^{initial}). \end{aligned} \tag{3.10}$$

Hereafter, it also affects the calculation of the virtual force generated from the visual information, F_x^{ref}. Therefore, the converted value of virtual force F_{img}^{ref} can be further elaborated as

$$\begin{aligned} F_{img}^{ref} &= S_x(F_x^{ref}) \\ &= S_x(M\ddot{p}_x^{ref}) \\ &= M\left\{K_{\mathrm{pv}}S_x(p_x^{ref}) + K_{\mathrm{vv}}S_x(\dot{p}_x^{ref})\right\} \\ &= M(K_{\mathrm{pv}}x_{img}^{ref} + K_{\mathrm{vv}}\dot{x}_{img}^{ref}). \end{aligned} \tag{3.11}$$

3.4 Integration of Force-Based Compliance Control Utilizing Visual Information with Haptic Bilateral Control System

As described in the preceding section, a virtual force can be generated from information gathered from the vision system. The integration of a force-based compliance controller utilizing visual information with the haptic system can support a task involving careful and precise contact. The integration of these control methods, including the scaling and magnification factor of a static camera (eye-to-hand approach), is a novelty of this study.

For the respective changes in a specific object's location or position captured by the vision sensor, the force-based compliance controller will generate equivalent dedicated forces to trigger the whole system to take action. A generated force may produce changes in the computed force of the control system for both the master and slave manipulators, along with changes in its position feedback. To realize the integration with bilateral contact motion, the average value of the master and slave motor's position x_{bil}^{ave} will be considered as a feedback for the force-based controller, where

$$x_{bil}^{ave} = \frac{1}{2}(x_{\mathrm{m}}^{res} + x_{\mathrm{s}}^{res}). \tag{3.12}$$

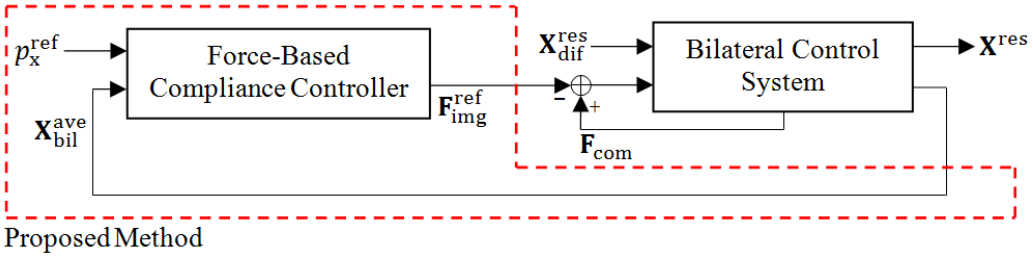

Figure 3.7: Integration between force-based compliance controller and bilateral control system

Thus, the summation result of the image acceleration $\ddot{x}_{img}^{ref}$ of the force-based compliance controller can be written as

$$\ddot{x}_{img}^{ref} = K_{\mathrm{pv}}(x_{img}^{ref} - x_{bil}^{ave}) + K_{\mathrm{vv}}(\dot{x}_{img}^{ref} - \dot{x}_{bil}^{ave}). \tag{3.13}$$

To maintain the stability of the control strategy, the produced virtual force will be treated as a command value in the force common mode of the bilateral control system. It will serve as a force reference for the master and slave manipulator. Hence, from (3.11), the total computed force F_{com} of the system can be described as

$$\begin{aligned} F_{com} &= F_m + F_s - F_{img}^{ref} \\ &= 0. \end{aligned} \tag{3.14}$$

Figure 3.6 shows the integration of the force-based compliance controller with the bilateral control system. Further, it is demonstrated that this integration will depend on two conditions: 1) the output of the force-based controller (F_{img}^{ref}) will be used as an input to the bilateral system and 2) the output of the bilateral system (x_{bil}^{ave}) will be used as an input to the force-based compliance controller. Thus, the system will be the same as the conventional bilateral control if these two conditions are excluded. The complete block diagram of this integration system with the implementation of low pass filter (LPF) are depicted in Figure 3.8 and Figure 3.9.

3.4.1 Parameter Setting

In this study, all of the control feedback are developed based on the second-order system. The parameter setting for the control system should satifying the critical damping effect on the transfer function output.

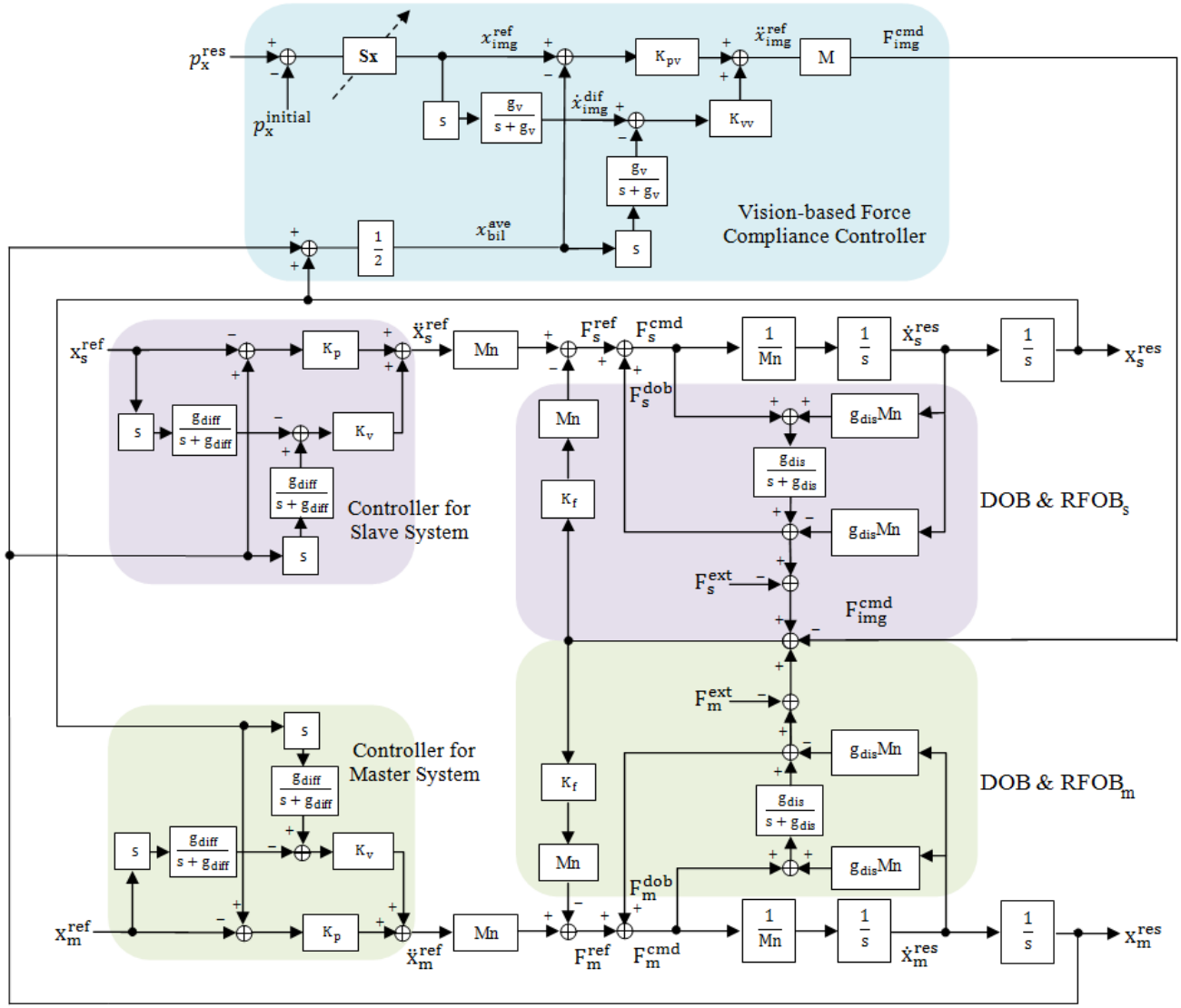

Figure 3.8: Overall block diagram of force-based compliance control utilizing visual information with haptic bilateral control system

The standard second order form of the close-loop transfer function can be expressed as

$$2^{nd}order form \quad = \quad \frac{{\omega_n}^2}{s^2 + 2\zeta\omega_n s + {\omega_n}^2}. \tag{3.15}$$

Now, to achieve the critical damping effect, the damping ratio ζ should be set as 1.0. Then, the second order transfer function for the proportional derivative (PD) control system can be described as

$$\text{PD control} \quad = \quad \frac{K_\text{p}}{s^2 + K_\text{v}s + K_\text{p}}. \tag{3.16}$$

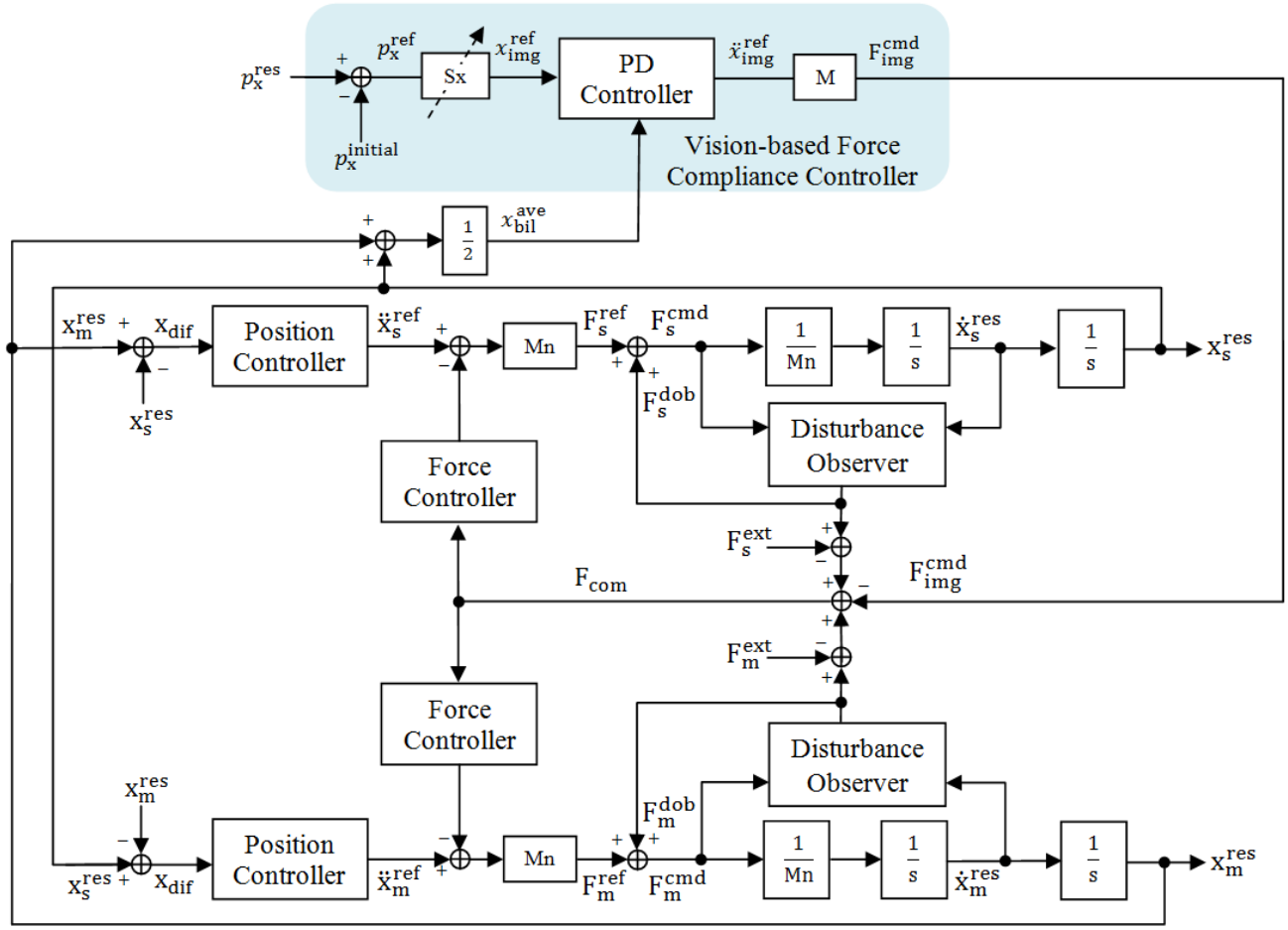

Figure 3.9: Simplified block diagram of the proposed system

Thus, it causes the calculation of natural angular frequency ω_n as

$$\omega_n \quad = \quad \sqrt{K_\mathrm{p}} = \frac{1}{2} K_\mathrm{v} \tag{3.17}$$

where K_p is the position coefficient and K_v is the velocity coefficient of the manipulator system.

As to achieve a good position response between the master and slave manipulator system, the ω_n for the manipulator is set at 100 rad/s. Hence, it causes the position gain K_p and velocity gain K_v value are calculated as 10000 and 200, respectively. As described in Section 2.3, the value of cut-off frequency g for the implemented low pass filter (LPF) also can be set as 600 rad/s.

The aim of this research is want to perform the soft navigation of visual servoing system. Thus, it will resulted the generation of low stiffness between the generated force by the compliance controller and the response force by the bilateral manipulators. As to achieve these condition, the compliance controller's ω_n value should be set lower than the setting value for

the manipulators. Then, throughout the study, the natural angular frequency ω_n value is set as 50 rad/s, that generates the K_{pv} and K_{vv} values as 2500 and 100, respectively. However, the cut-off frequency value of LPF for vision is decided base on the performance of the vision sensor (camera) which will be elaborated in detail in next section. In addition, the virtual mass of the object M_i value for the compliance controller is set as 1.0 kg, to represent the whole considered detected object marker in the vision system.

3.5 Simulation of the Control Method

This section will shows the theoretical analysis of the proposed vision-based force compliance controller that performs by the simulation. The analysis will discusses the control performance of the system which based on certain criterions; video frame sampling period, actuator inertia and controller gain.

3.5.1 Simulation setup

The control performance of the proposed compliance controller with the bilateral master–slave system is simulated by using the Cygwin Terminal of C programming language architecture. It is conducted using the Windows7 based personal computer (PC) with the Intel Core i7-2600 3.40GHz processor and 4GB memory. The analysis will be focused on the performance of the vision-based force compliance controller with the 1 degree-of-freedom bilateral actuator (master and slave) system. The simulation time of all the control performance analysis is fixed at only 10 seconds with the Step input command. The Step input command is represents the sudden transformation of the detected object as much as 1 mm at 1 seconds of simulation times.

3.5.2 Control performance based on the video frame sampling speed

In general, the tracking performance of the control method will be affected by the equipment or hardware limitation. Since the proposed compliance controller is based on the visual information, thus the performance of the camera that used to provide the image information should be studied.

The video frame sampling period of the camera is one of the factor that can influence the performance of the system. As to get the good response for the bilateral system, the designed programming should be conducted with high speed of sampling time. In this case, it has been

Table 3.1: The different of parameter setting of each cases

Case	Video frame rate	Cutoff frequency
Case 1	0.10×10^{-3} s	1.00 rad/s
Case 2	0.10×10^{-3} s	600 rad/s
Case 3	33.0×10^{-3} s	1.00 rad/s
Case 4	33.0×10^{-3} s	600 rad/s

set at 0.10 ms to achieve stability and high disturbance rejection. Anyway, recently there are no camera that can provide the video frame rate such that speed. Thus, the comparison between the control performance which based on the different video frame sampling speed will be analyzed.

Further, the different speed of the frame rate also will provides different frequency generation. Hence, the performance of the control method will be influenced by the designed value of controller's cutoff frequency. Thus, the analysis of different cutoff frequency value will be also be considered.

The resolution of images also influence the performance of the system. High resolution images provide much more detailed information regarding objects in view. However, processing a high resolution images would require higher processing speed and more memory [164]. Thus, longer processing time is required as the resolution of the image gets higher. Yet, it will decreases the number of sampling speed and affected the control performance of the system.

The simulation for the control system is conducted in four different cases. The differents of each cases are described as in Table 3.1. Case 1 and Case 2 use the same sampling speed as the simulation sampling time (0.10×10^{-3}s). Moreover, Case 3 and Case 4 use the different sampling speed as to represent the frame rate of the conventionally available USB web camera (30 fps). All cases uses the same parameters of $K_p = 10000$, $K_v = 200$, $K_{pv} = 2500$, $K_{vv}= 100$, $M_n = 0.5$ kg and $M_i = 1.0$ kg.

Simulation result

Figure 3.10 to Figure 3.13 shows the results of the simulation that contains force, position and position error for Case 1, Case 2, Case 3 and Case 4 respectively. Those results can be analyzed in two categories; force response and position response.

• Force Response

From the graphs of Case 1 and Case 2, eventhough the system uses the same sampling rate, chosen the different cutoff frequency of the compliance controller will affected the generation of force response. It can be seen as in the Figure 3.10((a) and (b)) and Figure 3.11((a) and (b)) where the cutoff frequency value = 1.00 rad/s is applied to Case 1, and 600 rad/s is applied to Case 2. For Case 1, the bilateral manipulator generates about 1.3N impulse force during the beginning cycle of the implied Step input. It was to comply with the generation of virtual force by the vision-based compliance controller that generates 2.6N of impulse force. However, for Case 2, the master and slave manipulators generates about 31N and compliance controller generates about 62N of impulse force.

On the other hand, for Case 3 and Case 4, when the sampling rate of the image from the camera is getting lower (33 ms), the manipulators that ran with higher sampling speed, will provides different performance as being compare to the results in Case 1 and 2. It can be referred to the graphs as depicted in Figure 3.12((a) and (b)) and Figure 3.13((a) and (b)). For Case 3, when the cutoff frequency is set at 1.00 rad/s, the bilateral manipulator generates about 5N of impulse force with the settling time of 1.131s. While the compliance controller generates about 10N impulse force. Besides that, in Case 4, when the cutoff frequency is set at 600 rad/s, both master–slave manipulators generates about 65N impulse force as to respond to the generated 130N of virtual force by the compliance controller. Anyway, the settling time for this case is getting longer as long as 3.892s. The system took longer time to stay in steady state condition.

• Position Response

The position response for Case 1, 2, 3 and 4 can be seen in Figure 3.10(c), 3.11(c), 3.12(c) and 3.13(c), respectively. While its position error can be obtained in Figure 3.10(d), 3.11(d), 3.12(d) and 3.13(d), respectively. The error is calculated as

$$x_{error} = \frac{1}{2}(x_m^{res} + x_s^{res}) - x_{img}^{ref}. \tag{3.18}$$

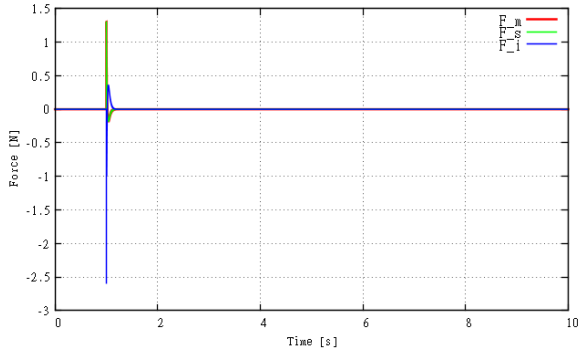

(a) Force response

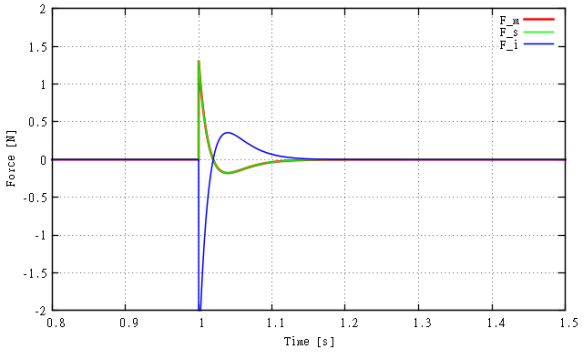

(b) Magnification of force response

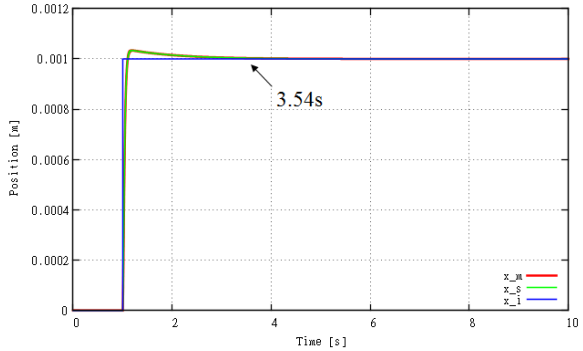

(c) Position response

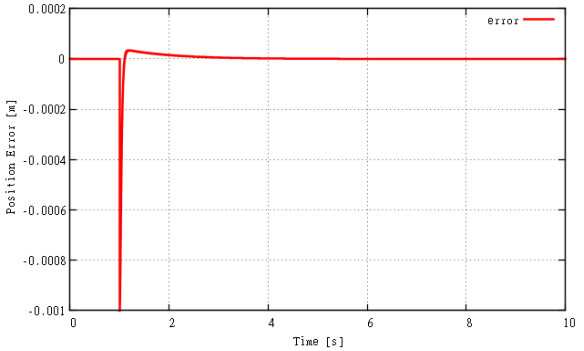

(d) Position error response

Figure 3.10: Force, position, and position error responses of simulation on Case 1

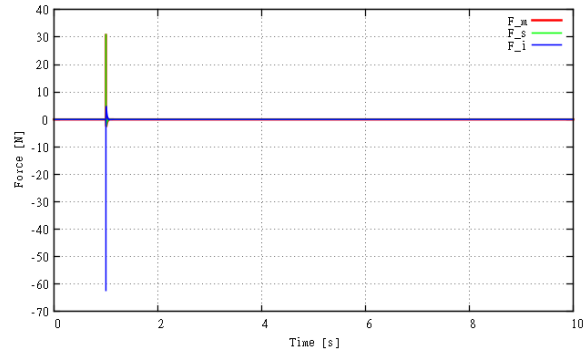

(a) Force response

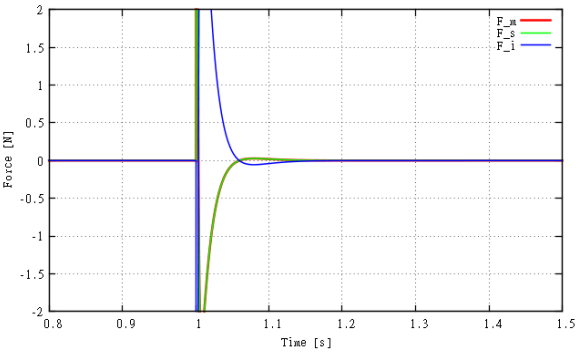

(b) Magnification of force response

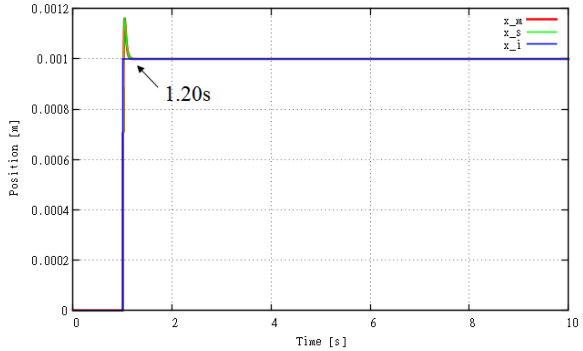

(c) Position response

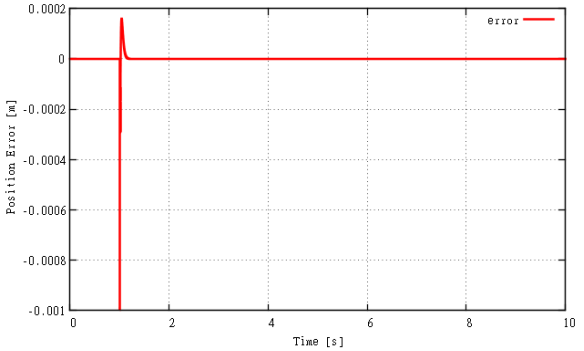

(d) Position error response

Figure 3.11: Force, position, and position error responses of simulation on Case 2

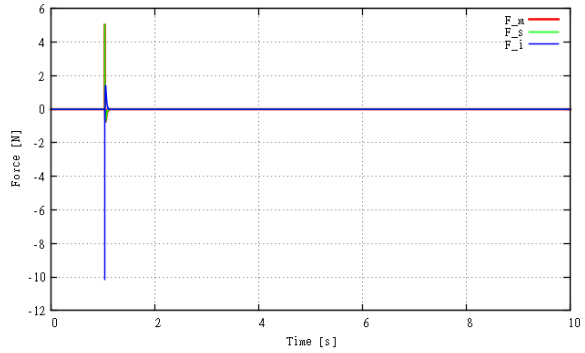

(a) Force response

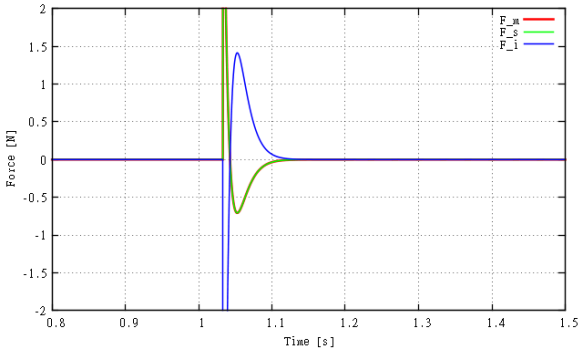

(b) Magnification of force response

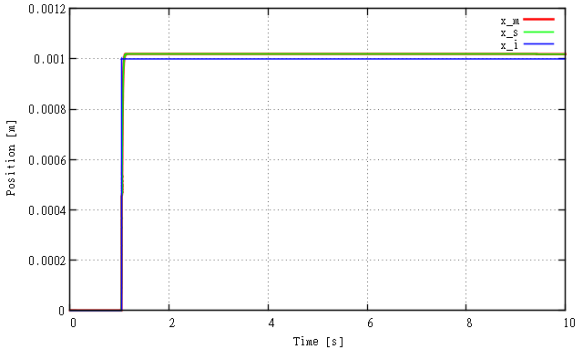

(c) Position response

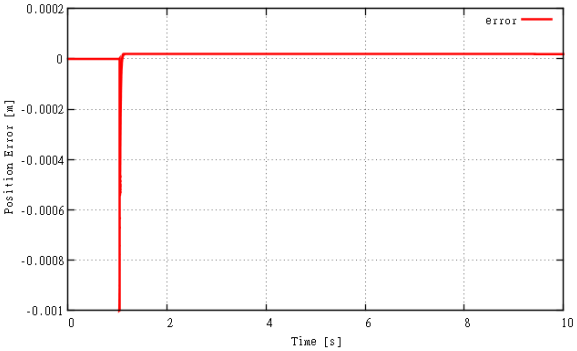

(d) Position error response

Figure 3.12: Force, position, and position error responses of simulation on Case 3

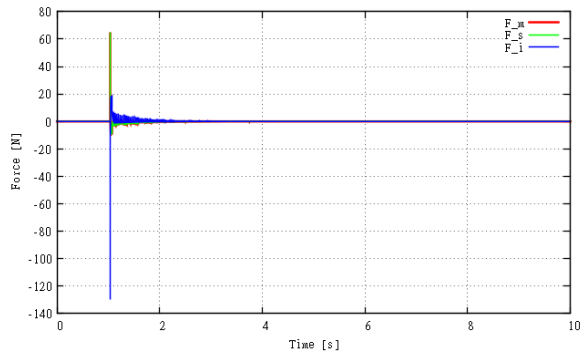

(a) Force response

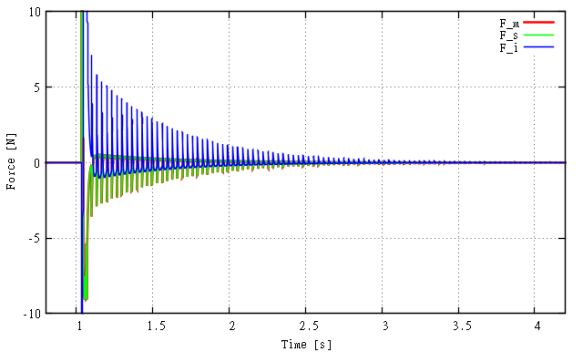

(b) Magnification of force response

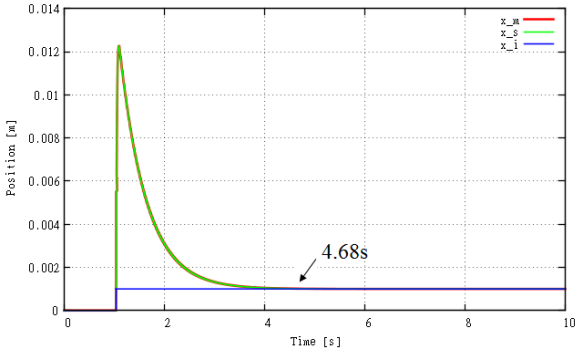

(c) Position response

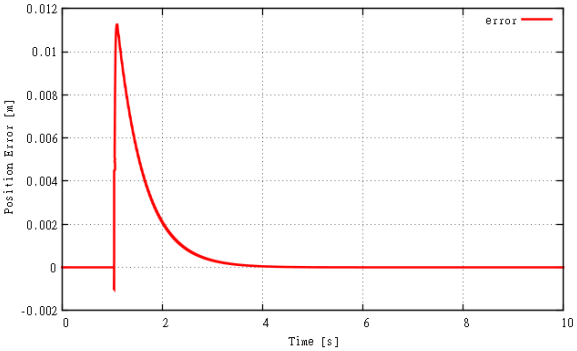

(d) Position error response

Figure 3.13: Force, position, and position error responses of simulation on Case 4

From the results, Case 1 and Case 3 shows only a small position error of about 20 μm. However, Case 2 generates about 160 μm of position error, while Case 4 generates about 11.3 mm of position error. It seems that the error are getting bigger if the cutoff frequency of the compliance controller is set at a high value.

3.5.3 Control performance based on the actuator mass

The performance of the control method can be observed by considering the mass of the actuator. The objective of this simulation is want to analyze the effect of generated force by the different actuator's mass value.

The simulation is conducted in two situation. The first situation, the master and slave manipulator's nominal mass are set at 0.5 kg each. While in the second situation, the master and slave manipulator's nominal mass are set at 10 kg each. Both situations use the same parameter of K_p = 10000, K_v = 200, K_{pv} = 2500, K_{vv}= 100, M_i = 1 kg and the system's sampling time = 0.1 ms. The effect of the response force by the different inertia of the actuator will be studied.

Simulation result

The simulation result for the control performance of the system which based on the actuator mass can be seen as depicted in Figure 3.14 and Figure 3.15. The results are categorized into the force and position response respectively.

• Force Response

The force response for this simulation is same as plotted in Figure 3.10. The master manipulator generates the same 1.3N of impulse force as the slave manipulator. While the compliance controller generates 2.6N of impulse force as to response to the Step input command.

However, when the inertia of the actuators are getting bigger, the generated impulse force has hiking up to about 26N each. Although the compliance controller generates the same 2.6N of impulse force. This result can be found as shown in Figure 3.15(a) and (b).

• Position Response

Even though the system's force response gave different value for the different inertia point, the system still can provides the small value of position error. From the graphs plotted in Figure 3.14(c) and 3.15(c), both system shows the same position response result with the position error

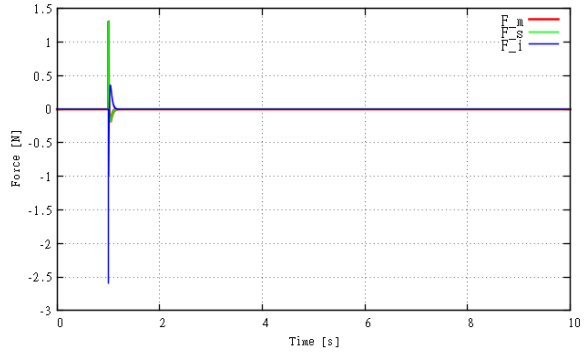

(a) Force response

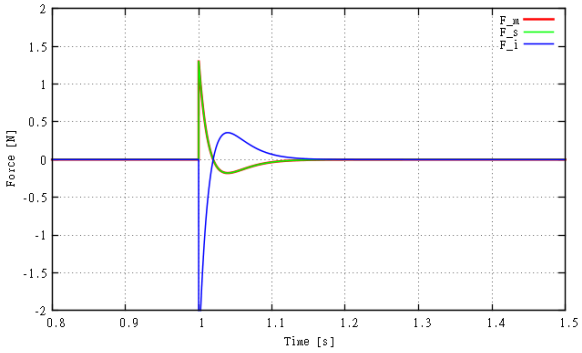

(b) Magnification of force response

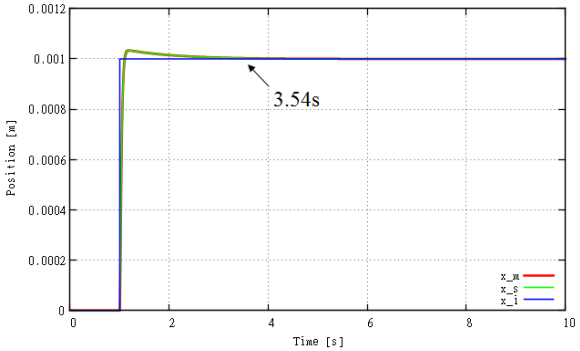

(c) Position response

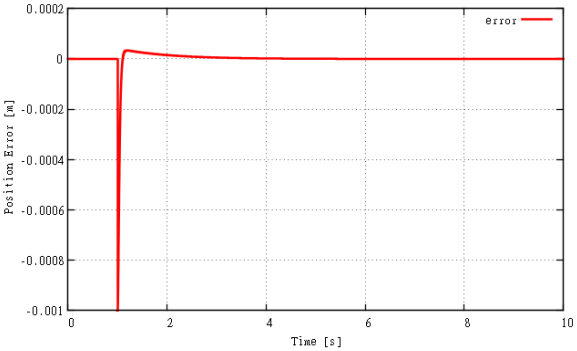

(d) Position error response

Figure 3.14: Force, position, and position error responses of simulation with $M_n = 0.50$kg

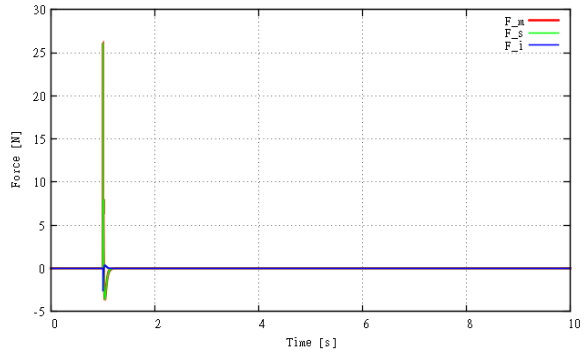

(a) Force response

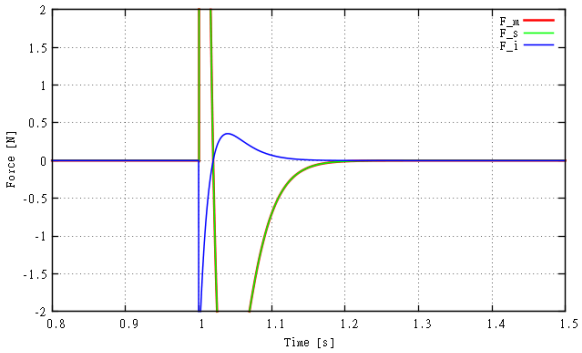

(b) Magnification of force response

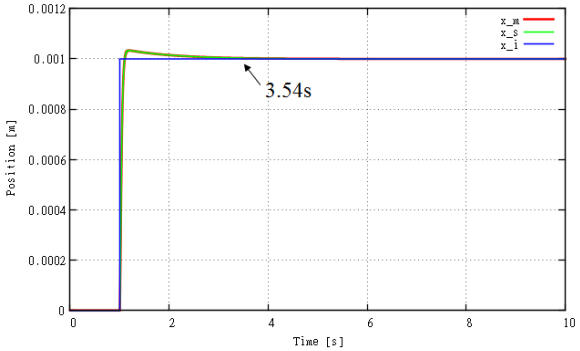

(c) Position response

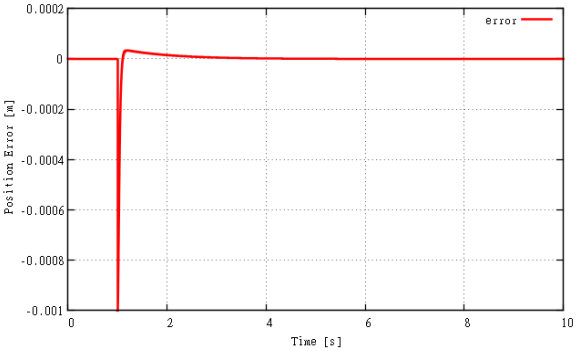

(d) Position error response

Figure 3.15: Force, position, and position error responses of simulation with $M_n = 10.0$kg

value as small as 20 μm. Its settling time were achieved at 3.54s of simulation time.

3.5.4 Control performance based on the controller gain

The control performance of the proposed system also can be measured by analysing the parameter setting of compliance controller's gain value. It can be noticed that, all the previous simulation which in subsection 3.5.2 and subsection 3.5.3, uses the compliance controller position gain K_{pv} and velocity gain K_{vv} as 2500 and 100, respectively. It shows that the controller's natural angular frequency has been set at ω_n = 50 rad/s, half of the value for the bilateral manipulator, ω_n = 100 rad/s. This is to realize the soft navigation and low stiffness control system.

Thus, this simulation is conducted to find any changes in the performance response of the system. The vision-based force compliance controller's natural angular frequency is increased to ω_n = 200 rad/s. Hence, it will resulted the changes in controller's gain value, to be as K_{pv} = 40000 and K_{vv} = 400. The other simulation parameters are set as K_p = 10000, K_v = 200, M_n = 0.5 kg, M_i = 1 kg and the system's sampling time = 0.1 ms.

Simulation result

Figure 3.16 shows a simulation results for the control performance which based on the different controller's gain value. The result can be discussed in two categories; force response and position response.

• Force Response

As the ω_n value for the compliance controller be increased to 200 rad/s, the controller had generated the 40N of impulse force which then resulted the generation of 20N force for each master and slave manipulators. On the other hand, even though the generation of impulse force had increased, but the system's force response achieved the shortest settling time which converged at 1.055s. It can be referred to the graphs in Figure 3.16(a) and (b), respectively.

• Position Response

Based on the position response graph as depicted in Figure 3.16(c), the system can response very well to the respective position command. It only produces less than 10 μm of position error, which is the smallest error as compared to the other previous simulations. The response of this position error can be seen as plotted in Figure 3.16(d).

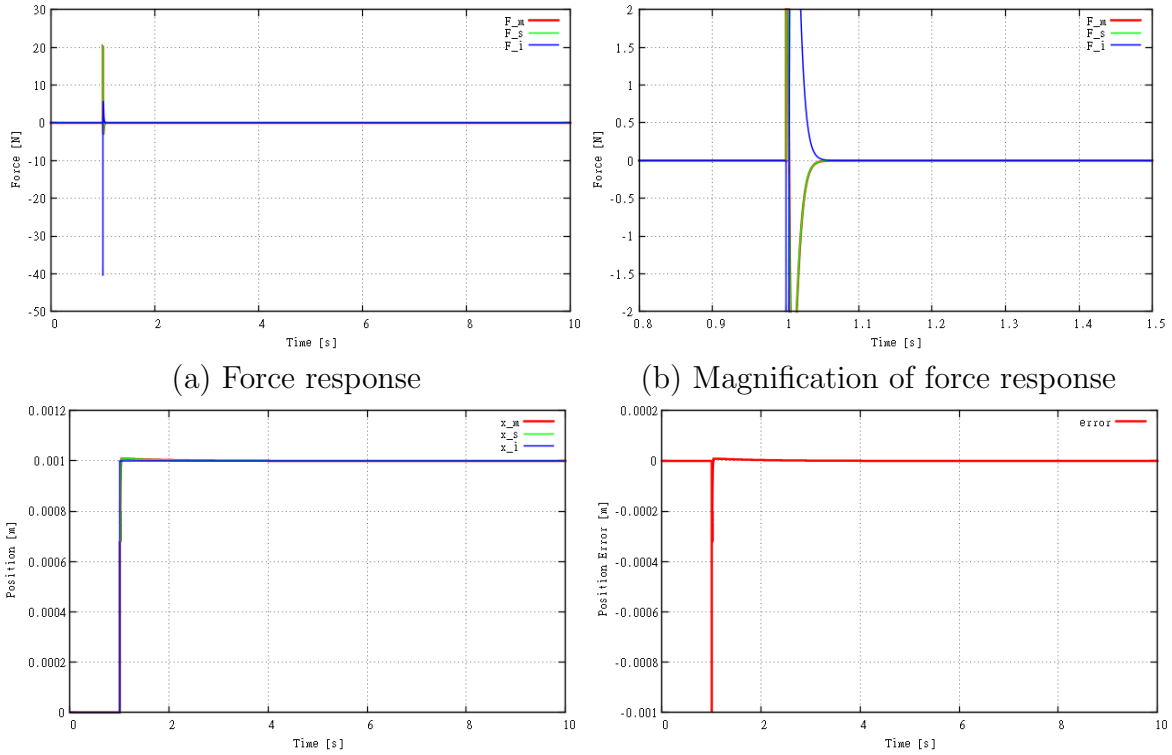

(a) Force response

(b) Magnification of force response

(c) Position response

(d) Position error response

Figure 3.16: Force, position, and position error responses of simulation with $\omega_n = 200$rad/s

3.5.5 Discussion

In general, the performance of the proposed control method can be summarized as below

- Video frame sampling speed

  The faster video frame sampling speed, will produce the better control performance. It also can reduce the error and noise in the system.

- Cutoff frequency

  The lower the cutoff frequency value of the compliance controller, the better control performance can be achieved. The lower value will make the system force response reach shortest settling time in steady state motion.

- Actuator mass

  As the mass of the actuator become large, its inertia also being increase synchronously. Thus, the initial force to move the actuator increasingly hiking.

- Controller gain

  The bigger compliance controller's gain value, the better performance can be achieved. As the gain value be increased, the system can converge to the response command quickly. Yet, it resulted the small value in position error. However, it hard for the system to perform the soft navigation task.

3.6 Summary

In this chapter, the vision-based system which including its four step image-processing techniques has been described. Then, there also the full explanation about the advent of the vision-based force compliance control method and its concept. Next, the integration method between the virtual force compliance controller and the bilateral control system has been introduced. Finally, in the last section of this chapter, the simulation of the proposed control method has been conducted and its control performance result has been analyzed.

Chapter 4

Confirmation of the Scaling Effect

In the previous chapter, I have explained the basic concept of the proposed vision-based force compliance control method. In the meantime, the integration method between the proposed technique with the bilateral control system also has been described.

In this chapter, I will clarify about the different of generated force produces by the scaling effect. This confirmation is crucial in order to ensure that the force generates by the compliance controller is the same even if the object image is enlarged or undergone the magnification process. Different scale of viewed object size will result in different generated force by the controller. Thus, this effect should be encountered to get the same.

At first, the chapter will begin with the explanation of what is scaling effect and how it can be occured. Next, I will explain about how to encounter the effect by the implementation of one variable in the compliance controller. Further, the experimental setup and its result will be elaborate to study the effect in the discussed topic.

4.1 Introduction

The advent of real-time vision navigation in the haptic environment has led to the development of the latest technologies. In this study, the authors considered how the object can be tracked and a kind of image processing approach needs to be used. It can be referred to the others finding. For instance, Kapoor *et al*. proposed a new potential function-based modelling approach for real-time object tracking by using single camera. The concept of attractor and repeller inside a potential field had been introduced to classify different direction of motion in image plane [165]. Moreover, Kim *et al*. had developed the tracking method that uses real-time template matching of image processing technique. They had developed a haptic interaction

method for a deformable object manipulation system considering image processing and physical based modelling techniques without the use of force sensor [2]. Whilst, Tamadazte *et al.* had proposed a new control law based on the use of pure image signal (pixel intensity) called as photometric-based approach [156].

The establishment of the visual-haptic integration especially in the bilateral control system has triggered the compliance's performance study as done by Kuschel *et al.*. He and his team proposed the combination of nonredundant position and force information to estimate compliance by a weighted summation process [161]. Furthermore, Muis *et al.* introduced the technique of dual compliance controller that uses a trajectory estimation from produced force for automated pushing operation [159]. Nakajima *et al.* also contributed to this bilateral control study that used the environmental information of position and posture of target object obtained by the camera [158]. Motoi *et al.* also proposed the force-based variable compliance control method for bilateral system with different degrees of freedom (DOF) [166].

The authors also consider about the control technique. Previously, Taghirad *et al.* has proposed a 3-D pose estimation of rigid object by only one camera by using Kalman observer and extended Kalman filter (EKF) [155]. In the other hand, a visual servoing method based on disturbance observer has been introduced by Lee *et al.* to improve visual servoing performance [167]. The authors consider to apply this research to control the medical robotic manipulators. For instance, in case of beating heart surgery application, the investigation of the control strategies for an active stabilizer dedicated to beating heart coronary artery bypass grafting has been done in a high speed visual servoing medical robot [168]. Navkar *et al.* also provides a study of both real-time visualization and force-feedback based guidance for maneuvering tool safely inside the dynamic environment of a heart left ventricle [169]. All the related study has been considered in line with the development of this research.

Hereinafter, this chapter explains a new bilateral control method with vision-based guidance and elaborates its scaling effect. The visual force compliance control is adopted to the navigation. The experiments demonstrate the validity and different scaling performance of the proposed method.

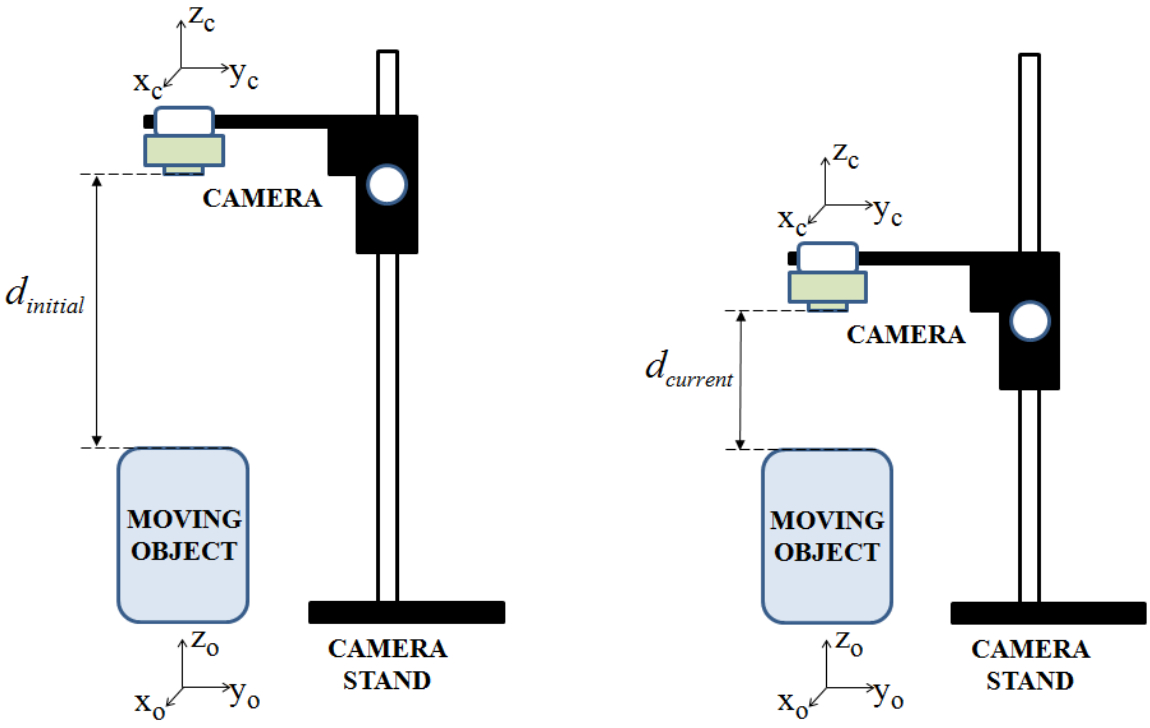

(a) Initial camera–object distance setting (b) New camera–object distance setting

Figure 4.1: The different camera height that create different camera–object distances

4.2 Scaling Effect

The navigation process for the moving object uses a camera that is located above the object (facing down). As described in the previous chapter, the camera is mounted on an adjustable camera stand that allows it to be raised to different heights. This is also known as the camera distance magnification process. The height of the camera is justified as the distance d between the camera and the object surface. Figure 4.1 shows the different height positions of the camera that create the different distance between camera and object. As in Figure 4.1(a), initially the camera is set at a height and the distance between camera and object is measured as $d_{initial}$. When the object undergone the magnification process, the camera is set to a lower height that the camera–object distance is measured as $d_{current}$, as depicted in Figure 4.1(b).

The object's size may appear to be bigger if the camera is lowered down. This makes it look like another object mass is being used for the navigation process. Thus, as a countermeasure to this effect, a new generalization of the distance's magnification function α needs to be considered

and can be stated as

$$\alpha = \frac{d_{initial}}{d_{current}} \tag{4.1}$$

where $d_{initial}$ is the initial distance between the camera and the object, and $d_{current}$ is the current distance between the camera and the object after being magnified. The values of scaling factor S_x and the distance magnification function α are changed in a relative way by this magnification effect.

Now, by considering the distance's magnification function, the virtual force generated from the visual information for the manipulator's force reference F_{img}^{cmd} can be revised as follows:

$$\begin{aligned} F_{img}^{cmd} &= \alpha F_{img}^{ref} \\ &= \alpha M(K_{\mathrm{pv}} x_{img}^{ref} + K_{\mathrm{vv}} \dot{x}_{img}^{ref}). \end{aligned} \tag{4.2}$$

Hence, from (4.2), the total computed force F_{com} of the system can be described as

$$\begin{aligned} F_{com} &= F_m + F_s - F_{img}^{cmd} \\ &= 0. \end{aligned} \tag{4.3}$$

It is found that if the camera is close to the object, or if the camera zooms in, the virtual force based on visual information can be magnified. The complete flow of the block diagram of this integration system is depicted in Figure 4.2.

4.3 Experiments

In this section, the experimental setup and dedicated steps are elaborated to confirm the validity of the proposed method. The performance of this proposed method will be discussed in the next section.

4.3.1 Experimental Setup

In this experiment, two X-Y tables are used as the master and slave manipulator systems. Each manipulator can be moved in the horizontal (x-plane) and vertical (y-plane) directions. A horizontal movement is used to give a response for the position and force feedback from the generated virtual force utilizing visual information. A vertical movement is used for the purpose of object manipulation using the stick attached to the manipulator to feel its stiffness.

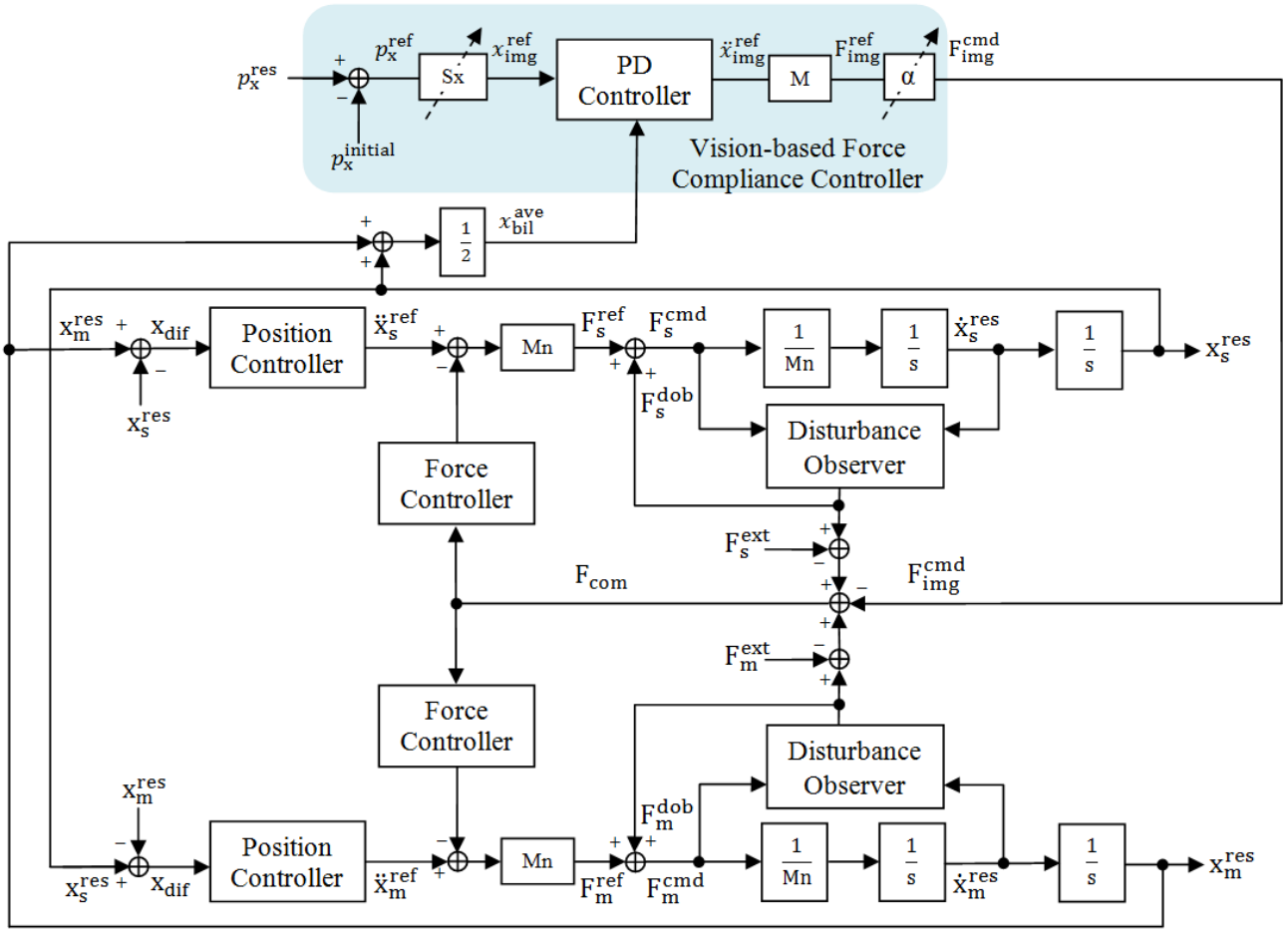

Figure 4.2: Overall block diagram of the system with magnification scaling consideration.

The vision sensor used in this experiment is a standard web camera with a maximum resolution of 1280 × 1024 pixels and a frame rate of 30 fps. This camera does not have a zoom function. The magnification process needs to be done manually. It is mounted on a camera stand with an adjustable height. The performance of the virtual force generated by this intentional camera visualization will be evaluated and kept for reference and further enhancement. Figure 4.3 shows the experimental setup for this experiment.

The camera needs to track a moving object. In this study, a rectangular object is used (8 cm length × 4 cm width × 6 cm height). The object is made of foam sponge and is white in color. The object marker is attached to its surface. It is mounted on one linear motor so that a designed standard repeated movement can be utilized. In addition, the various positions of 2-cm red, green, and yellow lines are printed out and placed in the background of the object. This is to show the effectiveness of the image-processing technique. The positions of the object

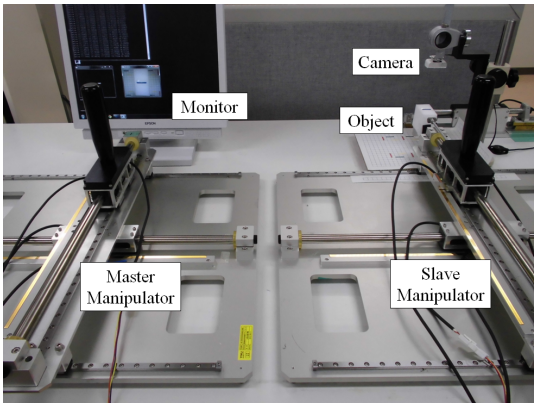

Figure 4.3: Experimental setup of force-based compliance control utilizing visual information with haptic bilateral system

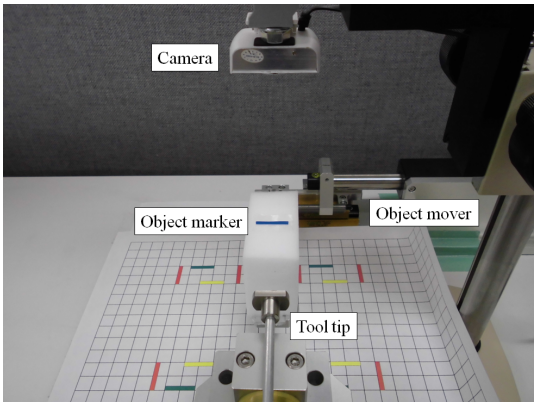

Figure 4.4: Positioning of object for navigation purposes

and its mover are shown in Figure 4.4.

The image-processing program was developed using the OpenCV library under the Microsoft Visual Studio software. It is driven by the Windows 7 operating system with an Intel Core 2 Duo microprocessor chip. The developed program will process the captured image and send the resulting coordinate to the bilateral controller with a sampling time of 33 ms. At the same time, the bilateral controller is driven by a real time Linux operating system with the same type of microprocessor through a PCI motor driver connection. The sampling time for the bilateral controller is set to 0.1 ms. These two computers communicate through a standard UTP network cable.

4.3.2 Experimental Measures

In order to show the validity of the proposed system, the experiments are conducted based on several steps. Specifically, there are two experiments with the same repeated task but different camera magnifying conditions. The steps of the task are described below.

• Step 1: The object is moved 2.00 cm to the left and back to the original position. Continuously, it is moved 2.00 cm to the right and back again to the original position. The linear motor that acts as the object's mover is programmed to perform these movements with a sinus command characteristic. This step is conducted during the period of 10 to 29 s of the experimental time. At this point, an attempt is made to show how the bilateral control of the master and slave system responds to the generated virtual force.

• Step 2: A 20.0-N force is exerted at the master manipulator side. This force is exerted horizontally in the left direction of the X-Y table. This step is conducted during the period of 30 to 39 s of the experimental time. Here, the responses of the slave manipulator and force-based compliance controller utilizing visual information are analyzed.

• Step 3: A 2.50-kg cylindrical block is placed at the slave manipulator side (on the left), and it acts like an obstruction object. Then, the same 20.0-N force is exerted at the master manipulator. This step is conducted during the period of 40 to 49 s of the experimental time. This is done to examine the extent of the reaction of the bilateral system and force-based compliance system.

• Step 4: This step is conducted for object manipulation purposes. The master manipulator approaches and touches the object. It is moved vertically. The stiffness characteristic of the object that is manipulated by the tooltip at the slave manipulator can be felt by the operator. This step is conducted during the period of 50 to 59 s of the experimental time.

The steps mentioned above needed to be performed for each experiment. Initially, the experiment was conducted with the distance d, between the camera and the object set at 20.0 cm. Then, for the second experiment, the distance was set at 10.0 cm to utilize the magnification zooming-in function. In order to confirm the validity of the proposed integration method, the

experimental results for two cases are compared: one using the proposed method and the other using the conventional bilateral control without the integration of the force-based compliance controller utilizing visual information. In this case, although there was no integration with the force-based compliance controller, the data from the camera were still recorded to show the movement of the object. Moreover, to reduce the noise generated by the web camera, the filter was designed and applied to the system. The noise should have been greatly reduced. Thus, a small cutoff frequency value was considered. Table 4.1 lists the control parameters used for the bilateral controller and force-based compliance controller for the entire experiment. The damping ratio characteristics for both systems were designed to allow critical damping with the natural angular frequency ω_n equal to 100 rad/s for the bilateral controller and 50.0 rad/s for the visual force controller. The designed values were experimentally tuned to obtain the best performance. These had to meet the requirement of soft navigation with low stiffness manipulation to assist operators. The response data for each manipulator and camera were recorded and saved for the analysis.

4.3.3 Experimental Results and Discussion

The effectiveness of the image-processing techniques can be assessed by referring to the visualization results, as shown in Figure 4.5. Based on that figure, the program successfully detected the blue line marker even though there was a variety of colors in the background. It filtered out all the other image information, which left only one line of white pixels that represented the intentional object marker. It was also successful at locating the centroid point by referring to the detected corners. The size comparison could easily be made between the camera–object distances of 20.0-cm and 10.0-cm. The resulting pixel length of the object marker was longer when the distance was 10.0-cm compared to the 20.0-cm distance, which resulted in a smaller S_x value. The object size was also magnified. The value for the weighting magnification function α in the second experiment can be calculated as follows:

$$\alpha = \frac{20.0cm}{10.0cm} = 2.00. \tag{4.4}$$

After the scaling conversion, the center point coordinate of the object marker was sent to the bilateral controller in real time when the experiment was conducted.

The recorded data for each experiment are plotted in several graphs, as depicted in Figure 4.6 to Figure 4.9. The data are divided into the position, force, and velocity responses for the

Table 4.1: System parameters

Parameters	Description	Values
K_{p}	Position gain of manipulator system	1.00×10^4
K_{pv}	Position gain of vision system	2.50×10^3
K_{v}	Velocity gain of manipulator system	200
K_{vv}	Velocity gain of vision system	100
K_{f}	Force gain of manipulator system	1.00
g_{dis}	Cutoff frequency of DOB	600 rad/s
g_{diff}	Cutoff frequency of LPF	600 rad/s
g_{v}	Cutoff frequency of LPF for vision	1.00 rad/s
M_{n}	Mass of the motor	0.50 kg
M	Virtual mass of the moving object	1.00 kg

horizontal and vertical movements of the haptic manipulators. The performance of the proposed method and its comparison with the conventional method will be explained further.

Position Response

The bilateral system provided a good position tracking response with the proposed method. This can clearly be seen in Figure 4.6((a) and (d)), and Figure 4.8((a) and (d)). At the same time, it also managed to give a good reaction to a synchronous move following the tracking position of the object created by the virtual force. For the horizontal movements of the 20.0-cm camera–object distance, the application of a 20.0-N force to the master manipulator affected the position change on both bilateral systems. There was a displacement of approximately 7 mm, and it could only generate a displacement of approximately 6 mm if there was an obstacle on the slave side. Here, the effectiveness of the compliance controller could be clearly shown when the image had been magnified. When the camera–object distance was set at 10.0-cm, even though the same 20.0-N force was applied, both manipulators could only generate displacements

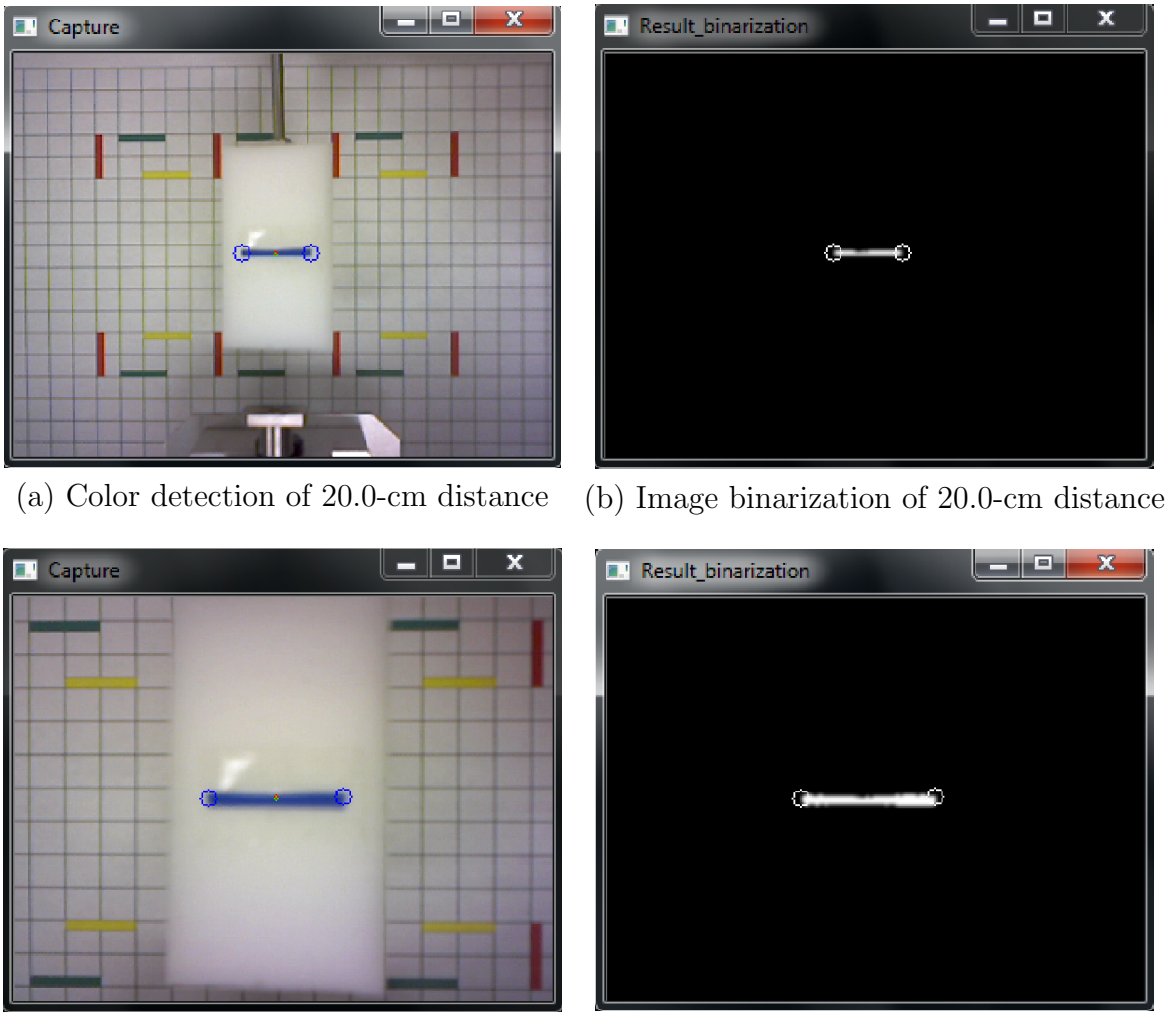

(a) Color detection of 20.0-cm distance (b) Image binarization of 20.0-cm distance

(c) Color detection of 10.0-cm distance (d) Image binarization of 10.0-cm distance

Figure 4.5: Visualization of image-processing techniques for 20.0-cm and 10.0-cm camera–object distances

of approximately 3.5 mm (without an obstacle) and 3 mm (with an obstacle). It seemed to be more difficult to manipulate the bilateral manipulator when magnification was applied (it became more strained).

In contrast, the bilateral system could not track and follow the movements of the object if the conventional method was applied, as shown in Figure 4.7(a) and Figure 4.9(a). Thus, when a 20.0-N force was exerted, the bilateral manipulator was moved but did not have the ability to go back to its original position. Further, the operator had to move it to the original position manually to commence the manipulation task.

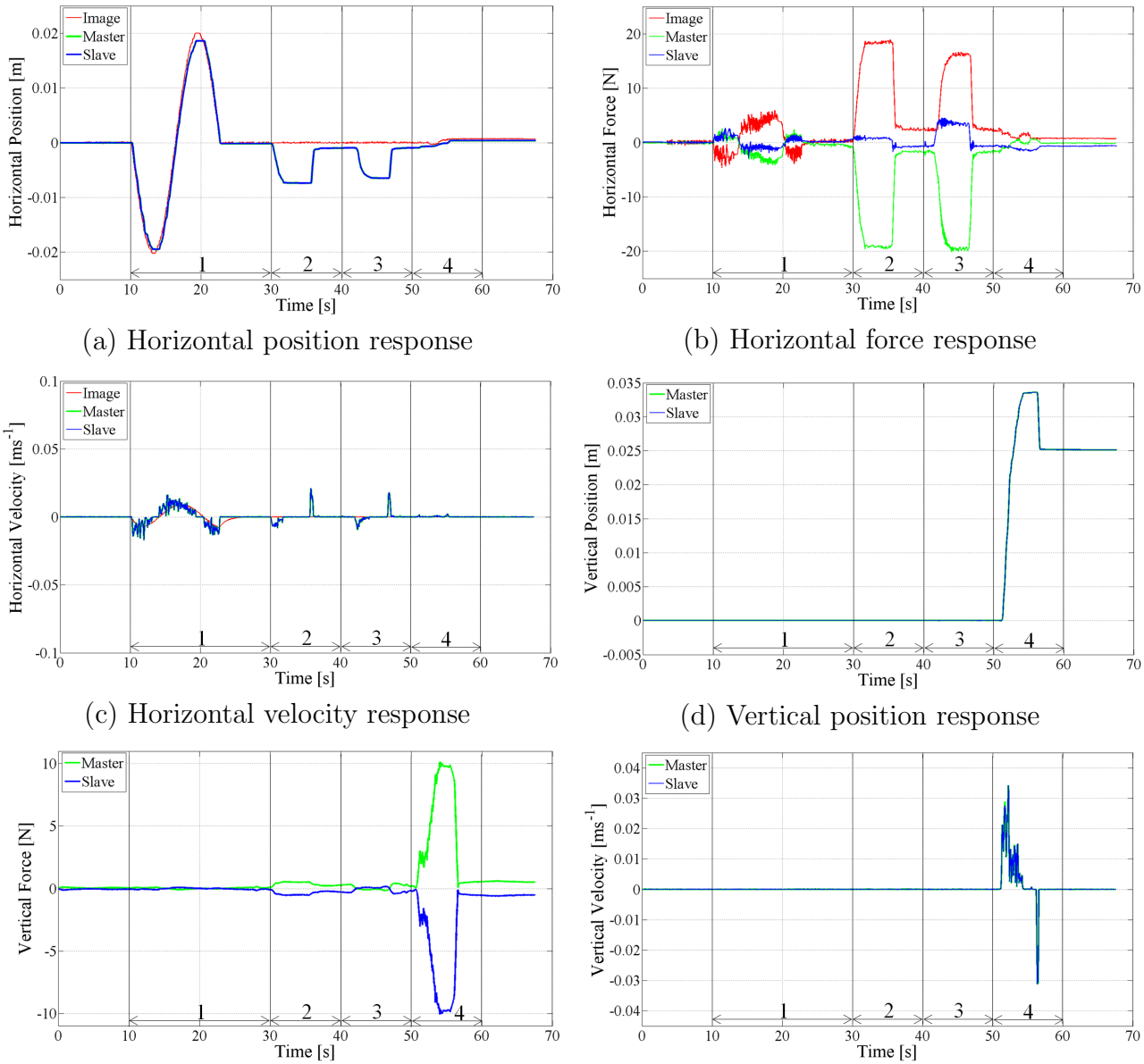

(a) Horizontal position response

(b) Horizontal force response

(c) Horizontal velocity response

(d) Vertical position response

(e) Vertical force response

(f) Vertical velocity response

Figure 4.6: Position, force, and velocity responses of horizontal and vertical manipulator movements for 20.0-cm camera–object distance by proposed method

Force Response

The effects of the force responses of horizontal movements when utilizing the proposed method can be seen in the graphs in Figure 4.6(b) and Figure 4.8(b). These graphs clearly show that a large force was generated by the force-based controller in response to an object movement if it was magnified, compared to the case when it was not. It can also be noticed that the

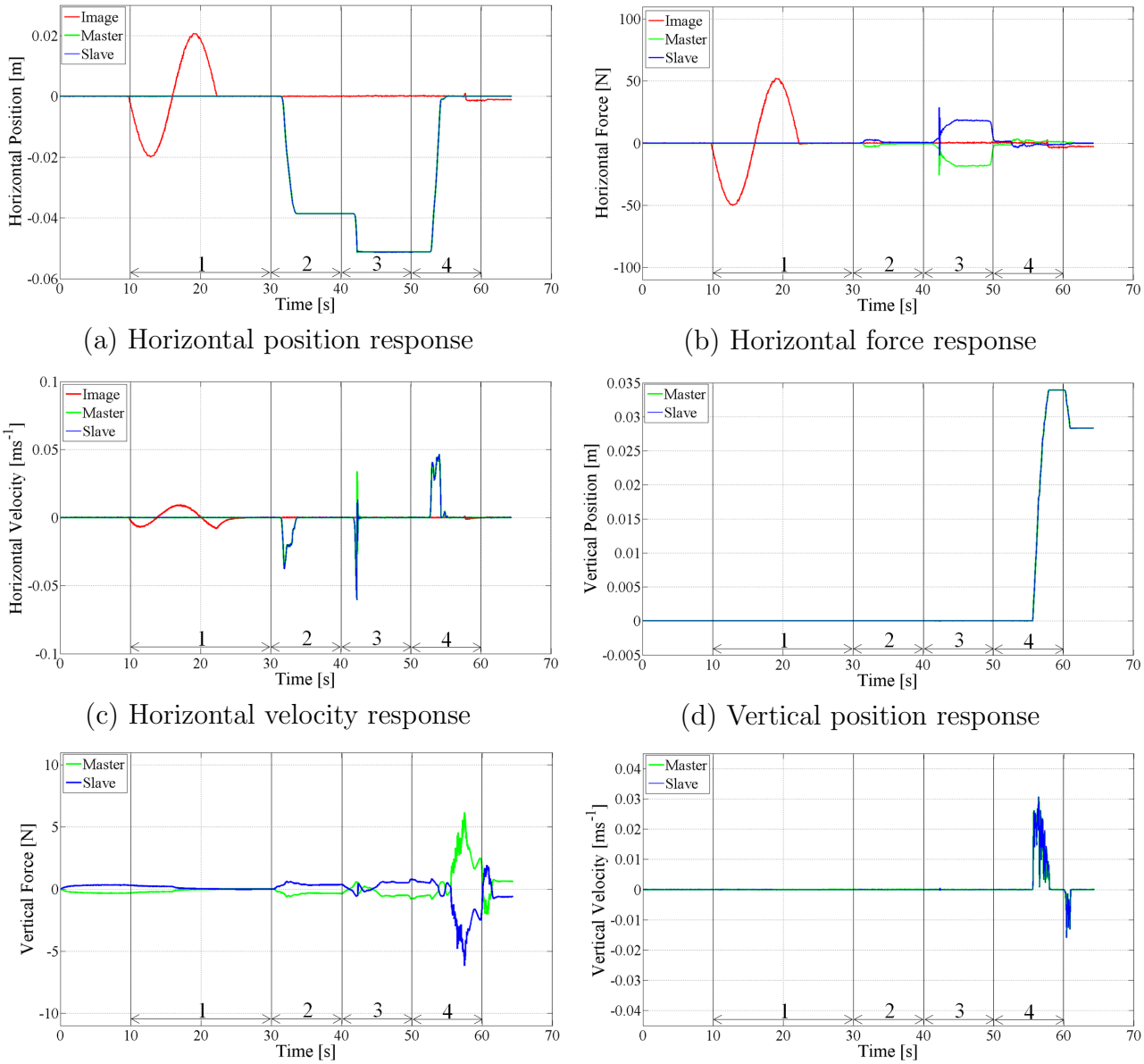

(a) Horizontal position response

(b) Horizontal force response

(c) Horizontal velocity response

(d) Vertical position response

(e) Vertical force response

(f) Vertical velocity response

Figure 4.7: Position, force, and velocity responses of horizontal and vertical manipulator movements for 20.0-cm camera–object distance by conventional method

integration system gave a correct response when the summation of the bilateral force was equal to the generated virtual force, as predicted. In step 3 of the experimental measures, the presence of an obstacle on the slave side caused the generation of a feedback force (f_s). Because of this, an equal virtual force was generated to balance the total computed force responses.

On the other hand, even though the movement of the object generated the force, there were no effects with the conventional method. This can be seen in Figure 4.7(b) and Figure

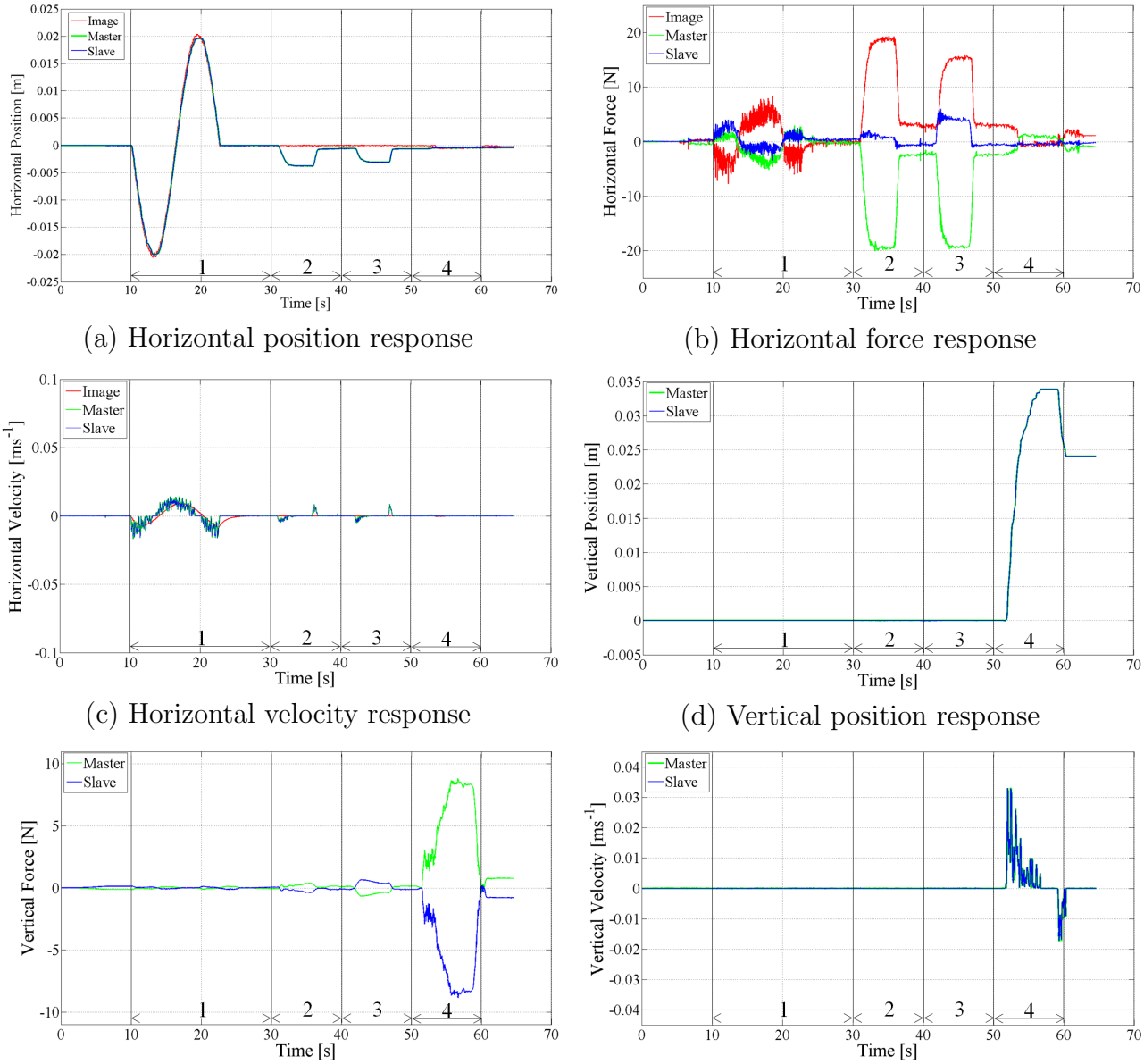

(a) Horizontal position response

(b) Horizontal force response

(c) Horizontal velocity response

(d) Vertical position response

(e) Vertical force response

(f) Vertical velocity response

Figure 4.8: Position, force, and velocity responses of horizontal and vertical manipulator movements for 10.0-cm camera–object distance by proposed method

4.9(b), where neither manipulator was moved during object navigation. In step 2 and step 3, the object was not moved, but was static at the initial position. Thus, no virtual force was produced. Consequently, even though the master and slave manipulators moved, there was no reflection in the virtual force compliance controller. When the 20.0-N force was applied, the resultant forces were the same whether the camera was magnified or not.

Although the experiments performed in this study considered only the horizontal movements

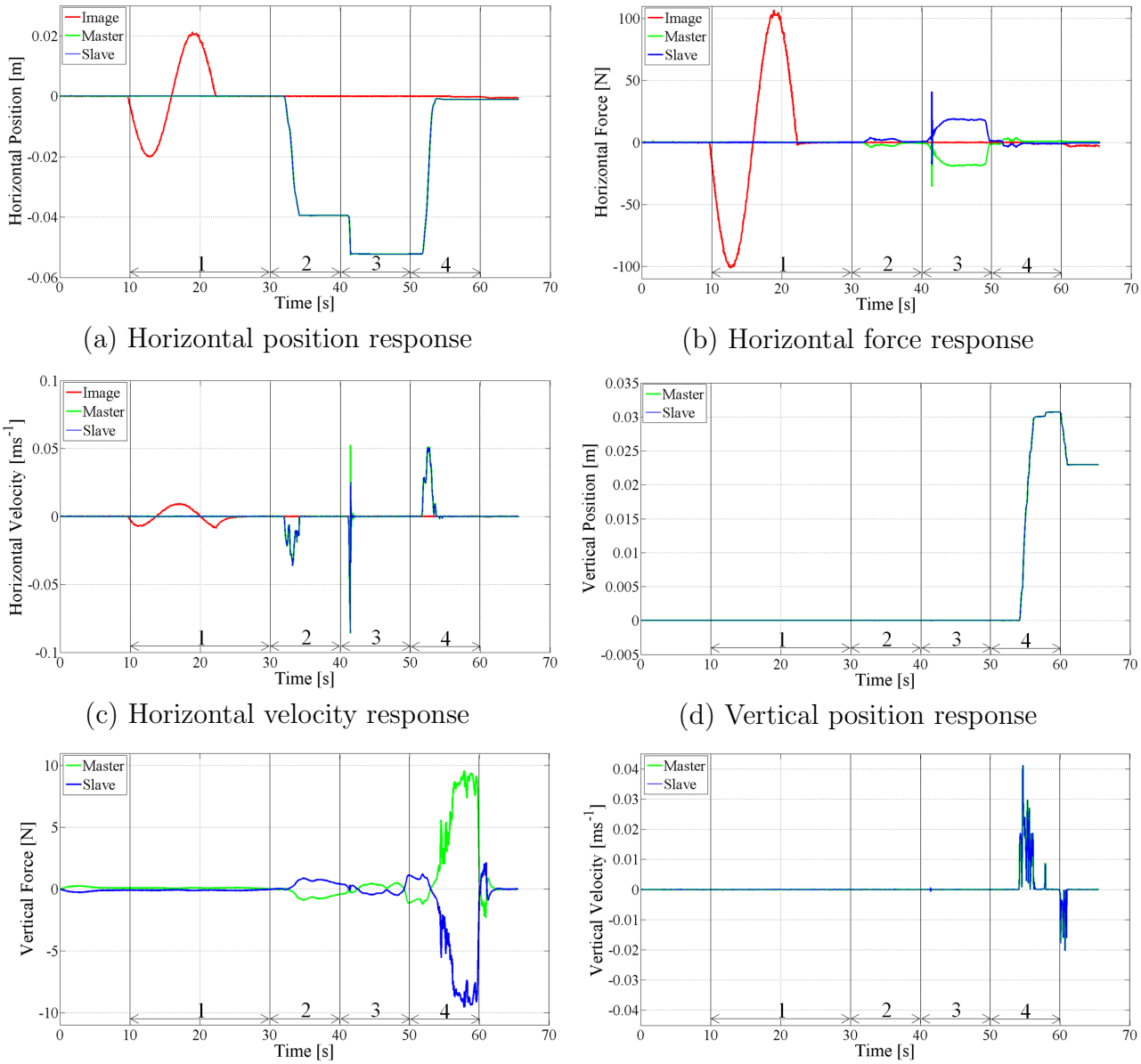

(a) Horizontal position response

(b) Horizontal force response

(c) Horizontal velocity response

(d) Vertical position response

(e) Vertical force response

(f) Vertical velocity response

Figure 4.9: Position, force, and velocity responses of horizontal and vertical manipulator movements for 10.0-cm camera–object distance by conventional method

of an object, the vertical manipulator movements were also recorded to show the ability to feel the object's stiffness with haptic manipulation, together with the servoing tasks. This means that the operator can feel the haptic sensation of an object even if the object is moving. The position and force responses of these manipulation activities can be seen in Figure 4.6((d) and (e)) and Figure 4.8((d) and (e)) with the proposed method and in Figure 4.7((d) and (e)) and Figure 4.9((d) and (e)) without the proposed method.

The results show that the purpose of motion navigation with soft tracking of the moving object was achieved. The dedicated compliance controller was applied only to the horizontal axis and not to the vertical axis. Therefore, in the horizontal direction, the operator could feel the virtual force generated by the force-based compliance controller utilizing visual information, plus the environmental impedance. The operator could not directly feel the environmental stiffness. This is a kind of trade-off. If the stiffness of the compliance controller increases, almost rigid tracking with a hard virtual force feel can be realized. However, if this parameter is decreased to a low number, a human will feel the relative environmental stiffness (from the slave side). Yet, this will also decrease the motion tracking performance. Moreover, on the vertical axis, there was no influence from the compliance controller. Thus, the operator could accurately feel the stiffness of the object. These effects confirmed the validity of the proposed system.

Velocity Response

The velocity responses of horizontal movements in both experiments are plotted in Figure 4.6(c), Figure 4.7(c), Figure 4.8(c), and Figure 4.9(c), whereas Figure 4.6(f), Figure 4.7(f), Figure 4.8(f), and Figure 4.9(f) show the velocity responses of the vertical manipulator movements during the contact task. Noises seem to be present in the graphs. These noises can clearly be seen, especially during step 1 of the motion navigation task by the proposed method. It also reflected the generated force response.

These noises were caused by two factors: the hardware and software limitations. For the hardware constraint, a web camera with a low frame rate (30 Hz) and low resolution was used in the experiments. Thus, this low-performance camera generated much noise. The generation of much noise was also due to a software limitation, where a difference between the sampling times for the image-processing and manipulator controller was set. A delay occurred by this difference in the sampling times. In addition, the communication line between the two computers produced a poor response signal to the control part. Thus, it generated the noises in the system.

In the future, the hardware limitation can be overcome by using a higher frame rate camera. As for the software constraint, the implementation of a multi-rate sampling control technique and/or interpolation technique can realize a noise reduction.

4.4 Simulation

As to confirm the results that gathered from the experiments, the simulation is conducted. There are two kind of simulations which simulates the response on Step 1 and Step 2, as same as the steps in the experiment. Those simulations also devided into two categories which depicts the difference between the 20.0-cm and 10.0-cm of camera–object distances. The simulations uses the same parameter as used in the experiments.

4.4.1 Simulation Results

The simulation results can be found as plotted in Figure 4.10 to Figure 4.13. Figure 4.10 and Figure 4.11 shows the simulation results for Step 1. While, Figure 4.12 and Figure 4.13 shows the results for Step 2.

In Step 1, when the height of the camera is reduced, the generation of compliance force become bigger. It seems that the response force is doubled as compared to original 20.0-cm distance. It can be referred to the figures as depicted in Figure 4.10((a) and (b)) and Figure 4.11((a) and (b)). In the meantime, the manipulators can follows the movements of the object with minimum position error. The position responses on Step 1 can be referred in Figure 4.10((c) and (d)) and Figure 4.11((c) and (d)). It shows almost the same position results.

In Step 2, when the position of the master manipulator is changed to the position of 0.01m, the 25N force is needed to move it to that location. Thus, as a response, the compliance controller also generates the same 25N force as a feedback. It can be referred as in Figure 4.12(a) and (b). However, when the distance between camera and object is reduced, to move the master manipulator to the same location (0.01m), the 50N force is required. It shown that the needed force is doubled. The results can be seen as plotted in Figure 4.13(a) and (b). The slave system gave a good position response as same as the master manipulator for both camera height simulation results. It can be found as in Figure 4.12((c) and (d)) and Figure 4.13((c) and (d)).

As a conclusion, the simulations of Step 1 and Step 2 with the comparison on the different camera-object distance, had confirmed the responses of the experimental results. Here, applied scaling of the camera will resulted the generation of different compliance force response even though the distance movements of the object are same.

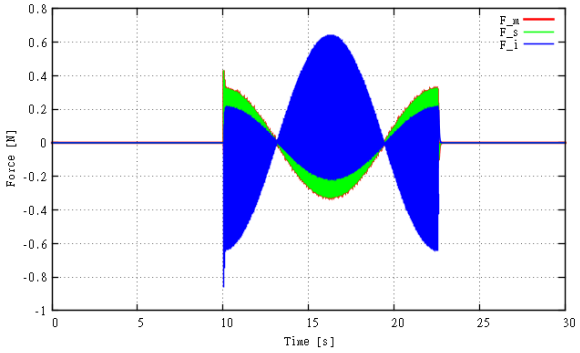

(a) Force response

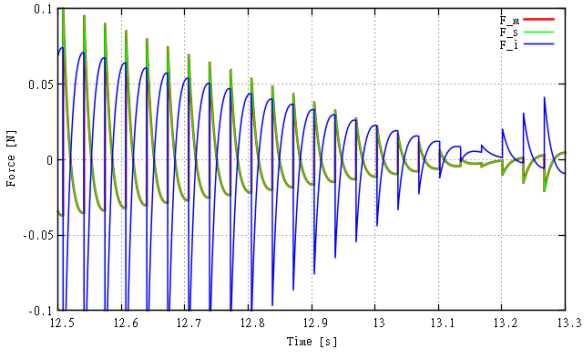

(b) Magnification of force response

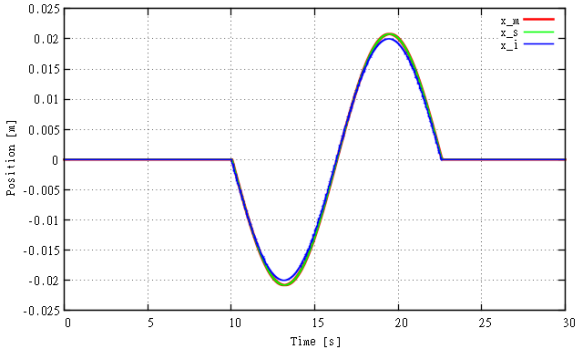

(c) Position response

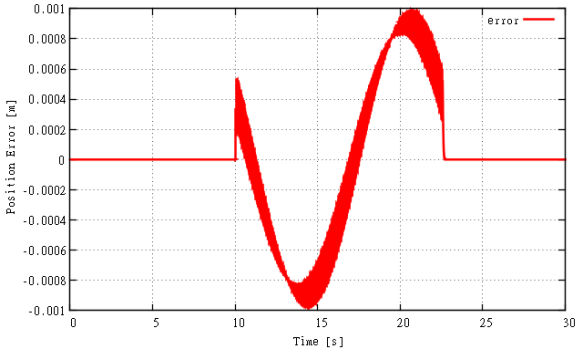

(d) Position error response

Figure 4.10: Force, position, and position error responses of simulation on Step 1 for 20.0-cm camera–object distance

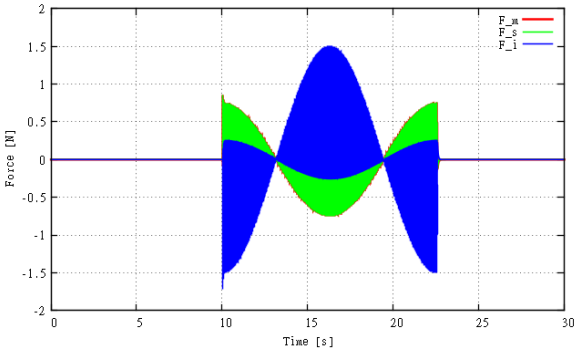

(a) Force response

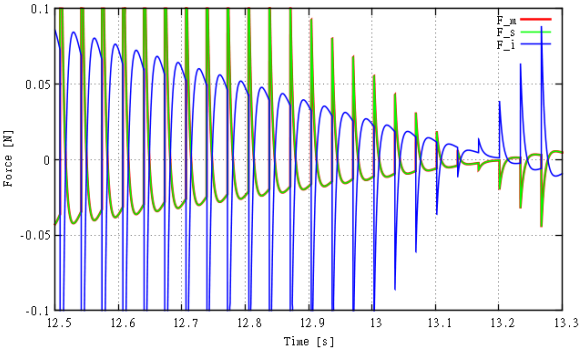

(b) Magnification of force response

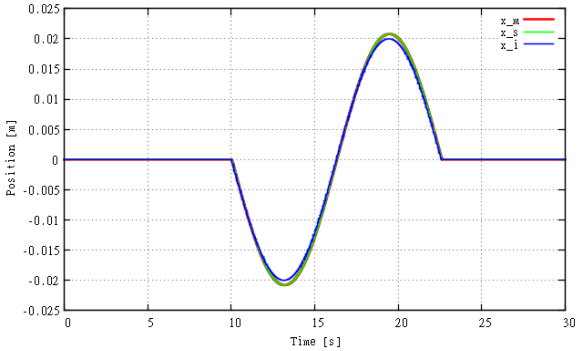

(c) Position response

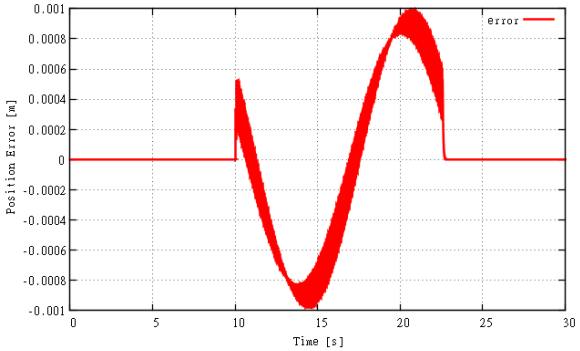

(d) Position error response

Figure 4.11: Force, position, and position error responses of simulation on Step 1 for 10.0-cm camera–object distance

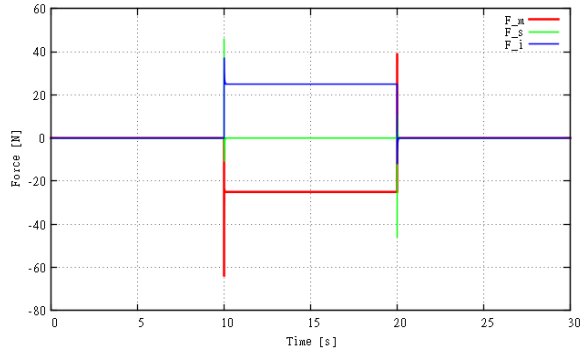

(a) Force response

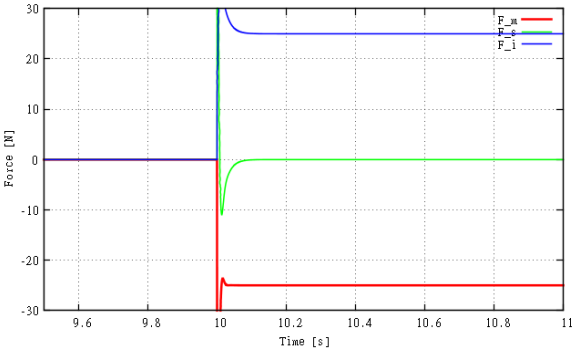

(b) Magnification of force response

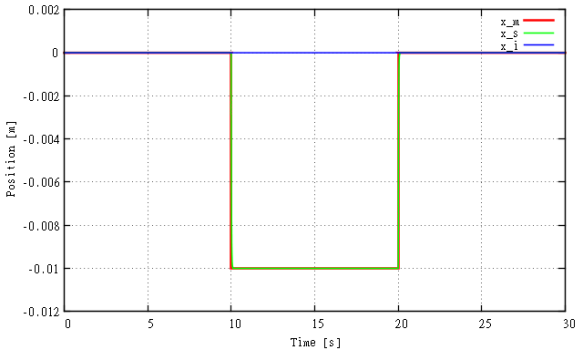

(c) Position response

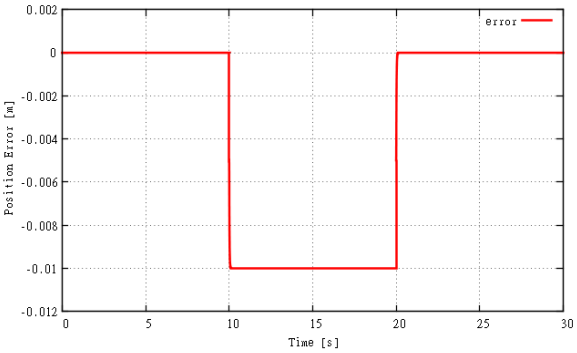

(d) Position error response

Figure 4.12: Force, position, and position error responses of simulation on Step 2 for 20.0-cm camera–object distance

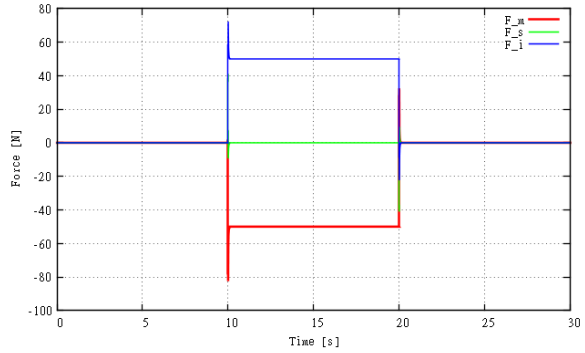

(a) Force response

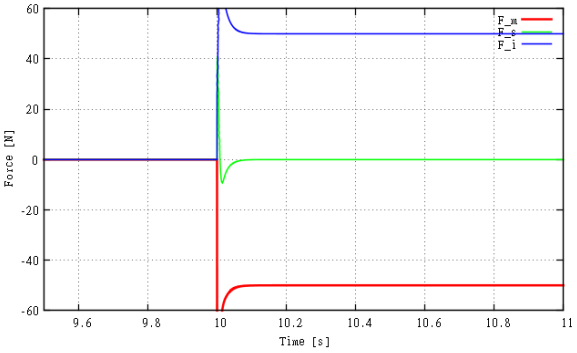

(b) Magnification of force response

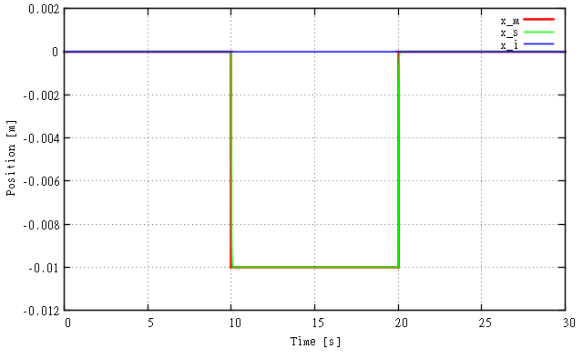

(c) Position response

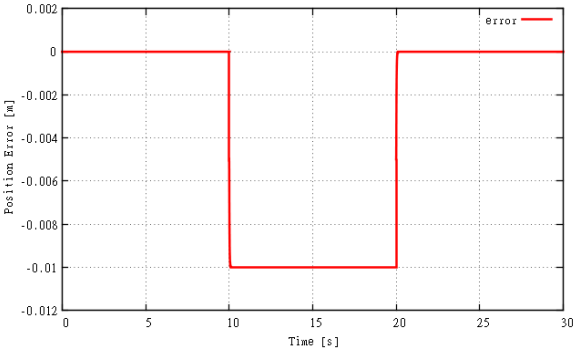

(d) Position error response

Figure 4.13: Force, position, and position error responses of simulation on Step 2 for 10.0-cm camera–object distance

4.5 Summary

In this chapter, I have explained about the scaling effect in the generation of virtual force by the vision-based force compliance controller. Initially, in the first section, the concept of scaling effect to the proposed system has been introduced. Then, four sets of experiments were conducted to show the comparison between the proposed method with the conventional method and together with the different height of camera–object distances. The validity of the proposals are verified by the experimental results. Its utility also are confirmed by the simulation outputs.

Chapter 5

Vision-based Disturbance Observer

In the previous chapter, I have explained the different of generated force produces by the scaling effect in the proposed vision-based force compliance control method. The effect can be encountered by the implementation of one variable in the proposed compliance controller.

In this chapter, I will explain about the improvement of the tracking performance by the implementation of a vision-based disturbance observer in the proposed method. Camera resolution also plays an important role in the accuracy of tracking data. As the generated force is fully dependant on the image information from the camera, tracking performance will also depend on the quality of that image. In order to decrease the disturbance effect form by the image information, a suppression method should be introduced.

I will begin with the construction of the vision-based disturbance observer method. Then, I will explain about how to implement it in the proposed integrated vision-based bilateral control system. Next, the experimental setup and its result will be elaborate to analyse the performance in the discussed topic.

5.1 Introduction

Recently, a perfect and robust requirement of the moving target tracking techniques in motion navigation has gained the attention. Several related control systems have been developed and discussed about its importance and originality.

One of the solutions is the vision-based navigation method. The uses of vision system had shown its robustness that can reduce the dependence on any position or force sensors. It was reported that it were successfully be applied in servoing for micromanipulation application [156] [170] and as an assistance in medical beating heart surgery [168] [169]. As the modelling of its

control design gets more complex, the kind of disturbance observer [167] has to be implemented to suppress any related modelling error or interruption [171] during the navigation task.

In the field of haptic, focused on the visual servoing controller for bilateral system application, [166] [172] were shown its potential that can produces the force-based feedback by the useful image information. However, the integration method of any designed vision-based disturbance observer to the bilateral motion control still lack and never be implemented. The consideration of this technique is important in order to attain a robust tracking of the target object.

Therefore, this chapter introduces the control algorithm of integration method for the implementation of disturbance observer that based on the visual information in bilateral haptic system. This observer can compensate the modelling error or any related force-based disturbance that occur in the integration of the system. The robust tracking of the target object will be considered as an objective to be achieved by the implementation of the vision-based disturbance observer (VDOB). It will be integrated with the bilateral manipulators controller and vision-based force compliance controller.

5.2 A Construction of Vision-based Disturbance Observer

In this section, a control structure for the vision-based disturbance observer is presented. After that, the proposed integration method with the present bilateral system will be introduced.

5.2.1 Vision-based Disturbance Observer Methodology

An implementation of an observer in a system can identify adherence to a given input. Hence, information from this observer needs to be used together with the input signal as a feedback to compensate any modelling error or disturbance that will occur.

In the development of the proposed method, the output signal information from the bilateral manipulator system need to be justified either it can comply or not, with the motion navigation by using the input from the vision-based force compliance controller. Thus, the kind of disturbance observer needs to be implemented to this system where its inputs are referred as from the visual information.

As for the purposes to navigate the moving object, the generated force by the vision-based force compliance controller (VFCC) may implicate the manipulators of bilateral system. Therefore, the average velocity response of bilateral system $\dot{x}_{ave}^{bil}$ is considered as the feedback to the

designed observer. It will be compared with the original input signal (generated force) so that the observed disturbance force F_{VDOB} can be generated. As for minimizing any possible occured noise, the kind of low pass filter (LPF) design with the cut-off frequency g_{iDis} is included.

The input signal of this observer F_{cc} can be defined as

$$F_{cc} = F_{img}^{cmd} + F_{VDOB} \tag{5.1}$$

and the observed disturbance force F_{VDOB} can be calculated as

$$F_{VDOB} = \frac{\left(F_{cc} + \boldsymbol{\sigma}\dot{x}_{ave}^{bil}\right) g_{iDis}}{s + g_{iDis}} - \boldsymbol{\sigma}\dot{x}_{ave}^{bil} \tag{5.2}$$

where,

$$\boldsymbol{\sigma} = g_{iDis}\left(\frac{M_m + M_s}{2}\right). \tag{5.3}$$

Therefore, the VDOB will be functioned as a feedforward controller for dynamic object tracking. It will generates the compensation value for compensates the steady state error in the system.

5.2.2 Integration with the Bilateral Motion Control System

As mentioned in previous subsection, the designed vision-based disturbance observer is integrated with the bilateral manipulator system. The generated force response F_{cc} will be fed into the reaction force observer (RFOB) of the bilateral control. Thus, in order to fulfil the requirement of haptic bilateral control system, the total computed force f_{com} for the overall system can be stated as

$$\begin{aligned} F_{com} &= F_m + F_s - F_{cc} \\ &= 0. \end{aligned} \tag{5.4}$$

Figure 5.1 depicts the structure of the vision-based disturbance observer's block diagram. While, Figure 5.2 shows the block diagram of the integration of VFCC and bilateral system with proposed Vision-based Disturbance Observer (VDOB).

5.3 Experiments

This section will describe the setup for the experiments that needs to be conducted. After that, the results obtained from the experiments will be discussed.

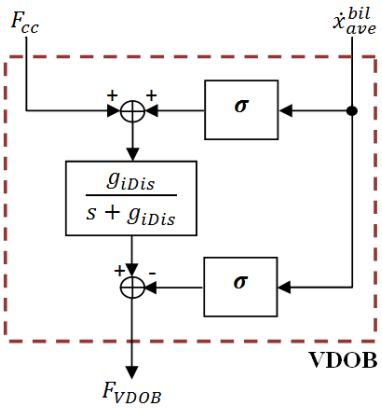

Figure 5.1: Vision-based Disturbance Observer (VDOB)

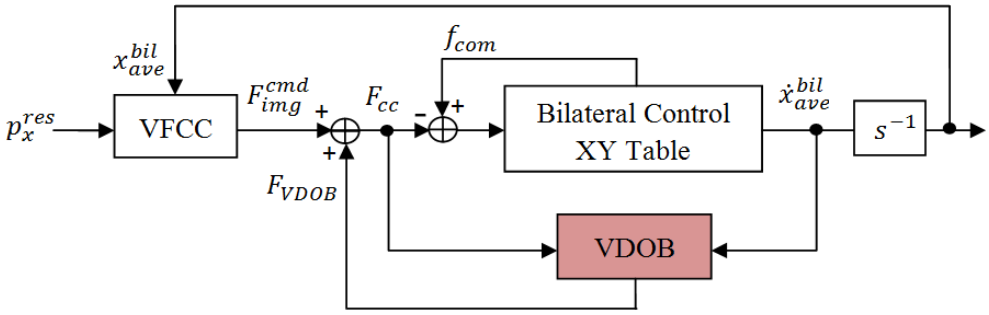

Figure 5.2: Block diagram of the system with proposed Vision-based Disturbance Observer

5.3.1 Experimental Setup

In order to validate the robustness of the proposed method, two experiments need to be performed. The first experiment is implemented only with the integration of bilateral manipulator control with vision-based force compliance controller. The second experiment is conducted in combination of bilateral manipulator control, vision-based force compliance controller and the vision-based disturbance observer. The difference between these two experiments will be evaluated to study the robust performance of the intended technique.

Each of the experiments include two steps. The designed steps are as below;

• Step 1: the slave manipulator navigates the moving object and tracks its motion path. The object is attached in one linear motor (object's mover) and programmed to be moved in sinusoidal characteristic, 2 cm to the right and 2 cm to the left from the original position of the object. The tracking performance of the system will be recorded and analyzed. It will be conducted from 10 to 30 s of experimental time.

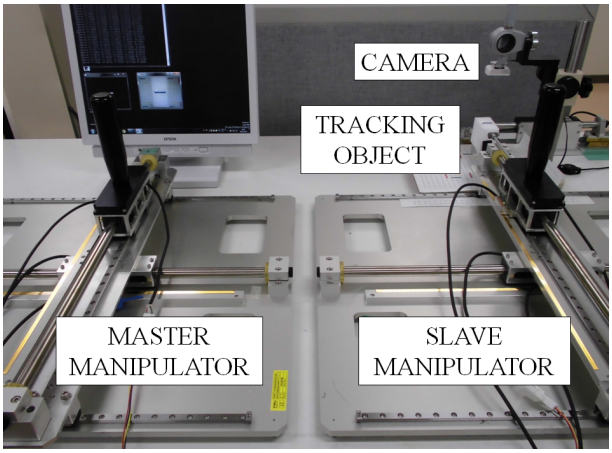

Figure 5.3: Experimental setup for the vision-based force compliance controller with the bilateral haptic system

• Step 2: the object is not moving. About 6-N force will be given to the master manipulator as a disturbance force. The force is exerted by pushing the manipulator's knob to the left direction. The effect of this disturbance force to the overall system will be recorded and evaluated. It will be conducted from 30 to 40 s of experimental time.

Those two experiments will be carried out with the use of the parameter as stated in Table 5.1. The ζ is set as 1.0. While, the natural angular frequency ω_n are set as 100 rad/s for the manipulator system and 50 rad/s for the vision system, with critical damping ratio characteristic to obtain superior performance. The cutoff frequency values are justified by considering the signal to noise ratio (SNR) effects on the system. The manipulators' movements are controlled and recorded by the LINUX operating system (OS) computer. While the image information that is captured by the usb camera is processed by another computer with the Windows 7 OS. The real time image informations gathered are sent to the LINUX computer that is connected with the UDP network cable. Figure 5.3 shows the arrangement of the experimental setup for the system.

Table 5.1: Parameters for the VDOB system

Parameters	Discription	Values
K_{p}	Position gain of manipulator system	1.00×10^4
K_{pv}	Position gain of vision system	2.50×10^3
K_{v}	Velocity gain of manipulator system	200
K_{vv}	Velocity gain of vision system	100
K_{f}	Force gain of manipulator system	1.00
g_{dis}	Cutoff frequency of DOB	600 rad/s
g_{iDis}	Cutoff frequency of VDOB	30 rad/s
g_{diff}	Cutoff frequency of LPF	600 rad/s
g_{v}	Cutoff frequency of LPF for vision	1.00 rad/s
M_{m}	Mass of the motor (Master)	0.50 kg
M_{s}	Mass of the motor (Slave)	0.50 kg
M	Virtual mass of the moving object	1.00 kg
S_x	Scaling conversion	0.38×10^{-3} m/pixel
α	Camera-Object distance ratio	1.00

5.4 Results and Discussion

The recorded data of the conducted experiments were plotted into three different graphs to specifically validate the performance of its responses. Those three graphs are; the position response, the position error and the force response, as shown in Figure 5.4 and Figure 5.5. The results of the experiment obtained without implementation of proposed method is shown in Figure 5.4, while Figure 5.5 shows the results acquired by integration of proposed method with the bilateral control system.

5.4.1 Position Response

During the first step of the conducted experiments, the bilateral manipulator of master and slave system had demonstrated its ability to navigate the moving object as depicted in Figure 5.4(a) and Figure 5.5(a). Whereas, there were differences between those graphs during the second

step of the conducted experiments. Upon the disturbance force applied to the system, it has caused the bilateral manipulator to have about 2 mm displacement from its original position as shown in Figure 5.4(a). In contrast, almost no displacement is observed in Figure 5.5(a) by the disturbance force impact.

5.4.2 Position Error

The error between the position response of bilateral manipulator feedback x_{ave}^{bil} and the captured image x_{img}^{ref} for both experiments are plotted as shown in Figure 5.4(b) and Figure 5.5(b). This error x_{err} can be calculated as

$$\boldsymbol{x_{err}} = x_{ave}^{bil} - x_{img}^{ref}. \tag{5.5}$$

As for the first experiment, without the proposed method, the system had generated about 1.5 mm of position error during Step 1 and 2 mm of position error during Step 2 as depicted in Figure 5.4(b). However, as for the second experiment, with the proposed method, the position errors generated by the system were only about 0.5 mm during Step 1 and almost no error during Step 2, as shown in Figure 5.5(b). By these results, the proposed technique has shown its aptitude and effectiveness to track the moving object with the minimal position error and gave a good response for the disturbance force as compared to the first experiment.

5.4.3 Force Response

The force response for the conducted experiment without the integration of vision-based disturbance observer is shown in Figure 5.4(c). From that figure, the bilateral manipulator system gave the feedback as for a response from the force generated by the vision-based force compliance controller. During Step 1, the force generated by the master and slave manipulator are not in the same value because of its low stiffness's controller design but still complies with the total force of the system f_{com}. Thus, during Step 2, as 6-N force exerted to the master manipulator, reversal force by the compliance controller is generated. However, the responded forces cannot maintain at the zero force level even without any object's movement and disturbance force.

Conversely, by the proposed method, the forces generated by the master and slave manipulators of the bilateral system during navigation task are almost at the same value, as can be seen

in Figure 5.5(c). Besides to be able to comply with the f_{com} condition, the generated system force also can maintain almost at the zero force level apart of Step 1 and Step 2. With this accomplishment, the proposed vision-based disturbance observer has demonstrated its robustness either for the motion navigation or against any disturbance force.

From the experimental results, the noise that appeared due to the low quality of the usb camera can be found. The different sampling rates of the vision system program (1 kHz) compared to the bilateral control's (10 kHz) had caused a delay in a system, thereby generated the noise. For future development, these effect will be reduced by replacing the usb camera with the high performance camera having a higher frame rates and considering the multirate sampling method. The stability of the system and its noise sensitivity will also be observed.

5.5 Summary

In this chapter, I have described the design method of Vision-based Disturbance Observer (VDOB) for the proposed VFCC methodology. Then, this method is implemented in the bilateral manipulator control system which produces new equation for the total force in common mode of the system. The experiments have been conducted to show the different between the proposed system without the VDOB and with the VDOB. Finally, the results were discussed in term of its position response, position error and force response.

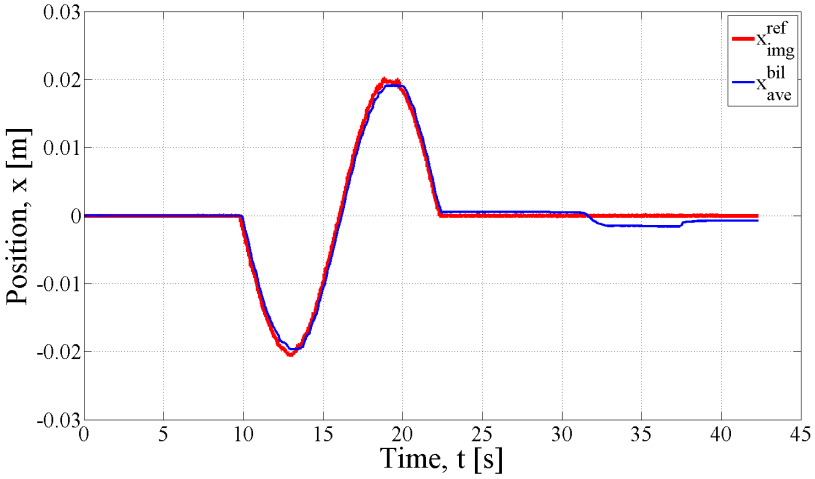

(a) Position response

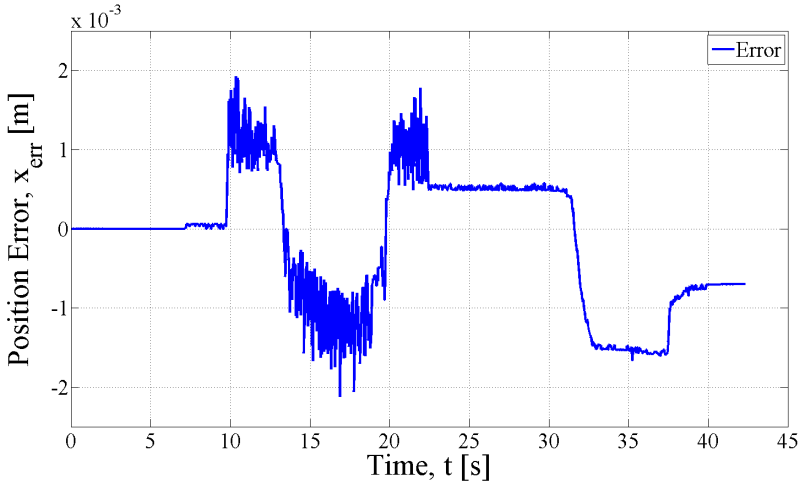

(b) Position error

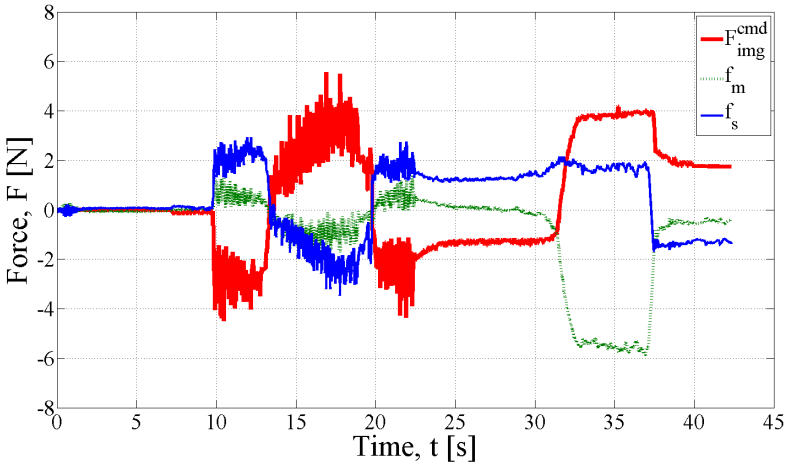

(c) Force

Figure 5.4: Experimental results of the system without Vision-based Disturbance Observer

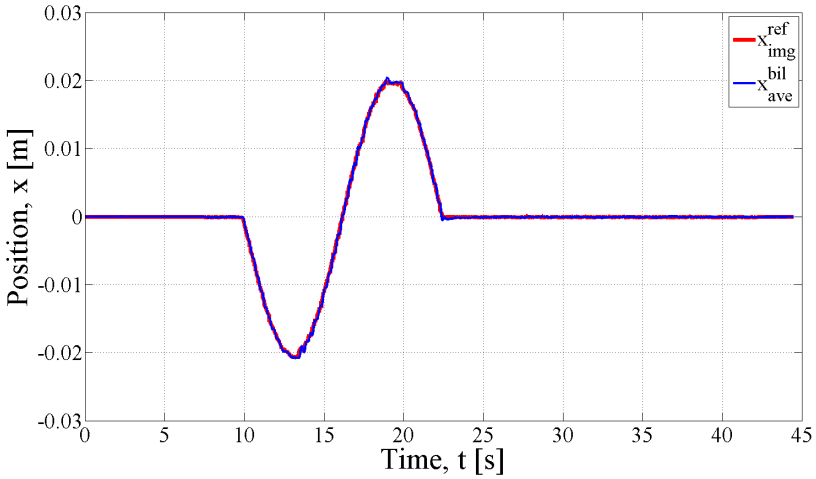

(a) Position response

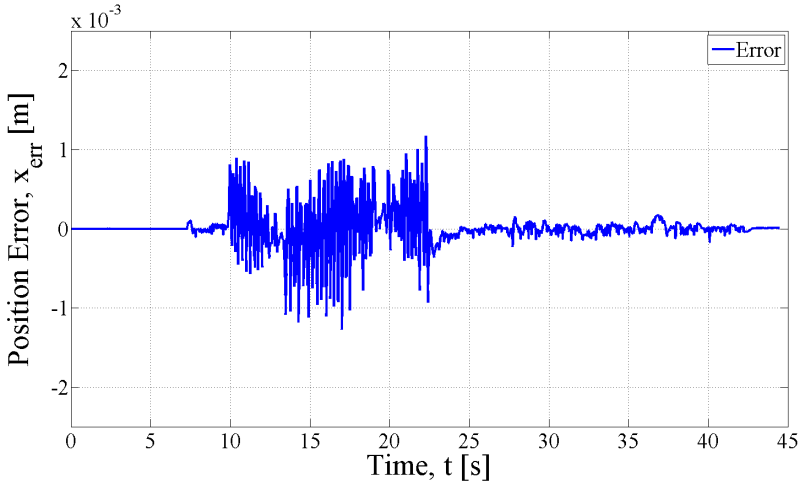

(b) Position error

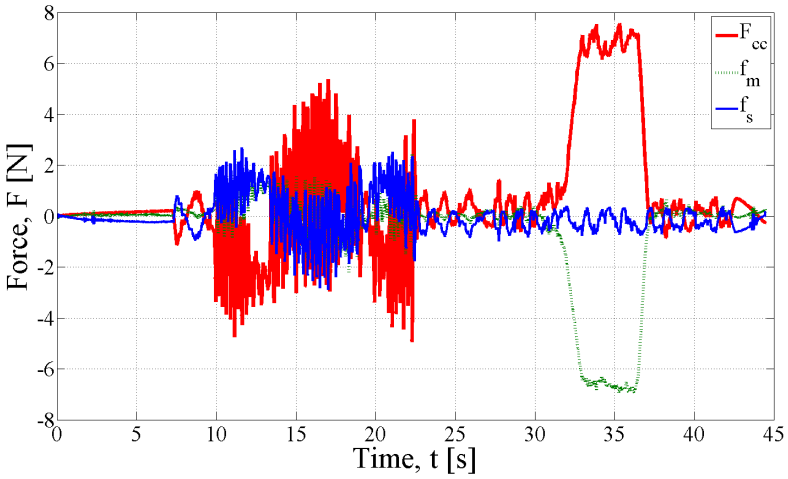

(c) Force

Figure 5.5: Experimental results of the system with proposed Vision-based Disturbance Observer

Chapter 6

Confirmation on the Object Rotational Effect

In the previous chapter, I have explained the technique on how to increase the tracking performance by the implementation of vision-based disturbance observer.

In this chapter, the explanation about the object tracking technique by the proposed method considering the object coordinate rotational effect, will be presented. This is crucial in order to enhance the robustness of the proposed vision-based compliance control method.

The chapter will be begun with the conception of object's rotational effect in the vision-based servoing method. Then, I will explain about how to integrate the enhancement method in the bilateral motion control system. Next, the experimental setup and its result will be elaborate to analyse the performance in the discussed topic.

6.1 Introduction

An implementation of force-based control in haptic application has gained much attention. Based on its popularity, many advanced technologies related to force-based research has been proposed. It can be referred to past articles such as force-based haptic training system [173], 6 degrees of freedom (DOF) haptic interfaced robot [174] and teleoperated robot-assisted surgery [175]. Further, the vibrancy of the research was enhanced by the involvement of the vision system as a part of haptic control. Various methods have been investigated, and some of them are about the angle of rotation of the navigated object.

The discretion of angle effect on servoing task has demonstrated its importance in the development of vision-based control system. One research was conducted considering the angle factor in controlling the direction of unmanned aerial vehicle (UAV) caused by a gust of wind [176]. The linearizing integration matrix has been proposed in the controller to generate wind correction angle. An automatically positioning of end-effectors to be centered in micro-environment [177] is another example of the rotational and positioning effect. An image-based PID visual servo controller and Kalman filter method had been implemented to position the end-effector's tip to the center field of view. Thus, the consideration of the object rotational effect in vision-based bilateral haptic control system is an interesting topic to be discussed.

Previously, the research which was based on the visual feedback that had been integrated with the bilateral haptic system was developed. The horizontal movement of the navigated object had been considered by the compliance controller to produce the dedicated virtual force [162]. In other related visual and haptic feedback study, the model-displaced teleoperation (MDT) approach was proposed by [178] to compensate the visual–haptic asynchrony issue. The vertical movement of an object had been highlighted in the research. However, both studies [162, 178] did not consider the rotational effect of the measured object in its trajectory movement. Thus, a method that emphasizes the trajectory alteration of the object and its effect on the haptic bilateral system, need to be developed. The consideration on the object's coordinate and orientation is important for the servoing application requiring parallel movement to the determined object surface.

Therefore, this chapter elaborates the virtual force trajectory projection for the integrated vision-based force compliance controller in bilateral control system that considering object coordinate into account. The proposed method will deliberates an orientation of the object on its coordinate which reflect to the servoing manipulator trajectory. By considering the rotational matrix in the proposed controller, the projection of respective trajectory can be realized. This method can transform the servoing trajectory of the manipulator depending on the moving object's rotation angle. Hence, the stiffness of the object can be rendered directly by the bilateral manipulators during navigation task.

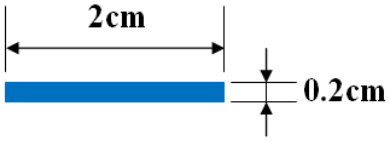

Figure 6.1: Blue line object marker dimension

6.2 Vision-based Force Compliance Controller with Object Rotational Effect

As defined in the Chapter 3, the vision-based force compliance controller (VFCC) is a kind of controller that can give the virtual force feedback to the system. The feedback force is generated by referring to the image information of the vision system. It will affect the horizontal movement of an object and/or manipulator, hence the actual condition (stiffness) of the object can be felt during the vertically manipulation of the manipulator. The concept of VFCC was introduced in detail by [162].

In this chapter, a condition of the navigated object with respect to the VFCC is considered. One of the conditions that can be accounted is an object's rotational effect. This effect occurs when the object is not moving straight in its original axes but move in a curve direction with perpendicular to the tooltips of slave manipulator. Thus, the force generated by the controller also must consider this object's condition transformation.

The detection of this rotational effect is measured by the vision system. The static visual sensor is used and located facing downward above the navigated object. A blue line objects marker with a length of 2 cm is used for the object detection, as shown in Figure 6.1. An image processing software of the vision system will do the colour recognition, image binarization, corner detection and centroid identification processes [172]. In addition to the ability of the corner detection process, by the detection of two corner with its' coordinate from the end parts of the line, the rotational angle can be calculated.

Figure 6.2 shows the detected two corners with respective rotational angle. From this figure, the rotational angle θ can be calculated as

$$\theta = \sin^{-1}\left(\frac{a}{c}\right) \tag{6.1}$$

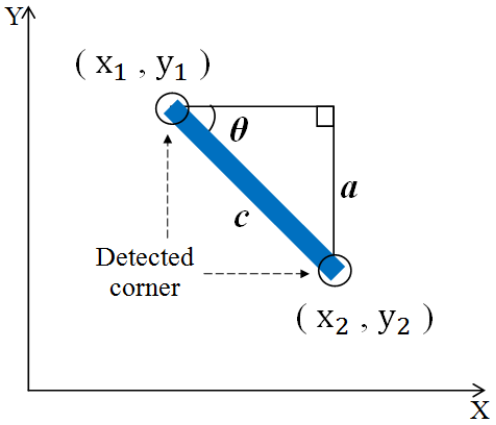

Figure 6.2: Rotational angle measures from the detected two corners

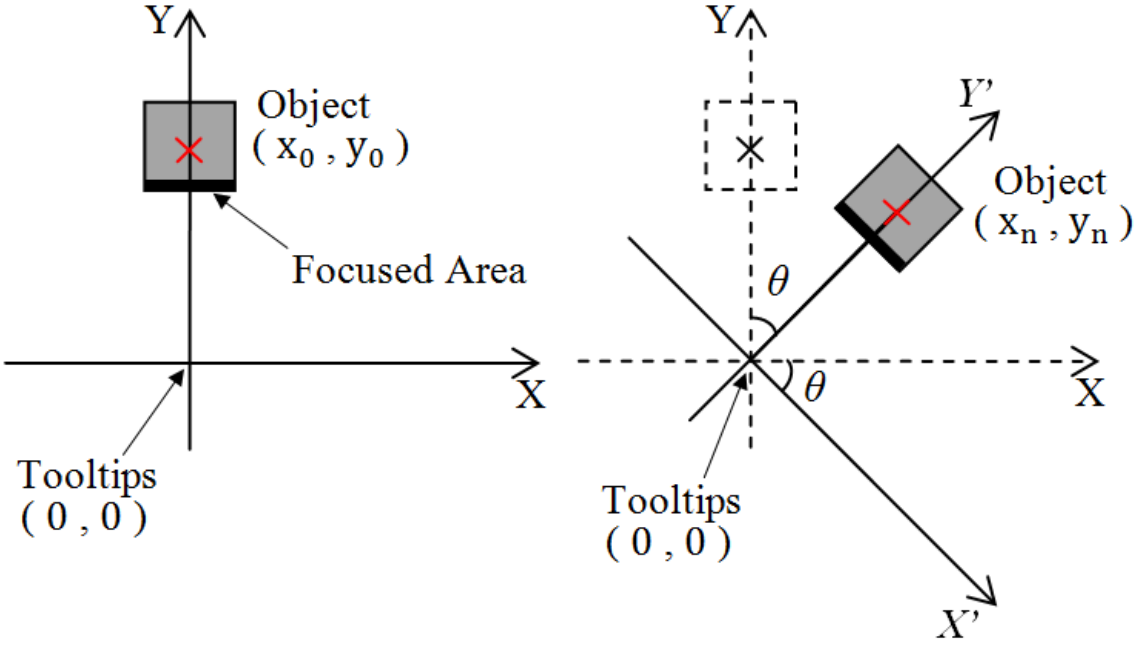

(a) (b)

Figure 6.3: Coordinate of the object (a)without rotational effect, and (b)with rotational effect of θ°

where,

$$a = y_2 - y_1$$

$$c = \sqrt[2]{(x_2 - x_1)^2 + (y_2 - y_1)^2}. \tag{6.2}$$

As shown in Figure 6.3(a), the object with a coordinate (x_0, y_0) will cause the VFCC to gen-

erate the responsive virtual force horizontally if the object or the tooltips is moved in horizontal direction (X-axis) [162]. The generated force will let the manipulator moves in parallel direction to the object's focused area/surface. In pixel value, the object's coordinate displacement p_{xy}^{ref} is obtained from the subtraction of current object's coordinate p_{xy}^{res} with initial coordinate $p_{xy}^{initial}$. However, if the object is moved to a new coordinate $(\mathrm{x_n}, \mathrm{y_n})$ with a rotational angle of θ° from its original position, the direction trajectory of generated virtual force also will be changed. Figure 6.3(b) shows the condition of the object with the rotational effect.

The horizontal and vertical axes of the object with respect to the tooltips will be twisted to a new horizontal and vertical axes (X', Y') as much as θ°. Thus, the calculation of produced force by the VFCC will encompass this rotational effect by using the rotational matrix formula, $\mathbf{R}$. The formula can be defined as

$$\mathbf{R} = \begin{pmatrix} \cos\theta & \sin\theta \\ -\sin\theta & \cos\theta \end{pmatrix}. \tag{6.3}$$

The $\mathbf{R}$ can realize the projection between the trajectory of X-Y and X'-Y'.

6.3 Integration of the Bilateral System with Vision-based Force Compliance Controller including the Rotational Effect

The VFCC can be integrated with the bilateral control system. As the object is navigated by the vision sensor, the generated virtual force will order the bilateral system to comply with the object's position. Thus, the bilateral manipulator may track the object movement and at the same time can feel/manipulate the objects.

Therefore, as prescribed in earliest chapter, by this integration the average position of bilateral manipulator $\mathbf{x}_{\mathrm{bil}}^{\mathrm{ave}}$ will be considered as an input to the VFCC. In this study, the object's rotational effect factor is considered. As a result, the acceleration reference $\ddot{\mathbf{x}}_{\mathrm{img}}^{\mathrm{ref}}$ for the VFCC controller can be described as

$$\ddot{\mathbf{x}}_{\mathrm{img}}^{\mathrm{ref}} = K_{\mathrm{pv}}\left(\mathbf{x}_{\mathrm{img}}^{\mathrm{ref}} - \mathbf{x}_{\mathrm{bil}}^{\mathrm{rot}}\right) + K_{\mathrm{vv}}\left(\dot{\mathbf{x}}_{\mathrm{img}}^{\mathrm{ref}} - \dot{\mathbf{x}}_{\mathrm{bil}}^{\mathrm{rot}}\right) \tag{6.4}$$

where

$$\mathbf{x}_{\text{img}}^{\text{ref}} = S_x p_{xy}^{ref} \tag{6.5}$$

and

$$\mathbf{x}_{\text{bil}}^{\text{rot}} = \mathbf{R}\mathbf{x}_{\text{bil}}^{\text{ave}}. \tag{6.6}$$

The $\mathbf{x}_{\text{img}}^{\text{ref}}$ is the object's position reference. It is obtained as a result from a multiplication of object's coordinate displacement in pixel value p_{xy}^{ref} with the scaling conversion factor S_x [163]. While K_{pv} and K_{vv} are position and velocity gains of VFCC controller respectively. Then, considering the virtual object's mass M, the virtual force $\mathbf{F}_{\text{img}}^{\text{ref}}$ can be calculated as

$$\mathbf{F}_{\text{img}}^{\text{ref}} = M\ddot{\mathbf{x}}_{\text{img}}^{\text{ref}}. \tag{6.7}$$

Further, the generated virtual force with respective rotational angle $\mathrm{F}_{\text{img}}^{\text{rot}}$ can be described as

$$\mathbf{F}_{\text{img}}^{\text{rot}} = \mathbf{R}^{-1}\mathbf{F}_{\text{img}}^{\text{ref}}. \tag{6.8}$$

In common mode, the calculation of the total feedback force for the integrated system $\mathbf{F}_{\text{com}}$ can be defined as

$$\mathbf{F}_{\text{com}} = \mathbf{F}_{\text{m}} + \mathbf{F}_{\text{s}} - \mathbf{F}_{\text{img}}^{\text{rot}}. \tag{6.9}$$

Figure 6.4 depicts the complete block diagram of integration between the bilateral control system and vision-based force compliance controller including the rotational matrix. While, the simplified diagram for the integrated system can be found as shown in Figure 6.5.

6.4 Experiments

In this section, the details about the experimental setup and the arrangement of the equipment will be explained. Subsequently, the steps to conduct the experiments will be described. Next, the results of the conducted experiments will be explained.

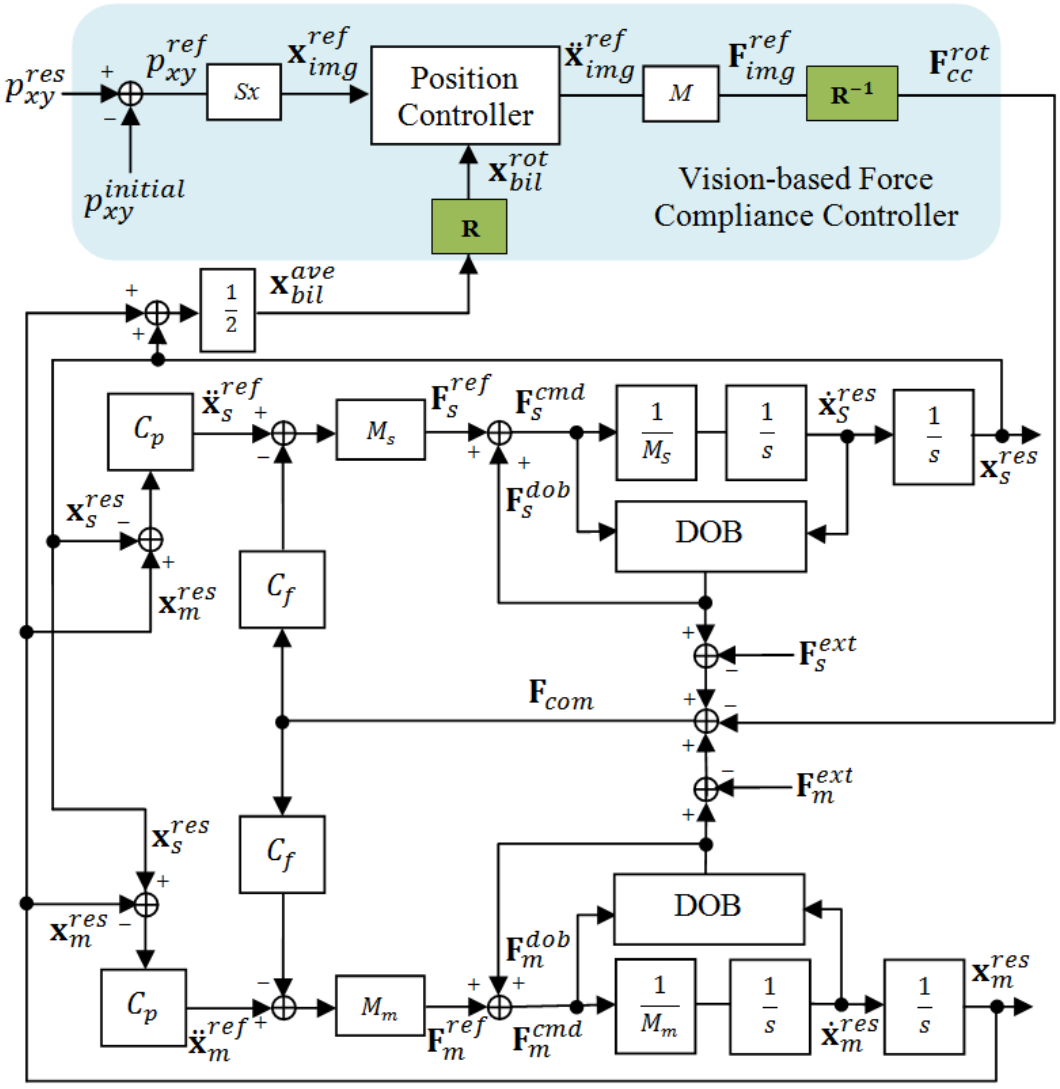

Figure 6.4: Complete block diagram of vision-based force compliance controller in bilateral master-slave haptic system with rotational effect

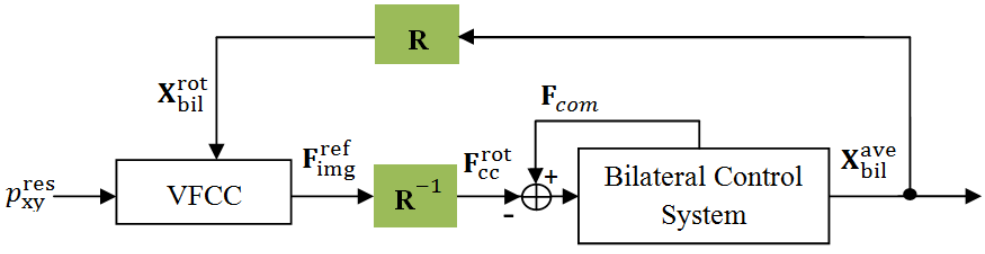

Figure 6.5: Integration of bilateral control system with VFCC considering the rotational matrix

6.4.1 Experimental Setup

As to prove the concept of the proposed method, the experiments of the integrated system are conducted. The experiments are performed using two sets of X-Y table as a bilateral master–

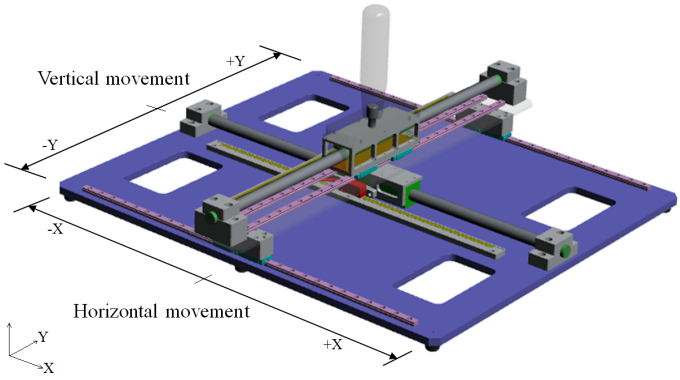

Figure 6.6: CAD diagram of X-Y table

slave manipulators system. One is a master manipulator and the other is a slave manipulator. Each set consists of two linear motors which were positioned perpendicular to each other to reflect the horizontal and vertical movements. Its movements are controlled by the Linux operating system (OS) computer. Figure 6.6 depicts the illustration of X-Y table used in the experiment.

As for the vision system, a conventional web camera (1.4 megapixels) with 30 fps, that is connected to the Windows 7 OS computer, is used. The camera is static and attached on the adjustable camera stand. It is located above the object with facing downwards as to navigate the object's movements. The real time image informations are captured, processed and after that are sent to the bilateral controller that is connected by UDP. The white foam, with the dimension of 8 cm $\times$ 6 cm $\times$ 4 cm and pasted with blue line marker, is used as the object. An arrangement for all the equipments is shown as in Figure 6.7.

Further, to confirm the validity of the proposed method, two experiments which used the different object's rotation condition are conducted. The first is without any rotation or $\theta = \angle 0^{\circ}$ and the second is with object's rotation at $\theta = \angle 45^{\circ}$. At this moment, the basic concept of the proposed method needs to be justified. Thus, the technique of static and not moving object is used in both experiments. Each experiment is conducted following several steps as below:

- Step 1: The master manipulator is moved horizontally to the right direction (+X).
- Step 2: The master manipulator is moved horizontally to the left direction (−X).
- Step 3: The master manipulator is moved vertically in forward direction (+Y).
- Step 4: The master manipulator is moved vertically in backward direction (−Y).
- Step 5: The master manipulator is moved diagonally to the right and forward direction at

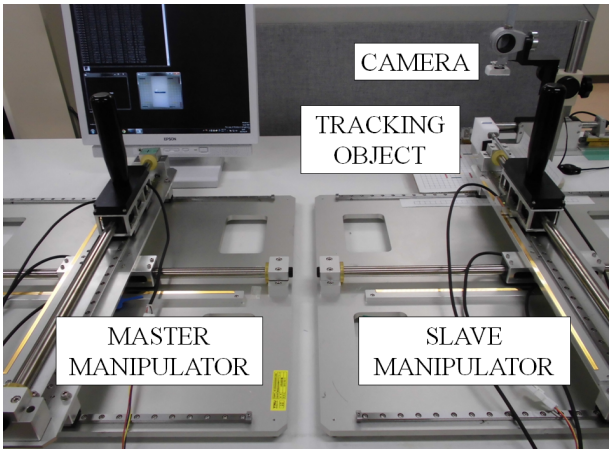

Figure 6.7: Experimental setup for the bilateral haptic system with vision-based force compliance controller

$\angle 45^\circ$ (+X and +Y).

• Step 6: The master manipulator is moved diagonally to the left and backward direction at $\angle 45^\circ$ (−X and −Y).

The first step is begun after 10 seconds of experimental times and the steps are updated for every 10 seconds interval times. The experiments are conducted based on the parameter values as given in Table 6.1. The responses position and force of horizontal and vertical manipulators of the bilateral system are recorded to be analyzed.

6.5 Results and Discussion

The vision system successfully detected the object and its changing angle. It can be referred to the captured images as shown in Figure 6.8 for $\theta = \angle 0^\circ$ and Figure 6.9 for $\theta = \angle 45^\circ$. The developed image processing software perfectly detected the blue line marker even though another colors are presented in the background.

The recorded data from both experiments is plotted in the responded graphs. The responses are divided into four categories which are the horizontal position and force of horizontal manipulator, and also the vertical position and force of vertical manipulator. Figure 6.10 depicts the manipulators' responses for $\theta = \angle 0^\circ$ while Figure 6.11 for $\theta = \angle 45^\circ$.

In the first experiment, by applying the force at the master manipulator (to move it to the

Table 6.1: Parameters for the object's rotational effect system

Parameters	**Discription**	**Values**
K_{p}	Position gain of manipulator system	1.00×10^4
K_{pv}	Position gain of vision system	1.00×10^4
K_{v}	Velocity gain of manipulator system	200
K_{vv}	Velocity gain of vision system	200
K_{f}	Force gain of manipulator system	1.00
g_{dis}	Cutoff frequency of DOB	600 rad/s
g_{diff}	Cutoff frequency of LPF	600 rad/s
g_{v}	Cutoff frequency of LPF for vision	1.00 rad/s
M_{m}	Mass of the motor (Master)	0.50 kg
M_{s}	Mass of the motor (Slave)	0.50 kg
M	Virtual mass of the moving object	1.00 kg
S_x	Scaling conversion	0.38×10^{-3} m/pixel

directions as mentioned in the experimental steps), the bilateral horizontal manipulators make only a little displacement (almost zero) for each type of movements which corresponded to the generated force by the VFCC as shown in Figs. 6.10(a) and (b). The VFCC generates the corresponding virtual force to maintain the position of horizontal manipulators. At this stage of the conventional VFCC method, the system shows its ability when the vertical manipulator can be moved freely in the vertical direction as depicted in Figs. 6.10(c) and (d). Indeed, the generated virtual force is only applied at the horizontal movements of the system's manipulators. Thus, in vertical direction of manipulating task to contact with the object, the original stiffness of the object can be felt [162].

As for the second experiment, the manipulators are hard to be moved either in the horizontal or in the vertical direction of the X-Y tables. These are proved by the generated horizontal and vertical forces as shown in Figs. 6.11(b) and (d). This is because of the alteration of original manipulator's servoing trajectory. In this situation, the navigation trajectory is rotated $\angle 45^\circ$ as same as the object's coordinates orientation. Thus, the trajectory of the generated virtual force also is changed. In contrast, the manipulators can easily be moved in diagonal directions of $\theta = \angle 45^\circ$ (Step 5 and 6). It shows that the original behavior of VFCC which only affected to the horizontal movements, can be utilized. Further, the original stiffness of the object can

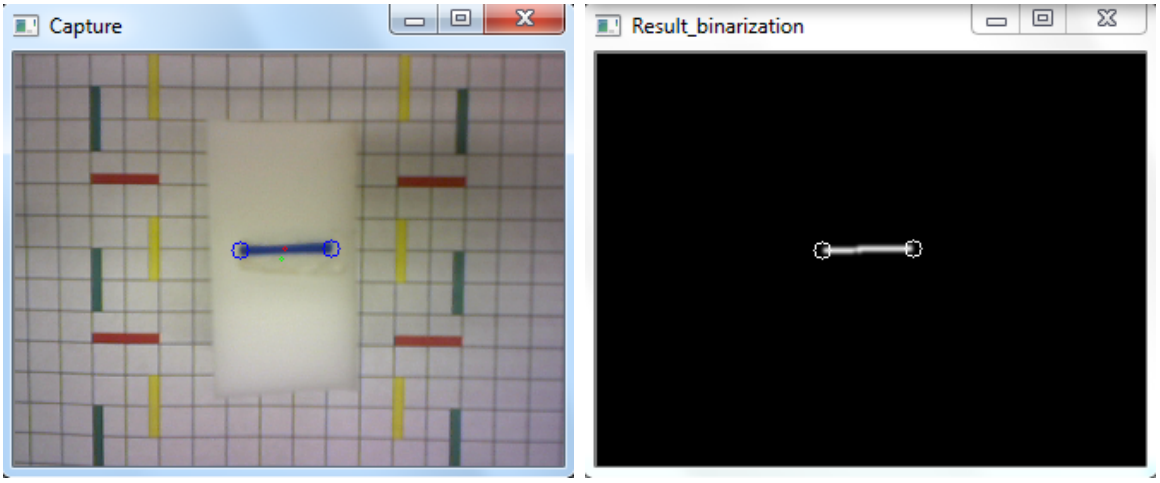

(a) (b)

Figure 6.8: Image processing results for (a) detection of object's marker, and (b) binarization output of the detected object's marker, at $\theta = \angle 0^{\circ}$

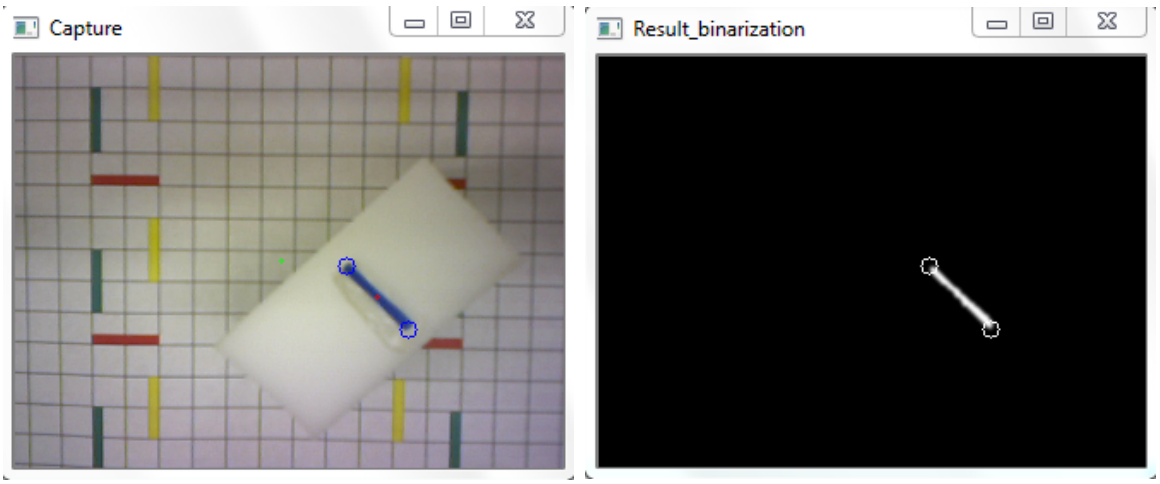

(a) (b)

Figure 6.9: Image processing results for (a) detection of object's marker, and (b) binarization output of the detected object's marker, at $\theta = \angle 45^{\circ}$

be felt [162] even by manipulating the manipulator in diagonal directions ($\theta = \angle 45^{\circ}$). The displacements in horizontal and vertical position for the manipulators can be found as plotted in graphs of Figs. 6.11(a) and (c). For both cases, since the virtual force generated by the VFCC only being applied to the horizontal manipulator, no data on the virtual force is recorded for force response graphs as in Figure 6.10(d) and Figure 6.11(d).

The proposed method shows its utility by rotating the respective X-axis of the system to the new X'-axis which corresponding to the object's rotational effect. As a result, the operator

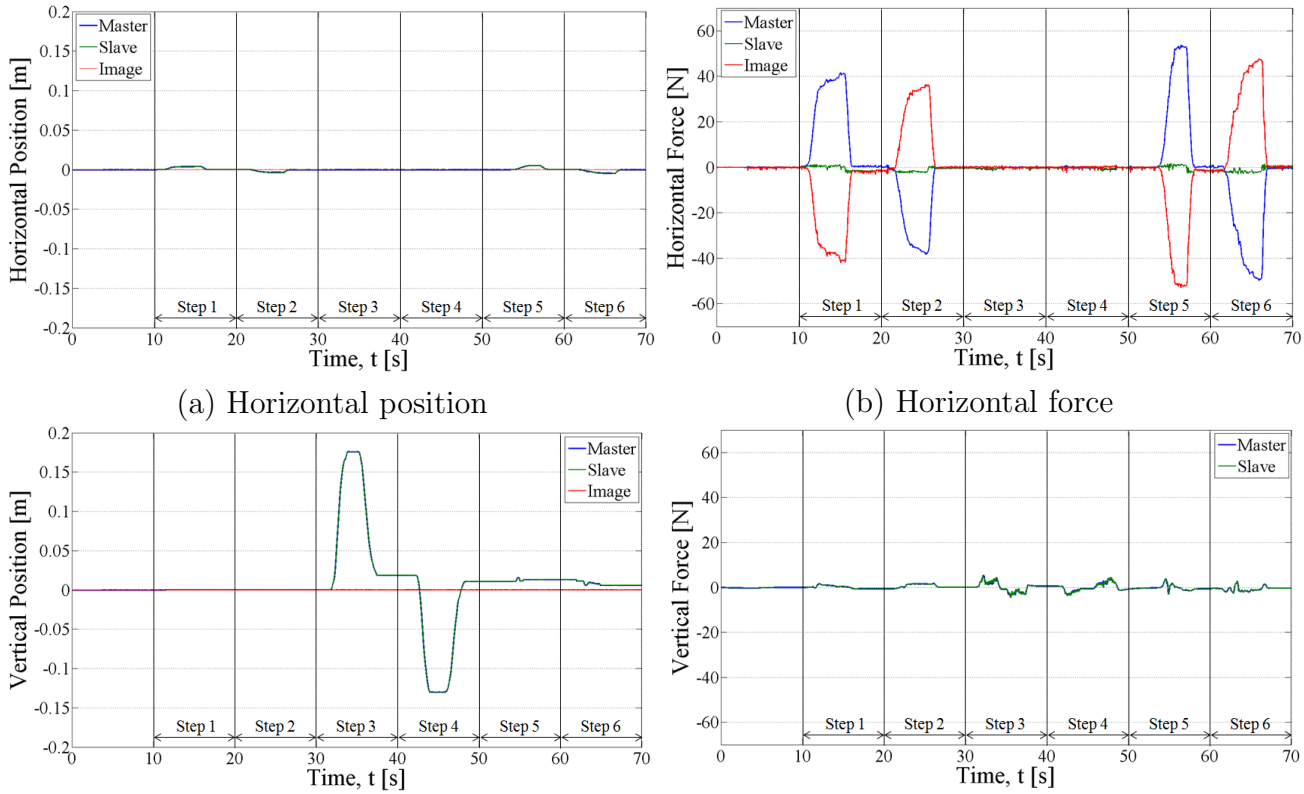

(a) Horizontal position

(b) Horizontal force

(c) Vertical position

(d) Vertical force

Figure 6.10: Experimental results of the system without rotational effect ($\theta = \angle 0°$)

at the master manipulator can freely feel the stiffness of the object (by the slave manipulator) even if the object rotates.

6.6 Summary

In this chapter, the concept of object coordinate rotational effect is introduced. This concept is applied to the proposed integrated vision-based force compliance controller with the bilateral motion control system. As the coordinate of the object is changed, which also including its rotational effect, the axis of the generated force will also get changed in parallel with the rotated axes. The experimental result had confirmed the utility of this method.

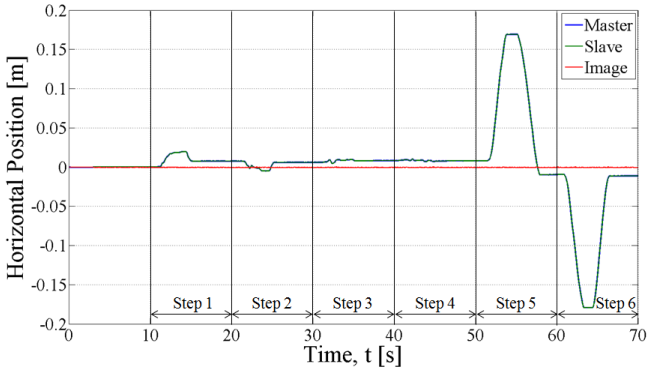

(a) Horizontal position

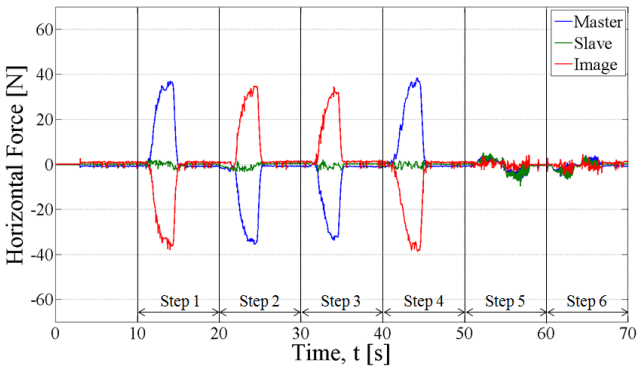

(b) Horizontal force

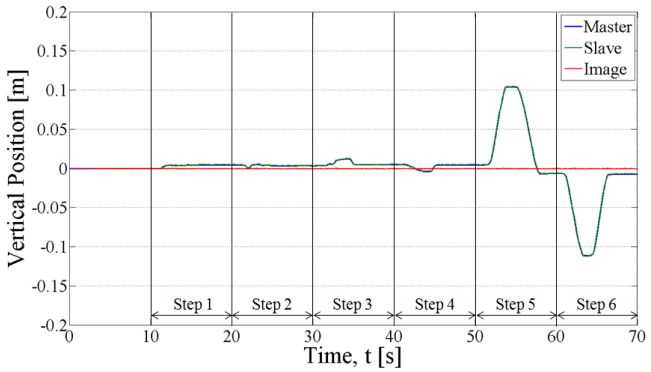

(c) Vertical position

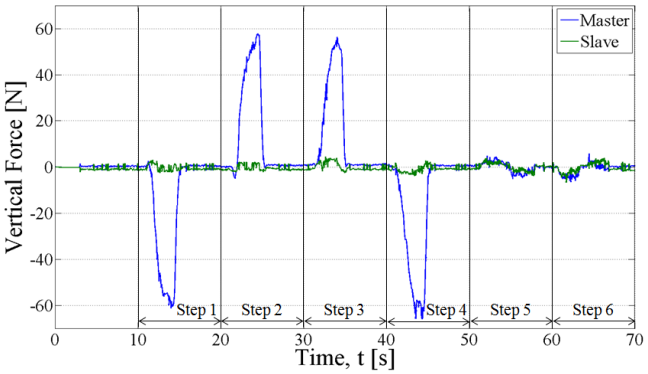

(d) Vertical force

Figure 6.11: Experimental results of the system with rotational effect ($\theta = \angle 45°$)

Chapter 7

Generalized Conclusions

7.1 Executive Summary

In this portion, the conclusions for each chapter, from chapter 1-6 will be explained. In total, this thesis is divided into 7 chapters including this chapter, the generalized conclusions. At the end of this thesis, there are appendix sections that included the special research report, the list of publications and the list of research awards.

In Chapter 1, the background of the research was presented. A vast of literature reviews of past research by other researcher were defined. The reviews cover the topic that related to this study such as in the area of haptic, disturbance observer (DOB), reaction force observer (RFOB), bilateral motion control, vision-based system, visual servoing technique and image processing method. Based on the reviews, it has motivates the author to conduct a research and proposed the new method in haptic bilateral motion control which based on the visual servoing technique.

Hereinafter, Chapter 2 explains the basic concept of motion control for robust bilateral haptic system. To achieve a robust acceleration based control system, the DOB and RFOB control method can be used. Thus, the concepts of both methods were presented in details. In the meantime, the bilateral master–slave manipulator's basic control approach is also introduced. The bilateral control concept uses the total acceleration $\ddot{x}_{dif}$ calculation in the differential mode and total force F_{com} calculation in the common mode on both master and slave systems.

Furthermore, Chapter 3 presents a novel technique of combination and integration of haptic

system with vision-based force compliance controller (VFCC). The system incorporated the bilateral control of master and slave devices with the visual servoing and navigation method. The uniqueness of this proposed system, compared to the other system, is in its ability to treat the visual navigation's of specific object information as a beneficial force that affected the whole system's position and/or force feedback. Hardware components, image processing techniques and control methodologies of the proposed system are presented. The simulation of the proposed control method is conducted which based on the Step input command to study the control performance of the proposed system.

Moreover, Chapter 4 explains the confirmation of the scaling effect on the generated force by the proposed VFCC controller. The scaling effect will occur if the magnification process of the image is held. The system's validity was shown by enhancing a haptic bilateral control's ability to track a moving object without any direct contact. Four experiments were conducted with different camera and object distances to evaluate the effectiveness of the system with and without the implementation of the proposed method. The techniques for a single camera, eye-to-hand approach for this force-based compliance control were considered and discussed. The weighting magnification function α between the camera and the object could be changed according to the size in the image plane. Based on the experimental results, it was verified that the magnification effect for the same object size caused different position and force responses in the horizontal manipulation task. It was also found that the camera–object distance was directly proportional to the scaling ratio between the original size object and the camera captured size. The proposed method of integrating the force-based compliance controller utilizing visual information with a haptic bilateral motion system will be effective at realizing tasks involving careful and precise contact, e.g., microscopic tele-manipulation.

In Chapter 5, the concept of vision-based disturbance observer (VD0B) for bilateral haptic system is introduced. The explanation of the proposed integration technique between the VDOB and VFCC controller is presented. Subsequently, the comparison of its robustness among the present bilateral control is discussed by referring to the conducted experimental data. As a result, the implementation of vision-based disturbance observer that was integrated with the haptic bilateral control system can improved the tracking performance generated by the vision-based force compliance controller (VFCC). Further, the proposed method can compensates the modelling error or occurred force disturbance in the designed system. Thus, the robustness of

the navigating the target object can be achieved.

Lastly, Chapter 6 presents a trajectory navigation method of generating the virtual force by the vision-based force compliance controller (VFCC). The object's rotational effect had been considered in line with the virtual force generation direction in the bilateral manipulator system. The control methodologies for the proposed technique and its experimental results were presented. The projection of new manipulator's navigation trajectory based on the object orientation was realized by considering the **R** (rotational matrix) in the system. Thus, the original behavior of the VFCC (generated force for horizontal manipulator movements) can be utilized. The effectiveness of the proposed method had been examined and discussed. As to confirm the concept of the proposed method, two experiments using two sets of X-Y table had been conducted. From the experimental results, it had been confirmed that the generated force manipulated from the image information of object's trajectory may responses to the system's trajectory respectively. Hence, the proposed method is effective in the applications for the tele-manipulation process of the moving object with specified object's surface.

7.2 Future Research

There are several future works which can be considered and have not done yet because of time limitation. The topics that could be explored and will be the near future research topics are listed as below.

- Implementation of this integration method in more complex trajectories. For further work, this method can be implemented in more complex trajectories, including a redundant manipulator to evaluate its robustness. In this research, the proposed vision-based force compliance control method is applied to be integrated with the bilateral haptic system only with 2 degree-of-freedom (DOF) manipulators.

- Visual servoing technique by using high speed frame-based camera. High speed camera can provide a better image acquisition. Thus, a high speed, high resolution camera can be used to get more precise image information signal of the navigated object from a remote environment. In this study, the object image only be captured by using the conventional USB web-camera with 1.3 megapixels of pixel resolution.

- Implementation of a robust detection method of tracking object. In this study, the image information is gathered based on the blue line marker that pasted on the object surface. For an implementation of tracking method in real application, a robust detection method of the object should be studied. It can be done by referring to the criterion of the object itself, such as shape, color and size.

- Implementation of an image processing on a Linux-based operating system. Conducting the image processing technique on the non real-time operating system will decelerate the performance of the produced response. Thus, in the future a real-time-based operating system should be used for the whole experimental architecture including the image processing method.

Bibliography

[1] M. Lin and K. Salisbury, "Haptic Rendering–Beyond Visual Computing," *IEEE Computer Graphic Application*, Vol. 24, No. 2, pp. 22-23, 2004.

[2] J. Kim, F. J. Sharifi and J. Kim, "A Haptic Interaction Method using Visual Information and Physically Based Modeling," *IEEE Trans. on Mechatronics*, Vol. 15, No. 4, pp. 636-645, 2010.

[3] T. Hachisu, A. Lecuyer, G, Cirio, M. Marchal and H. Kajimoto, "Pseudo-Haptic Feedback Augmented with Visual and Tactile Vibrations," *in Proceedings of the IEEE International Symposium on Virtual reality Innovation*, pp. 327-328, 2011.

[4] R. Cortesao, J. Park and O. Khatib, "Real-Time Adaptive Control for Haptic Telemanipulation With Kalman Active Observers," *IEEE Transactions on Robotics*, Vol. 22, No. 5, pp. 987-999, 2006.

[5] D. Yamashiro, S. Tanaka and H. T. Tanaka, "Active Estimation of Friction Properties with Haptic Vision," *in Proceedings of the International Conference on Control, Automation, Robotics and Vision*, pp. 17-20, 2008.

[6] T. Amemiya and H. Gomi, "Camera pose estimation with a two-dimensional marker Grid for haptic navigation," *in Proceedings of the IEEE Virtual Reality (VR)*, pp. 143-144, 2013.

[7] L. M. D. Diodato, R. Mraz, S. N. Baker and S. J. Graham, "A Haptic Force Feedback Device for Virtual Reality-fMRI Experiments," *IEEE Transactions on Neural Systems and Rehabilitation Engineering*, Vol. 15, No. 4, pp. 570-576, 2007.

[8] K. Inoue and Y. Okamoto, "Vision-Based Detection of Finger Touch for Haptic Device Using Transparent Flexible Sheet," *in Proceeings of the IEEE International Conference on Robotics and Automation*, pp. 665-670, 2009.

[9] K. Sato, K. Kamiyama, H. Nii, N. Kawakami and S. Tachi, "Measurement of Force Vector Field of Robotic Finger using Vision-based Haptic Sensor," *in Proceedings of the IEEE/RSJ International Conference on Intelligent Robots and Systems*, pp. 488-493, 2008.

[10] J. D. Brown, A. Paek, M. Syed, M. K. O'Malley and P. A. Shewokis, "Understanding the Role of Haptic Feedback in a Teleoperated/Prosthetic Grasp and Lift Task," *World Haptics Conference (WHC)*, pp. 271-276, 2013.

[11] A. Mkhitaryan and D. Burschka, "Vision Based Haptic Multisensor for Manipulation of Soft, Fragile Objects," *IEEE Sensors*, Vol. 0, No. 1, pp. 1-4, 2012.

[12] A. Bolopian, Z. Ni, J. Agnus, R. Benosman and S. Regnier, "Stable Haptic Feedback based on a Dynamic Vision Sensor for Microrobotics," *in Proceedings of the IEEE/RSJ International Conference on Intelligent Robots and Systems*, pp. 3203-3208, 2012.

[13] Z. Ni, A. Bolopion, J. Agnus, Ryad Benosman and S. Regnier, "Asynchronous Event-Based Visual Shape Tracking for Stable Haptic Feedback in Microrobotics," *IEEE Transactions on Robotics*, Vol. 28, No. 5, pp. 1081-1089, 2012.

[14] M. Ammi and A. Ferreira, "Realistic Visual and Haptic Rendering for Biological-Cell Injection," *in Proceedings of the IEEE International Conference on Robotics and Automation*, pp. 18-23, 2005.

[15] M. Ammi, H. Ladjal and A. Ferreira, "Evaluation of 3D Pseudo-Haptic Rendering using Vision for Cell Micromanipulation," *in Proceedings of the IEEE/RSJ International Conference on Intelligent Robots and Systems*, pp. 2115-2120, 2006.

[16] A. D. Greer, P. M. Newhook and G. R. Sutherland, "Human–Machine Interface for Robotic Surgery and Stereotaxy," *IEEE/ASME Transactions on Mechatronics*, Vol. 13, No. 3, pp. 355-361, 2008.

[17] C. Casellato, A. Pedrocchi, G. Zorzi, L. Vernisse, G. Ferrigno and N. Nardocci, "EMG-Based Visual-Haptic Biofeedback: A Tool to Improve Motor Control in Children With Primary Dystonia," *IEEE Transactions on Neural Systems and Rehabilitation Engineering*, Vol. 21, No. 3, pp. 474-480, 2013.

[18] S. Akhter, J. Mirsalahuddin, F. B. Marquina, S. Islam and S. Sareen, "A Smartphone-Based Haptic Vision Substitution System for the Blind," *in Proceedings of the IEEE 37th Annual Northeast Bioengineering Conference (NEBEC*, pp. 1-2, 2011.

[19] L. Bowers, M. Bowler and F. Amirabdollahian, "Haptic Cues for Vision Impaired Art Makers: "Seeing" through Touch," *in Proceedings of the IEEE International Conference on Systems, Man, and Cybernetics*, pp. 547-552, 2013.

[20] K. K. Lee, G. Batz and D. Wollherr, "Basketball robot: Ball-On-Plate with Pure Haptic Information," *in Proceedings of the IEEE International Conference on Robotics and Automation*, pp. 2410-2415, 2008.

[21] D. J. Agravante, A. Cherubini, A. Bussy and A. Kheddar, "Human-Humanoid Joint Haptic Table Carrying Task with Height Stabilization using Vision," *in Proceedings of the IEEE/RSJ International Conference on Intelligent Robots and Systems*, pp. 4609-4614, 2013.

[22] A. Widmer and Y. Hu, "Integration of the Senses of Vision and Touch in Perceiving Object Softness," *in Proceedings of the Canadian Conference on Electrical and Computer Engineering*, pp. 1353-1356, 2007.

[23] A. Widmer and Y. Hu, "The role of viewing angle in integrating the senses of vision and touch for perception of object softness," *Canadian Journal on Electrical and Computer Engineering*, Vol. 32, No. 4, pp. 193-198, 2007.

[24] S. Katsura, Y. Matsumoto and K. Ohnishi, "Modeling of Force Sensing and Validation of Disturbance Observer for Force Control," *IEEE Transactions on Industrial Electronics*, Vol. 54, No. 1, pp. 530-538, 2007.

[25] K. Ohishi, K. Ohnishi and K. Miyachi, "Torque-speed regulation od DC-motor based on load torque estimation method," *in Proceedings of IPEC-Tokyo*, pp. 1209-1218, 1983.

[26] E. Sariyildiz and K. Ohnishi, "A Guide to Design Disturbance Observer based Motion Control Systems," *in Proceedings of International Power Electronics Conference*, pp. 2483-2488, 2014.

[27] Q. W. Jia, "Disturbance Rejection Through Disturbance Observer With Adaptive Frequency Estimation," *IEEE Transactions on Magnetics*, Vol. 45, No. 6, pp. 2675-2678, 2009.

[28] R. G. Montague, C. M. Bingham and K. Atallah, "Dual-observer-based position-servo control of a magnetic gear," *IET Electric Power Applications*, Vol. 5, No. 9, pp. 708-714, 2011.

[29] K. S. Kim, K. H. Rew and S. Kim, "Disturbance Observer for Estimating Higher Order Disturbances in Time Series Expansion," *IEEE Transactions on Automatic Control*, Vol. 55, No. 8, pp. 1905-1911, 2010.

[30] H. Kobayashi, S. Katsura and K. Ohnishi, "An Analysis of Parameter Variations of Disturbance Observer for Motion Control," *IEEE Transactions on Industrial Electronics*, Vol. 54, No. 6, pp. 3413-3421, 2007.

[31] A. Tesfaye, H. S. Lee and M. Tomizuka, "A Sensitivity Optimization Approach to Design of a Disturbance Observer in Digital Motion Control Systems," *IEEE/ASME Transactions on Mechatronics*, Vol. 5, No. 1, pp. 32-38, 2000.

[32] M. Bertoluzzo, G. S. Buja and E. Stampacchia, "The performance analysis of a high-bandwidth torque disturbance observer compensator," *IEEE/ASME Transactions on Mechatronics*, Vol. 9, No. 4, pp. 653-660, 2004.

[33] S. Katsura, K. Irie and K. Ohishi, "Wideband Force Control by Position-Acceleration Integrated Disturbance Observer," *IEEE Transactions on Industrial Electronics*, Vol. 55, No. 4, pp. 1699-1706, 2008.

[34] Z. Gao, X. Shi and S. X. Ding, "Correspondence Systems With Application to Sensor Fault Estimation," *IEEE Transactions on Systems, Man, and Cybernetics, Part B (Cybernetics)*, Vol. 38, No. 3, pp. 875-880, 2008.

[35] J. Yang, S. Li and X. Yu, "Sliding-Mode Control for Systems With Mismatched Uncertainties via a Disturbance Observer," *IEEE Transactions on Industrial Electronics*, Vol. 60, No. 1, pp. 160-169, 2013.

[36] J. Han, "From PID to Active Disturbance Rejection Control," *IEEE Transactions on Industrial Electronics*, Vol. 56, No. 3, pp. 900-906, 2009.

[37] Z. Y. Chu, J. Cui and F. C. Sun, "Fuzzy Adaptive Disturbance-Observer-Based Robust Tracking Control of Electrically Driven Free-Floating Space Manipulator," *IEEE Systems Journal*, Vol. 8, No. 2, pp. 343-352, 2014.

[38] D. Xing, J. Su, Y. Liu and J. Zhong, "Robust approach for humanoid joint control based on a disturbance observer," *IET Control Theory and Applications*, Vol. 5, No. 14, pp. 1630-1636, 2011.

[39] S. Komada, N. Machii and T. Hori, "Control of Redundant Manipulators Considering Order of Disturbance Observer," *IEEE Transactions on Industrial Electronics*, Vol. 47, No. 2, pp. 413-420, 2000.

[40] W. Kim, D. Shin, D. Won and C. C. Chung, "Disturbance-Observer-Based Position Tracking Controller in the Presence of Biased Sinusoidal Disturbance for Electrohydraulic Actuators," *IEEE Transactions on Control Systems Technology*, Vol. 21, No. 6, pp. 2290-2298, 2013.

[41] S. Sadhu and T. K. Ghoshal, "Sight Line Rate Estimation in Missile Seeker Using Disturbance Observer-Based Technique," *IEEE Transactions on Control Systems Technology*, Vol. 19, No. 2, pp. 449-454, 2011.

[42] K. Natori and K. Ohnishi, "A Design Method of Communication Disturbance Observer for Time-Delay Compensation, Taking the Dynamic Property of Network Disturbance Into Account," *IEEE Transactions on Industrial Electronics*, Vol. 55, No. 5, pp. 2152-2168, 2008.

[43] E. Kim and S. Lee, "Output Feedback Tracking Control of MIMO Systems Using a Fuzzy Disturbance Observer and its Application to the Speed Control of a PM Synchronous Motor," *IEEE Transactions on Fuzzy Systems*, Vol. 13, No. 6, pp. 725-741, 2005.

[44] S. H. Lee, H. J. Kang and C. C. Chung, "Robust Fast Seek Control of a Servo Track Writer Using a State Space Disturbance Observer," *IEEE Transactions on Control Systems Technology*, Vol. 20, No. 2, pp. 346-355, 2012.

[45] M. T. White, M. Tomizuka and C. Smith, "Improved Track Following in Magnetic Disk Drives Using a Disturbance Observer," *IEEE/ASME Transactions on Mechatronics*, Vol. 5, No. 1, pp. 3-11, 2000.

[46] T. R. Grochmal and A. F. Lynch, "Precision Tracking of a Rotating Shaft With Magnetic Bearings by Nonlinear Decoupled Disturbance Observers," *IEEE Transactions on Control Systems Technology*, Vol. 15, No. 6, pp. 1112-1121, 2007.

[47] W. H. Chen, D. J. Ballance, P. J. Gawthrop and J. O'Reilly, "A Nonlinear Disturbance Observer for Robotic Manipulators," *IEEE Transactions on Industrial Electronics*, Vol. 47, No. 4, pp. 932-938, 2000.

[48] W. H. Chen, "Disturbance Observer Based Control for Nonlinear Systems," *IEEE/ASME Transactions on Mechatronics*, Vol. 9, No. 4, pp. 706-710, 2004.

[49] A. Mohammadi, M. Takavoli and H. J. Marquez, "Disturbance observer-based control of non-linear haptic teleoperation systems," *IET Control Theory and Applications*, Vol. 5, No. 18, pp. 2063-2074, 2011.

[50] M. Chen and S. S. Ge, "Direct Adaptive Neural Control for a Class of Uncertain Nonaffine Nonlinear Systems Based on Disturbance Observer," *IEEE Transactions on Cybernetics*, Vol. 43, No. 4, pp. 1213-1225, 2013.

[51] E. Sariyildiz and K. Ohnishi, "A Comparison Study for Force Sensor and Reaction Force Observer based Robust Force Control Systems," *in Proceedings of the IEEE 23rd International Conference on Industrial Electronics*, pp. 1156-1161, 2014.

[52] E. Sariyildiz and K. Ohnishi, "An Adaptive Reaction Force Observer Design," *IEEE/ASME Transactions on Mechatronics*, Vol. 20, No. 2, pp. 750-760, 2015.

[53] T. Shimono, K. Nezu and M. Aboshi, "Variable Contact Force Control based on Reaction Force Control with Adjustment Ratio," *in Proceedings of the IEEE International Power Electronics Conference*, No. 2, pp. 2545-2550, 2010.

[54] T. Nozaki, T. Mizoguchi and K. Ohnishi, "Decoupling Strategy for Position and Force Control Based on Modal Space Disturbance Observer," *IEEE Transactions on Industrial Electronics*, Vol. 61, No. 2, pp. 1022-1032, 2014.

[55] A. C. Smith, F. Mobasser and K. H. Zaad, "Neural-Network-Based Contact Force Observers for Haptic Applications," *IEEE Transactions on Robotics*, Vol. 22, No. 6, pp. 1163-1175, 2006.

[56] T. T. Phuong, K. Ohishi, Y. Yokokura and C. Mitsantisuk, "FPGA-Based High-Performance Force Control SystemWith Friction-Free and Noise-Free Force Observation," *IEEE Transactions on Industrial Electronics*, Vol. 61, No. 2, pp. 994-1008, 2014.

[57] F. Mobasser and K. H. Zaad, "A Model-Independent Force Observer for Teleoperation Systems," *in Proceedings of the IEEE International Conference on Mechatronics and Automation*, pp. 964-969, 2005.

[58] N. Popescu, M. Ivanescu and D. Popescu, "Force Observer-Based Control for a Rehabilitation Hand Exoskeleton System," *in Proceedings of the 9th Asian Control Conference*, pp. 1-6, 2013.

[59] M. C. Lee, C. Y. Kim, B. Yao, W. J. Peine and Y. E. Song, "Reaction Force Estimation of Surgical Robot Instrument Using Perturbation Observer with SMCSPO Algorithm," *in Proceedings of the IEEE/ASME International Conference on Advanced Intelligent Mechatronics*, pp. 181-186, 2010.

[60] S. Katsura, Y. Matsumoto and K. Ohnishi, "Realization of "Law of Action and Reaction" by Multilateral Control," *IEEE Transactions on Industrial Electronics*, Vol. 52, No. 5, pp. 1196-1205, 2005.

[61] Y. Izumikawa, K. Yubai and J. Hirai, "Fault-Tolerant Control System of Flexible Arm for Sensor Fault by Using Reaction Force Observer," *IEEE/ASME Transactions on Mechatronics*, Vol. 10, No. 4, pp. 391-396, 2005.

[62] S. Katsura and K. Ohnishi, "Force Servoing by Flexible Manipulator Based on Resonance Ratio Control," *IEEE Transactions on Industrial Electronics*, Vol. 54, No. 1, pp. 539-547, 2007.

[63] S. Katsura, Y. Matsumoto and K. Ohnishi, "Analysis and Experimental Validation of Force Bandwidth for Force Control," *IEEE Transactions on Industrial Electronics*, Vol. 53, No. 3, pp. 922-928, 2006.

[64] T. J. Ren and T. C. Chen, "Modelling and control of a power-assisted mobile vehicle based on torque observer," *IET Control Theory and Applications*, Vol. 1, No. 5, pp. 1405-1412, 2007.

[65] K. Nam, H. Fujimoto and Y. Hori, "Advanced Motion Control of Electric Vehicles Based on Robust Lateral Tire Force Control via Active Front Steering," *IEEE/ASME Transactions on Mechatronics*, Vol. 19, No. 1, pp. 289-299, 2014.

[66] K. Ohishi, T. Miyazaki, K. Inomata, H. Yanagisawa, D. Koide and H. Tokumaru, "Robust Tracking Servo System Considering Force Disturbance for the Optical Disk Recording System," *IEEE Transactions on Industrial Electronics*, Vol. 53, No. 3, pp. 838-847, 2006.

[67] S. Yamaoka and K. Ohnishi, "Reaction Force Estimation of Piezoelectric Actuator by Charge Observation," *in Proceedings of the IEEE International Conference on Mechatronics (ICM)*, pp. 192-197, 2013.

[68] X. Wang, X. Sun, S. Li and H. Ye, "Output feedback domination approach for finite-time force control of an electrohydraulic actuator," *IET Control Theory and Applications*, Vol. 6, No. 7, pp. 921-934, 2012.

[69] T. S. Hwang and J. K. Seok, "Observer-Based Ripple Force Compensation for Linear Hybrid Stepping Motor Drives," *IEEE Transactions on Industrial Electronics*, Vol. 54, No. 5, pp. 2417-2424, 2007.

[70] C. Mitsantisuk, S. Katsura and K. Ohishi, "Force Control of Human – Robot Interaction Using Twin Direct-Drive Motor System Based on Modal Space Design," *IEEE Transactions on Industrial Electronics*, Vol. 57, No. 4, pp. 1383-1392, 2010.

[71] K. Iwazaki, K. Ohishi, Y. Yokokura, K. Kageyama, M. Takatsu and S. Urushihara, "Robust Sensorless Pressure Control of Electric Injection Molding Machine using Friction-Free Force Observer," *in Proceedings of the IEEE 13th International Workshop on Advanced Motion Control (AMC)*, pp. 43-48, 2014.

[72] Y. Ohba, M. Sazawa, K. Ohishi, T. Asai, K. Majima, Y. Yoshizawa and K. Kageyama, "Sensorless Force Control for Injection Molding Machine Using Reaction Torque Observer," *IEEE Transactions on Industrial Electronics*, Vol. 56, No. 8, pp. 2955-2960, 2009.

[73] T. Shimono, S. Katsura and K. Ohnishi, "Abstraction and Reproduction of Force Sensation From Real Environment by Bilateral Control," *IEEE Transactions on Industrial Electronics*, Vol. 54, No. 2, pp. 907-918, 2007.

[74] H. Tanaka, K. Ohnishi, H. Nishi, T. Kawai, Y. Morikawa, S. Ozawa and T. Furukawa, "Implementation of Bilateral Control System Based on Acceleration Control Using FPGA for Multi-DOF Haptic Endoscopic Surgery Robot," *IEEE Transactions on Industrial Electronics*, Vol. 56, No. 3, pp. 618-627, 2009.

[75] K. Tanida and K. Ohnishi, "Analysis of Operational Force Under Non-ideal Condition for Bilateral Control," *in Proceedings of IEEE 13th International Workshop on Advanced Motion Control (AMC)*, pp. 308-313, 2014.

[76] C. Mitsantisuk, K. Ohishi and S. Katsura, "Estimation of Action / Reaction Forces for the Bilateral Control Using Kalman Filter," *IEEE Transactions on Industrial Electronics*, Vol. 59, No. 11, pp. 4383-4393, 2012.

[77] C. Mitsantisuk and K. Ohishi, "Multi-Sensor Fusion Observer based Multilatral Control of Haptic Devices Without Force Sensor," *in Proceedings of the IEEE 13th International Workshop on Advanced Motion Control (AMC)*, pp. 79-84, 2014.

[78] A. Suzuki and K. Ohnishi, "Frequency-Domain Damping Design for Time-Delayed Bilateral Teleoperation System Based on Modal Space Analysis," *IEEE Transactions on Industrial Electronics*, Vol. 60, No. 1, pp. 177-190, 2013.

[79] A. Haddadi and K. H. Zaad, "Bounded-Impedance Absolute Stability of Bilateral Teleoperation Control Systems," *IEEE Transactions on Haptics*, Vol. 3, No. 1, pp. 15-27, 2010.

[80] R. Kubo, T. Shimono and K. Ohnishi, "Flexible Controller Design of Bilateral Grasping Systems Based on a Multilateral Control Scheme," *IEEE Transactions on Industrial Electronics*, Vol. 56, No. 1, pp. 62-68, 2009.

[81] D. Lee and P. Y. Li, "Passive bilateral control and tool dynamics rendering for nonlinear mechanical teleoperators," *IEEE Transactions on Robotics*, Vol. 21, No. 5, pp. 936-951, 2005.

[82] M. Tavakoli, A. Aziminejad, R. V. Patel and M. Moallem, "High-Fidelity Bilateral Teleoperation Systems and the Effect of Multimodal Haptics," *IEEE Transactions on Systems, Man, and Cybernetics, Part B (Cybernetics)*, Vol. 37, No. 6, pp. 1512-1528, 2007.

[83] P. H. Chang and J. Kim, "Telepresence Index for Bilateral Teleoperations," *IEEE Transactions on Systems, Man, and Cybernetics, Part B (Cybernetics)*, Vol. 42, No. 1, pp. 81-92, 2012.

[84] Q. M. Le, M. T. Pham, M. Tavakoli, R. Moreau, J. P. Simon and T. Redarce, "Bilateral Control of Nonlinear Pneumatic Teleoperation System With Solenoid Valves," *IEEE Transactions on Control Systems Technology*, Vol. 21, No. 4, pp. 1463-1470, 2013.

[85] A. Suzuki and K. Ohnishi, "Novel Four-Channel Bilateral Control Design for Haptic Communication Under Time Delay Based on Modal Space Analysis," *IEEE Transactions on Control Systems Technology*, Vol. 21, No. 3, pp. 882-890, 2013.

[86] D. Tian, D. Yashiro and K. Ohnishi, "Wireless Haptic Communication Under Varying Delay by Switching-Channel Bilateral Control With Energy Monitor," *IEEE/ASME Transactions on Mechatronics*, Vol. 17, No. 3, pp. 488-498, 2012.

[87] J. M. Daly and D. W. L. Wang, "Time-Delayed Output Feedback Bilateral TeleoperationWith Force Estimation for n-DOF Nonlinear Manipulators," *IEEE Transactions on Control Systems Technology*, Vol. 22, No. 1, pp. 299-306, .

[88] M. Franken, S. Stramigioli, S. Misra, C. Secchi and A. Macchelli, "Bilateral Telemanipulation With Time Delays : A Two-Layer Approach Combining Passivity and Transparency," *IEEE Transactions on Robotics*, Vol. 27, No. 4, pp. 741-756, 2011.

[89] S. Islam, P. X. Liu, A. E. Saddik and Y. B. Yang, "Bilateral Control of Teleoperation Systems With Time Delay," *IEEE/ASME Transactions on Mechatronics*, Vol. 20, No. 1, pp. 1-12, 2015.

[90] S. Nurung and I. Nilkhamhang, "A Robust Adaptive Algorithm for Bilateral Control System without Force Sensor with Time Delay," *in Proceedings of the SICE Annual Conference*, pp. 678-683, 2010.

[91] T. Ohta and T. Murakami, "A Stabilization Control of Bilateral System With Time Delay by Vibration Index—Application to Inverted Pendulum Control," *IEEE Transactions on Industrial Electronics*, Vol. 56, No. 5, pp. 1595-1603, 2009.

[92] V. Chawda and M. K. O'Malley, "Position Synchronization in Bilateral Teleoperation Under Time-Varying Communication Delays," *IEEE Transactions on Mechatronics*, Vol. 20, No. 1, pp. 245-253, 2015.

[93] Z. Y. Pan and J. Gu, "Adaptive robust control of bilateral teleoperation systems with unmeasurable environmental force and arbitrary time delays," *IET Control Theory and Applications*, Vol. 8, No. 15, pp. 1456-1464, 2014.

[94] T. Mizoguchi, T. Nozaki and K. Ohnishi, "Stiffness Transmission of Scaling Bilateral Control System by Gyrator Element Integration," *IEEE Transactions on Industrial Electronics*, Vol. 61, No. 2, pp. 1033-1043, 2014.

[95] S. Sakaino, T. Sato and K. Ohnishi, "Multi-DOF Micro-Macro Bilateral Controller Using Oblique Coordinate Control," *IEEE Transactions on Industrial Informatics*, Vol. 7, No. 3, pp. 446-454, 2011.

[96] O. Schreer, P. Eisert, P. Kauff, R. Tanger and R. Englert, "TOWARDS ROBUST INTUITIVE VISION-BASED USER INTERFACES," *in Proceedings of the ICME*, pp. 69-72, 2006.

[97] J. Sreng, A. Lecuyer, C. Megard and C. Andriot, "Using Visual Cues of Contact to Improve Interactive Manipulation of Virtual Objects in Industrial Assembly / Maintenance Simulations," *IEEE Transactions on Visualization and Computer Graphics*, Vol. 12, No. 5, pp. 1013-1020, 2006.

[98] B. Fang, F. Oliveira and F. Quek, "Using Vision Based Tracking to Support Real-Time Graphical Instruction for StudentsWho Have Visual Impairments," *in Proceedings of the*

IEEE Computer Society Conference on Computer Vision and Pattern Recognition - Workshops, pp. 9-14, 2010.

[99] J. Pomares and F. Torres, "Movement-Flow-Based Visual Servoing and Force Control Fusion for Manipulation Tasks in Unstructured Environments," *IEEE Transactions on Systems, Man and Cybernetics, Part C (Applications and Reviews)*, Vol. 35, No. 1, pp. 4-15, 2005.

[100] K. Kamiyama, K. Vlack, T. Mizota, H. Kajimoto, N. Kawakami and S. Tachi, "Vision-Based Sensor for Real- Time Measuring of Surface Traction Fields," *IEEE Computer Graphics and Applications*, pp. 68-75, 2005.

[101] R. Carloni, V. Lippiello, M. D'Auria, M. Fumagalli, A. Y. Mersha, S. Stramigioli and B. Siciliano, "Obstacle-Avoidance Techniques for Unmanned Aerial Vehicles," *IEEE Robotics and Automation Magazine*, pp. 22-31, 2013.

[102] C. S. Ha and D. Lee, "Vision-Based Teleoperation of Unmanned Aerial and Ground Vehicles," *in Proceedings of the IEEE International Conference on Robotics and Automation*, pp. 1465-1470, 2013.

[103] C. S. Ha and D. Lee, "Preliminary result of vision-based teleoperation of an UAV and UGVs team," *in Proceedings of the IEEE 10th International Conference on Ubiquitous Robots and Ambient Intelligence (URAI)*, pp. 128, 2013.

[104] E. C. D. Leon, V. P. Vega and E. Romero, "Visual Servoing for Constrained Planar Robots Subject to Complex Friction," *IEEE/ASME Transactions on Mechatronics*, Vol. 11, No. 4, pp. 389-400, 2006.

[105] C. H. Park and A. M. Howard, "Vision-based Force Guidance for Improved Human Performance in a Teleoperative Manipulation System," *in Proceedings of the IEEE/RSJ International Conference on Intelligent Robots and Systems*, pp. 2126-2131, 2007.

[106] N. Bartolini, G. Bongiovanni, T. F. L. Porta and S. Silvestri, "On the Vulnerabilities of the Virtual Force Approach to Mobile Sensor Deployment," *IEEE Transactions on Mobile Computing*, Vol. 13, No. 11, pp. 2592-2605, 2014.

[107] C. Liu and J. Wu, "Virtual-Force-Based Geometric Routing Protocol in MANETs," *IEEE Transactions on Parallel and Distributed Systems*, Vol. 20, No. 4, pp. 433-445, 2009.

[108] N. Oda, S. Mabuchi and N. Aizawa, "Interactive Control against Obstacle for Power Assisted Wheelchair by Vision-based Reaction Force Observer," *in Proceedings of the IEEE International Workshop on Advanced Motion Control*, pp. 216-221, 2010.

[109] P. K. Allen, B. Yoshimi and A. Timcenko, "Real-Time Visual Servoing," *in Proceedings of the IEEE International Conference on Robotics and Automation*, pp. 851-856, 1991.

[110] G. Simas, R. D. Bem, L. Novelo, G. Fickel and S. Botelho, "Visual Tracking Based on 3D Probabilistic Reconstruction," *in Proceedings of the IEEE International Conference and Workshops on Engineering of Computer Based Systems*, pp. 403-409, 2010.

[111] H. Hile, A. Liu, G. Borriello, R. Grzeszczuk and R. Vedantham, "Visual Navigation for Mobile Devices," *IEEE Multimedia*, pp. 16-25, 2010.

[112] F. B. Font, A. Burguera, A. Ortiz and G. Oliver, "Concurrent visual navigation and localisation using inverse perspective transformation," *Electronics Letters*, Vol. 48, No. 5, pp. 264-265, 2012.

[113] N. N. Bhat, "Real Time Robust Hand Gesture Recognition and Visual Servoing Nagaraj," *Annual IEEE India Conference (INDICON)*, pp. 1153-1157, 2012.

[114] R. Liu and Y. X. Wang, "Auditory Feedback and Sensory Substitution During Teleoperated Navigation," *IEEE/ASME Transactions on Mechatronics*, Vol. 17, No. 4, pp. 680-686, 2012.

[115] A. Goto and H. Fujimoto, "Proposal of 6 DOF Visual Servoing for Moving Object Based on Real-Time Distance Identification," *SICE Annual Conference*, pp. 3208-3213, 2008.

[116] M. Liu, C. Pradalier and R. Siegwart, "Visual Homing From Scale With an Uncalibrated Omnidirectional Camera," *IEEE Transactions on Robotics*, Vol. 29, No. 6, pp. 1353-1365, 2013.

[117] J. Gaspar, N. winters and J. S. Victor, "Vision-Based Navigation and Environmental Representations with an Omnidirectional Camera," *IEEE Transactions on Robotics and Automation*, Vol. 16, No. 6, pp. 890-898, 2000.

[118] L. Ge and Z. Jie, "A Real-time Stereo Visual Servoing for Moving Object Grasping Based Parallel Algorithms," *in Proceedings of the IEEE Conference on Industrial Electronics and Applications*, pp. 2886-2891, 2007.

[119] S. H. Han, W. H. Seo, K. S. Yoon and M. H. Lee, "Real-Time Control of an Industrial Robot Using Image-Based Visual Servoing," *in Proceedings of the IEEE/RSJ International Conference on Intelligent Robots and Systems*, pp. 1762-1767, 1999.

[120] H. Liu, D. Liu and Y. X. Yang, "Research of Real Time Robot Visual Servoing Based on Genetic Algorithm," *in Proceedings of the International Conference on Machine Learning and Cybernatics*, pp. 87-90, 2002.

[121] C. L. Hwang, Y. J. Chou and C. W. Lan, "Comparisons Between Two Visual Navigation Strategies for Kicking to Virtual Target Point of Humanoid Robots," *IEEE Transactions on Instrumentation and Measurement*, Vol. 62, No. 11, pp. 3050-3063, 2013.

[122] S. Ishikawa, H. Kuwamoto and S. Ozawa, "Visual Navigation of an Autonomous Vehicle Using White Line Recognition," *IEEE Transactions on Pattern Analysis and Machine Intelligence*, Vol. 10, No. 5, pp. 743-749, 1988.

[123] A. Cherubini, F. Spindler and F. Chaumette, "Autonomous Visual Navigation and Laser-Based Moving Obstacle Avoidance," *IEEE Transactions on Intelligent Transportation Systems*, Vol. 15, No. 5, pp. 2101-2110, 2014.

[124] S. Salazar, H. Romero, J. Gomez and R. Lozano, "Real-time Stereo Visual Servoing Control of an UAV having Eight-Rotors," *in Proceedings of the IEEE International Conference on Electrical Engineering, Computing Science and Automatic Control (CCE)*, pp. 1-11, 2009.

[125] L. Lucchese and S. K. Mitra, "A New Class of Chromatic Filters for Color Image Processing. Theory and Applications," *IEEE Transactions on Image Processing*, Vol. 13, No. 4, pp. 534-548, 2004.

[126] G. Langfelder, F. Zaraga, A. Longoni and C. Buffa, "Adaptation to the Scene in Color Imaging," *IEEE Sensors Journal*, Vol. 11, No. 9, pp. 1979-1986, 2011.

[127] G. Louverdis and I. Andreadis, "Design and Implementation of a Fuzzy Hardware Structure for Morphological Color Image Processing," *IEEE Transactions on Circuits and Systems for Video Technology*, Vol. 13, No. 3, pp. 277-288, 2003.

[128] P. Tokarczyk, J. D. wegner, S, Walk and K. Schindler, "Features, Color Spaces, and Boosting: New Insights on Semantic Classification of Remote Sensing Images," *IEEE Transactions on Geoscience and Remote Sensing*, Vol. 53, No. 1, pp. 280-295, 2015.

[129] V. Gradisnik, M. Pavlovic, B. Pivac and I. Zulim, "Study of the Color Detection of a-Si :H by Transient Response in the Visible Range," *IEEE Transactions on Electron Devices*, Vol. 49, No. 4, pp. 550-556, 2002.

[130] D. R. Martin, C. C. Fowlkes and J. Malik, "Learning to Detect Natural Image Boundaries Using Local Brightness, Color, and Texture Cues," *IEEE Transactions on Pattern Analysis and Machine Intelligence*, Vol. 26, No. 5, pp. 530-549, 2004.

[131] R. Ramanath, W. E. Snyder, Y. Yoo and M. S. Drew, "Color Image Processing Pipeline," *IEEE Signal Processing Magazine*, pp. 34-43, 2005.

[132] A. Koschan and M. Abidi, "Detection and Classification of Edges in Color Images," *IEEE Signal Processing Magazine*, pp. 64-73, 2005.

[133] S. Charaa and N. Ellouze, "Multiscale Product Edge Detection in Different Colour Spaces," *in Proceedings of the 11th IEEE International Conference on Information Technology: New Generations*, pp. 660-664, 2014.

[134] M. P. Krishna, A. Sriram and N. B. Puhan, "Clustering based Image Binarization in Palm Leaf Manuscripts," *in Proceedings of the IEEE International Advance Computing Conference (IACC)*, pp. 1060-1065, 2014.

[135] S. W. Jung, "Image Contrast Enhancement Using Color and Depth Histograms," *IEEE Signal Processing Letters*, Vol. 21, No. 4, pp. 382-385, 2014.

[136] H. Kavitha and M. V. Sudhamani, "Object Based Image Retrieval from Database Using Combined Features," *in Proceedings of the IEEE International Conference on Signal and Image Processing*, pp. 161-165, 2014.

[137] M. J. Chen, M. C. Chi, C.T. Hsu and J. W. Chen, "ROI Video Coding Based on H.263+ with Robust Skin-Color Detection Technique," *IEEE Transactions on Consumer Electronics*, Vol. 49, No. 3, pp. 724-730, 2003.

[138] L. Liu, N. Sang, S. Yang and R. Huang, "Real-Time Skin Color Detection under Rapidly Changing Illumination Conditions," *IEEE Transactions on Consumer Electronics*, Vol. 57, No. 3, pp. 1295-1302, 2011.

[139] G. Morel, E. Malis and S. Boudet, "Impedence Based Combination of Visual and Force Control", *in Proceedings of the 1998 IEEE International Conference on Robotics and Automation*, pp. 1743-1748, 1998.

[140] H. Kawai, T. Murao and M. Fujita, "Passivity-based Visual Force Feedback Control for Planar Manipulators with Eye-in-Hand Configuration", *in Proceedings of the* 16^{th} *IEEE International Conference on Control Applications*, pp. 1480-1485, 2007.

[141] J. Pomares, P. Gil, G. J. Garcia and F. Torres, "Visual - Force Control and Structured Light Fusion to Improve Recognition of Discontinuities in Surfaces", *in Proceedings of the IEEE Conference on Emerging Technologies and Factory Automation*, pp. 1044-1050, 2006.

[142] L. E. P. Williams, R. B. Loftin, H. A. Aldridge, E. L. Leiss and W. J. Bluethmann, "Kinesthetic and Visual Force Display for Telerobotics", *in Proceedings of the IEEE International Conference on Robotics and Automation*, pp. 1249-1254, 2002.

[143] M. Staniak, T. Winiarski and C. Zielinski, "Parallel Visual-Force Control", *in Proceedings of the IEEE/RSJ International Conference on Intelligent Robots and Systems*, pp. 937-942, 2008.

[144] H. Kawai, T. Murao and M. Fujita, "Passivity-based Dynamic Visual Force Feedback Control for Fixed Camera Systems", *in Proceedings of the* 16^{th} *IEEE International Symposium on Intelligent Control*, pp. 426-431, 2008.

[145] H. Huang, D. Sun, J. K. Mills and W. J. Li, "Visual-based Impedence Force Control of Three-dimensional Cell Injection System", *in Proceedings of the IEEE International Conference on Robotics and Automation*, pp. 4196-4201, 2007.

[146] C. S. Kim, W. H. Seo, S. H. Han and O. Khatib, "Fuzzy Logic Control of a Robot Manipulator Based on Visual Servoing", *in Proceedings of the IEEE International Symposium on Industrial Electronics*, Vol. 3, pp. 1597-1602, 2001.

[147] D. C. Ruspini, K. Kolarov and O. Khatib, "Haptic Interaction in Virtual Environments", *in Proceedings of the IEEE/RSJ International Conference on Intelligent Robots and Systems*, pp. 128-133, 1997.

[148] A. Namiki, Y. Nakabo, I. Ishii and M. Ishikawa, "High Speed Grasping Using Visual and Force Feedback", *in Proceedings of the IEEE International Conference on Robotics and Automation*, pp. 3195-3200, 1999.

[149] G. Ma, Q. Huang, Z. Yu, X. Chen, W. Zhang, J. Gao, L. Meng and Y. H. Liu, "A New Flexible Controller for a Humanoid Robot That Considers Visual and Force Information Interaction", *in Proceedings of the IEEE International Conference on Robotics and Automation*, pp. 1036-1041, 2014.

[150] W. Hou, S. Shen and A. Sterr, "An MRI Compatible Visual Force-Feedback System for the Study of Force Control Mechanics", *in Proceedings of the IEEE Engineering in Medicine and Biology Annual Conference*, pp. 3687-3690, 2005.

[151] K. Ohnishi, N. Matsui and Y. Hori, "Estimation, Identification, and Sensorless Control in Motion Control System," *Proceedings of the IEEE*, Vol. 82, No. 8, pp. 1253-1265, 1994.

[152] K. Ohnishi, S. Katsura and T. Shimono, "Motion Control for Real World Haptics," *IEEE Industrial Electronics Magazine*, Vol. 4, No. 2, pp. 16-19, 2010.

[153] T. Murakami, F. Yu, and K. Ohnishi, "Torque Sensorless Control in Multidegree-of-Freedom Manipulator," *IEEE Transactions on Industrial Electronics*, Vol. 40, No. 2, pp. 259-265, 1993.

[154] N. Oda, M. Ito and M. Shibata, "Vision-based Motion Control for Robotic Systems," *IEEJ Trans. on Electrical and Electronic Engineering*, Vol. 4, No. 2, pp. 176-183, 2009.

[155] H. D. Taghirad, S. F. Atashzar and M. Shahbazi, "Robust Solution on Three-dimensional Pose Estimation using Composite Extended Kalman Observer and Kalman Filter," *IET Computer Vision*, Vol. 6, No. 2, pp. 140-152, 2012.

[156] B. Tamadazte, N. L. F. Piat and E. Marchand, "A Direct Visual Servoing Scheme for Automatic Nanopositioning," *IEEE/ASME Trans. on Mechatronics*, Vol. 17, No. 4, pp. 728-736, 2012.

[157] W. Bachta, P. Renaud, E. Laroche, A. Forgione and J. Gangloff, "Active Stabilization for Robotized Beating Heart Surgery," *IEEE Trans. on Robotics*, Vol. 27, No. 4, pp. 757-767, 2011.

[158] Y. Nakajima, T. Nozaki, Y. Oyamada and K. Ohnishi, "Object-Coordinate Based Bilateral Control System using Visual Information," *IEEJ Trans. on Industry Applications*, Vol. 132, No. 3, pp. 374-380, 2012.

[159] A. Muis and K. Ohnishi, "Soft Pushing Operation with Dual Compliance Controllers Based on Estimated Torque and Visual Force," *IEEJ Trans. on Industry Applications*, Vol. 127, No. 5, pp. 518-527, 2007.

[160] N. V. Navkar, Z. Deng, D. J. Shah, K. E. Bekris and N. V. Tsekos, "Visual and Force-Feedback Guidance for Robot-Assisted Interventions in the Beating Heart with Real-Time MRI," *in Proceeding of IEEE International Conference on Robotics and Automation*, pp. 689-694, 2012.

[161] M. Kuschel, M. D. Luca, M. Buss and R. L. Klatzky, "Combination and Integration in the Perception of Visual-Haptic Compliance Information," *IEEE Trans. on Haptics*, Vol. 3, No. 4, pp. 234-244, 2010.

[162] M. H. Jamaluddin, T. Shimono and N. Motoi, "Haptic Bilateral Control System with Visual Force Compliance Controller," *in Proceeding of IEEE International Symposium on Industrial Electronics*, pp. 1-6, 2013.

[163] S. Hutchinson, G. D. Hager and P. I. Corke, "A Tutorial on Visual Servo Control," *IEEE Trans. on Robotics and Automation*, Vol. 12, No. 5, pp. 651-669, 1996.

[164] Y. M. Mustafah, T. Shan, A. W. Azman, A. Bigdeli and B. C. Lovell, "Real-Time Face Detection and Tracking for High Resolution Smart Camera System," *in Proceeding of IEEE 9th Biennial Conference of the Australian Pattern Recognition Society on Digital Image Computing Techniques and Applications*, pp. 387-393, 2007.

[165] R. Kapoor and A. Dhamija, "Fast Tracking Algorithm using Modified Potential function," *IET Computer Vision*, Vol. 6, No. 2, pp. 111-120, 2012.

[166] N. Motoi, T. Shimono, R. Kubo and A. Kawamura, "Force-based Variable Compliance Control Method for Bilateral System with Different Degrees of Freedom ," *Proceeding of IEEE International Workshop on Advanced Motion Control*, pp. 1-6, 2012.

[167] J. S. Lee, I. H. Suh, B. J. You and S. R. Oh, "A Novel Visual Approach involving Disturbance Observer ," *in Proceeding of IEEE International Conference on Robotics and Automation*, pp. 269-274, 1999.

[168] W. Bachta, P. Renaud, E. Laroche, A. Forgione and J. Gangloff, "Active Stabilization for Robotized Beating Heart Surgery," *IEEE Trans. on Robotics*, Vol. 27, No. 4, pp. 757-767, 2011.

[169] N. V. Navkar, Z. Deng, D. J. Shah, K. E. Bekris and N. V. Tsekos, "Visual and Force-Feedback Guidance for Robot-Assisted Interventions in the Beating Heart with Real-Time MRI ," *in Proceeding of IEEE International Conference on Robotics and Automation*, pp. 689-694, 2012.

[170] Y. H. Anis, M. R. Holl and D. R. Meldrum, "Automated Selection and Placement of Single Cells Using Vision-Based Feedback Control," *IEEE/ASME Trans. on Automation Science and Engineering*, Vol. 7, No. 3, pp. 598-606, 2010.

[171] Y. Tsutsumi, N. Oda, T. Murakami and K. Ohnishi, "A Construction of Observer-based Visual Servo Controller," *in Proceeding of IEEE Industrial Electronics Society*, Vol. 2, pp. 1109-1113, 1998.

[172] M. H. Jamaluddin, T. Shimono and N. Motoi, "A Scaling Effect of Visual Force in Haptic Bilateral Control System," *in IEEJ Technical Meeting of Industrial Instrumentation & Control and Mechatronics Control*, pp. 37-42, 2013.

[173] Y. Ohnishi and S. Katsura, "A Realization of Haptic Training System Based on Force Control," *in Proceedings of IEEE International Conference on Mechatronics*, pp. 510-515, 2013.

[174] V. M. Hung and U. J. Na, "Force Control of a New 6-DOF Haptic Interface for a 6-DOF Serial Robot," *in Proceedings of IEEE Control Automation and Systems*, pp. 1653-1658, 2010.

[175] O. Mohareri, S. E. Salcudean and C. Nguan, "Asymmetric force feedback control framework for teleoperated robot-assisted surgery," *in Proceedings of IEEE Robotics and Automation*, pp. 5800-5806, 2013.

[176] S. Mills, N. Aouf and L. Mejias, "Image Based Visual Servo Control for Fixed Wing UAVs Tracking Linear Infrastructure in Wind," *in Proceedings of IEEE International Conference on Robotics and Automation*, pp. 5769-5774, 2013.

[177] J. Liu, Z. Gong, K. Tang, Z. Lu and C. Ru, "Locating End-Effector Tips in Robotic Micromanipulation," *IEEE Transactions on Robotics*, pp. 1-6, 2013.

[178] X. Xu, G. Paggetti and E. Steinbach, "Dynamic Model Displacement for Model-mediated Teleoperation," *IEEE World Haptics Conference*, pp. 313-318, 2013.

[179] P. Poignet and M. Gautier, "Nonlinear Model Predictive Control of a Robot Manipulator", *in Proceedings of the IEEE Advanced Motion Control*, pp. 401-406, 2000.

[180] W. Shang and S. Cong, "Nonlinear Computed Torque Control for a High-speed Planar Parallel Manipulator", *Journal of Mechatronics*, Vol. 4, No. 2, pp. 987-992, 2009.

[181] A.R. Ridwan, M. I. S. Bony and I. I. Azad, "Performance Analysis of MPC in the Control of a Simple Motorized Nonlinear Model of a Robotic Leg", *International Journal of Computer Applications*, Vol. 54, No. 11, pp. 19-23, 2012.

[182] J. B. Rawlings, E. S. Meadows and K. R. Muske, "Nonlinear Model Predictive Control: A Tutorial and Survey", *in Proceedings of the International Symposium on Advanced Control of Chemical Processes*, pp. 185-197, 1994.

[183] C. Ekaputri and A. S. Rohman, "Implementation Model Predictive Control (MPC) Algorithm-3 for inverted Pendulum", *in Proceedings of the IEEE Control and System Graduate Research Colloqium*, pp. 116-112, 2012.

[184] F. Morabito, A. R. Teel and L. Zaccarian, "Nonlinear Antiwindup Applied to Euler-Lagrange Systems", *IEEE Transactions on Robotics and Automation*, Vol. 20, No. 3, pp. 526-537, 2004.

[185] T. Henmi, T. Ohta, M. Deng and A. Inoue, "Tracking Control of the Two-link Manipulator using Nonlinear Model Predictive Control", *in Proceedings of the IEEE International Conference on Networking, Sensing and Control*, pp. 761-766, 2009.

[186] Manjeet and P. Khatri, "Trajectory Control of Two Link Robotic Manipulator Using PID", *Golden Research Thoughts*, Vol. 3, No. 5, pp. 1-7, 2013.

[187] M. Khairudin, Z. Mohamed and A. R. Husain, "Dynamic Model and Robust Control of Flexible Link Robot Manipulator", *TELKOMNIKA*, Vol. 9, No. 2, pp. 279-286, 2011.

Appendix A

Trajectory Generation of 2-link Manipulator using Nonlinear Optimal Control Approach

A.1 Abstract

This paper addresses a solution for trajectory generation of two-link manipulator. The trajectory is generated by considering the nonlinear optimal control method which involving the use of Model Predictive Controller (MPC). There are two units in the MPC controller which are the internal plant model and the optimizer of cost function. In this paper, the simulations are conducted to compare the result between of the proposed method with different parameter setting values. The details concerning the implementation of this method will be discussed. The simulation results confirm the effectiveness of the proposed method.

A.2 Introduction

Recently, a lot of strategies have been introduced in order to control a robot [179]– [186]. In controlling the 2-link manipulator system, the dynamic effect of that manipulator will effect the performance of the controller. Some study had been conducted to generate the trajectory of manipulator system using the conventional computed torque control method but the response still not convince and needs the implementation with another observer [180]. The problem occur due to the implementation of linear control to the nonlinear system. Thus the nonlinear optimal

control technique should be used to tackle the nonlinearity effect.

One of the solutions is by implementing the nonlinear Model Predictive Control (MPC) method. The MPC is designed depending upon the past inputs and outputs, while the internal plant model will predicts the future output [181]. It is compared with reference value and the substracted result or future error is sent to the optimizer. The future inputs will be generated which finally becomes the past memory of the model for the next event. The iterative method is subsequently followed until it reaches close to the desired reference value [182]. This process always repeated so the output will be optimal [183].

This paper proposed the nonlinear MPC controller as for the optimal trajectory generation of 2-link manipulator. The trajectory will be simulated using MATLAB software including the MPC Toolbox. In the simulation, the controller's weighting parameters are set at certain values and the variation of these values will be compared based on the generated response. Its performance will be evaluated depending on two cases. The same cases also be applied by using the Linear Quadratic Regulator (LQR method) for effectiveness comparison.

The organization of this paper is as follows. The control methodologies of two-link manipulator system considering its dynamical model are described in section II. Subsequently, in section III, the simulation parameter to evaluate the system's effectiveness are explained. Additionally, the performance of the proposed method is discussed based on the obtained simulation results. Finally, section IV concludes the outcome of this paper.

A.3 Control Methods

In this section, the consideration of the dynamical model of two-link manipulator by the Euler-Lagrangian method will be explained. Next, the optimal control methods for the respective manipulator system will be explained.

A.3.1 Euler-Lagrangian method

Considering the dynamical model of two-link manipulator, the Euler-Lagrangian method can be used. The Lagrangian function $\mathcal{L}(\theta, \dot{\theta})$ are encompasses of kinetic energy function $K(\theta, \dot{\theta})$ and potential energy function $P(\theta, \dot{\theta})$ [184]. In general, kinetic energy function can be defined

as

$$K = \frac{1}{2}\sum_{i=1}^{2}\sum_{j=1}^{2} m_{ij}(\theta)\dot{\theta}_i\dot{\theta}_j \tag{A.1}$$

and potential energy function can be defined as

$$P = \sum_{i=1}^{2} gp_{ci}m_i. \tag{A.2}$$

Here, p_{ci} is the position of the centre of mass. Thus, the Lagrangian function can be written as

$$\mathcal{L}(\theta,\dot{\theta}) = K(\theta,\dot{\theta}) - P(\theta,\dot{\theta}). \tag{A.3}$$

A.3.2 Dynamic model of 2-link manipulator

Figure A.1 shows the configuration details of 2-link manipulator. From this figure, the parameters are described as below;

m_i = centre of mass (CoM) for link i-th

θ_i = angular variable for joint i-th

l_i = length for link i-th

s_i = distance between joint i and the CoM of the link i-th

g = gravity force along x_2 axis

where, $i = 1$ and 2.

The dynamical model of this manipulator is considered by the Euler-Lagrangian and it can be calculated as

• For link 1;

$$K_1 = \frac{1}{2}m_1 s_1^2\dot{\theta}_1^2 + \frac{1}{2}I_1\dot{\theta}_1^2 \tag{A.4}$$

and

$$P_1 = m_1 g s_1 sin\theta_1. \tag{A.5}$$

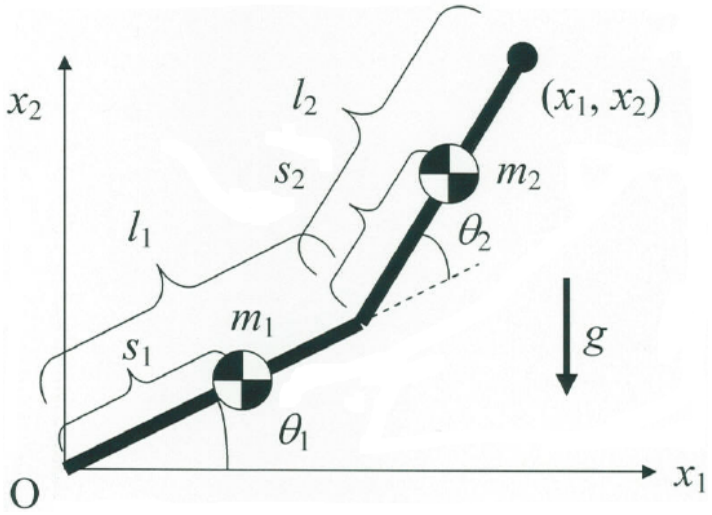

Figure A.1: The description of 2-link manipulator's configuration

• For link 2;

$$K_2 = \frac{1}{2} m_2 \left[l_1^2 \dot{\theta}_1^2 + s_2^2 (\dot{\theta}_1 + \dot{\theta}_2)^2 + 2 l_1 s_2 cos\theta_2 (\dot{\theta}_1^2 + \dot{\theta}_1 \dot{\theta}_2) \right] + I_2 (\dot{\theta}_1 + \dot{\theta}_2)^2 \tag{A.6}$$

and

$$P_2 = m_2 g \left[l_1 sin\theta_1 + s_2 sin(\theta_1 + \theta_2) \right]. \tag{A.7}$$

The calculations for kinetic energy are considering the inertia tensor I_i around the centre of mass of each link.

Furthermore, the complete Lagrangian function for this manipulator is calculated as

$$\mathcal{L} = K_1 + K_2 - P_1 - P_2. \tag{A.8}$$

Hereinafter, the resulted torques are defined as

$$\begin{aligned} \tau_1 = & \left[m_1 s_1^2 + I_1 + m_2 (l_1^2 + s_2^2 + 2 l_1 s_2 cos\theta_2) + I_2 \right] \ddot{\theta}_1 \\ & + \left[m_2 (s_2^2 + l_1 s_2 cos\theta_2) + I_2 \right] \ddot{\theta}_2 \\ & - m_2 l_1 s_2 sin\theta_2 (2 \dot{\theta}_1 \dot{\theta}_2 + \dot{\theta}_2^2) \\ & + m_1 g s_1 cos\theta_1 + m_2 g \left[l_1 cos\theta_1 + s_2 cos(\theta_1 + \theta_2) \right] \end{aligned} \tag{A.9}$$

and

$$\tau_2 = \left[m_2(s_2^2 + l_1 s_2 cos\theta_2) + I_2\right]\ddot{\theta}_1 + (m_2 s_2^2 + I_2)\ddot{\theta}_2 + m_2 l_1 s_2 sin\theta_2 \dot{\theta}_1^2 + m_2 g s_2 cos(\theta_1 + \theta_2). \quad \text{(A.10)}$$

The total torque $\boldsymbol{\tau}$ equation for the manipulator can be written in matrix form as

$$\boldsymbol{\tau} = \mathbf{M}(\boldsymbol{\theta})\ddot{\boldsymbol{\theta}} + \mathbf{C}(\boldsymbol{\theta}, \dot{\boldsymbol{\theta}})\dot{\boldsymbol{\theta}} + \mathbf{g}(\boldsymbol{\theta}) \quad \text{(A.11)}$$

where $\mathbf{M}, \mathbf{C}$ and $\mathbf{g}$ are manipulator's mass matrix, centrifugal (and coriolis) force and gravity torque, respectively. The term $\boldsymbol{\tau}$ is for $[\tau_1\ \tau_2]^T$ and $\boldsymbol{\theta}$ is for $[\theta_1\ \theta_2]^T$.

The manipulator's mass matrix $\mathbf{M}$, can be represented by

$$\mathbf{M} = \begin{bmatrix} M_{11} & M_{12} \\ M_{21} & M_{22} \end{bmatrix} \quad \text{(A.12)}$$

where

$$\begin{aligned} M_{11} &= m_1 s_1^2 + m_2(l_1^2 + s_2^2 + 2 l_1 s_2 cos\theta_2) + I_1 + I_2 \\ M_{12}, M_{21} &= m_2(s_2^2 + l_1 s_2 cos\theta_2) + I_2 \\ M_{22} &= m_2 s_2^2 + I_2 \end{aligned}$$

and the matrix for centrifugal and coriolis force $\mathbf{C}$ is represented as

$$\mathbf{C} = \begin{bmatrix} c_{11} & c_{12} \\ c_{21} & c_{22} \end{bmatrix} \quad \text{(A.13)}$$

where

$$\begin{aligned} c_{11} &= h\dot{\theta}_2 \\ c_{12} &= h(\dot{\theta}_1 + \dot{\theta}_2) \\ c_{21} &= -h\dot{\theta}_1 \\ c_{22} &= 0; \qquad h = -m_2 l_1 s_2 sin\theta_2. \end{aligned}$$

Finally, the gravity torque matrix $\mathbf{g}$ is represented as

$$\mathbf{g} = \begin{bmatrix} g_1 \\ g_2 \end{bmatrix} \quad \text{(A.14)}$$

where

$$g_1 = (m_1 s_1 + m_2 l_1) g cos\theta_1 + m_2 g s_2 cos(\theta_1 + \theta_2)$$
$$g_2 = m_2 g s_2 cos(\theta_1 + \theta_2).$$

The total torque equation for the manipulator can be simplified and written as

$$\boldsymbol{\tau} = \mathbf{M}(\boldsymbol{\theta})\ddot{\boldsymbol{\theta}} + \mathbf{b}(\boldsymbol{\theta}, \dot{\boldsymbol{\theta}}) \tag{A.15}$$

where $\boldsymbol{b}$ encompasses of matrix $\mathbf{C}$ and $\mathbf{g}$ as described below

$$\boldsymbol{b} = \mathbf{C}(\boldsymbol{\theta}, \dot{\boldsymbol{\theta}})\dot{\boldsymbol{\theta}} + \mathbf{g}(\boldsymbol{\theta}). \tag{A.16}$$

For this research, the manipulator is considered perfect by neglecting an internal friction effects.

Forward Dynamic

In order to calculates the resulted joint accelerations of the robot links, the forward dynamic technique can be used as a function of $\theta, \dot{\theta}$ and the input torques applied. It can be described as

$$\ddot{\boldsymbol{\theta}} = f(\boldsymbol{\theta}, \dot{\boldsymbol{\theta}}, \boldsymbol{\tau}). \tag{A.17}$$

Thus, the resulted joint accelerations for 2-link manipulator can be defined as

$$\ddot{\boldsymbol{\theta}} = \mathbf{M}(\boldsymbol{\theta})^{-1}[\boldsymbol{\tau} - \mathbf{b}] \tag{A.18}$$

where $\ddot{\boldsymbol{\theta}} = [\ddot{\theta}_1\ \ddot{\theta}_2]^T$.

A.3.3 Model Predictive Control (MPC)

Figure A.2 shows the general block diagram of MPC. The MPC controller block consists of two main parts which are the plant model and the optimizer (cost function) [185]. Figure A.3 shows the block diagram of MPC controlling method for 2-link manipulator system.

Internal Modeling

The predictive control method use the plant model in its controller. This model will be used for the generation of predicted output which be based on the predicted input given. The state-space formulations of the dynamics model may be obtained by defining the position/velocity state [186] as

$$x = [\boldsymbol{\theta}^T \dot{\boldsymbol{\theta}}^T]^T \tag{A.19}$$

and it can be written in the form of $\dot{x} = Ax + Bu$ as

$$\dot{x} = \begin{bmatrix} 0 & I \\ 0 & 0 \end{bmatrix} x + \begin{bmatrix} I \\ 0 \end{bmatrix} u. \tag{A.20}$$

Here, u is the control input as described in (A.18).

Reference Trajectory

The predictive control method of MPC is eloborated on Figure A.4. Given the set point trajectory on a receding horizon [0, h], the predicted process output $\hat{y}_P$ will reach the future set point following a reference trajectory y_R [179].

Performance index

The performance index may be a sum of the errors between the predicted output $\hat{y}_P$ and the reference trajectory y_R. It can be defined as

$$\Delta\boldsymbol{\theta} = \hat{y}_P(t+k) - y_R(t+k) \tag{A.21}$$

where k is the number of coincident time point. It also will depends on the different between the current input $u(t+k)$ and previous input $u(t)$ and can be described as

$$\Delta\boldsymbol{u} = u(t+k) - u(t) \tag{A.22}$$

where $\boldsymbol{u} = [u_1\ u_2]^T$.

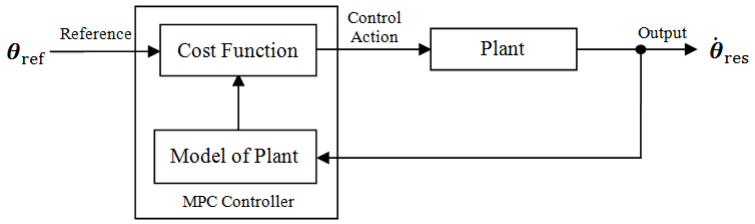

Figure A.2: General block diagram of Model Predictive Control

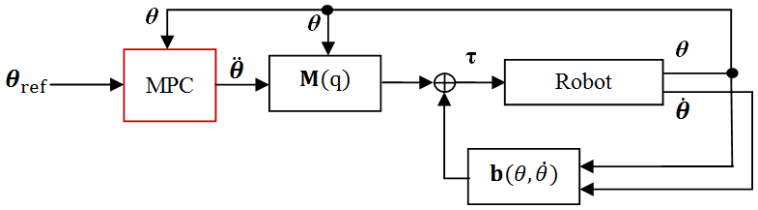

Figure A.3: 2-link manipulator with MPC's block diagram

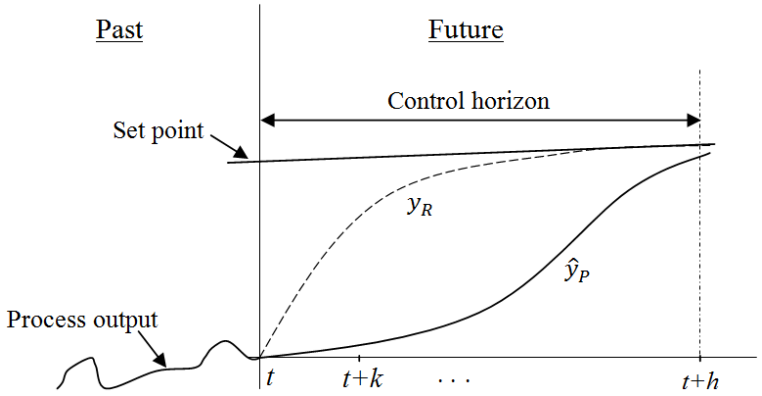

Figure A.4: Predictive control strategy

Thus the optimal cost function for the 2-link manipulator's predictive controller during $0 \leq t \leq T$ of its trajectory generation time can be written as

$$minJ \quad = \quad \int_0^T \left(\Delta\theta^T Q \Delta\theta + \Delta u^T R \Delta u\right) dt \tag{A.23}$$

where Q and R are the symmetric weighting matrices (diagonal) for the output and input respectively. Its values can be chosen within $0 \leq Q \leq 1$ for Q and $0 \leq R \leq 1$ for R [181].

A.3.4 Linear Quadratic Regulator (LQR)

Linear Quadratic Regulator (LQR) is a technique in modern control in which uses state-space approach to analyze such system [187]. The method of LQR will be used to compare with the

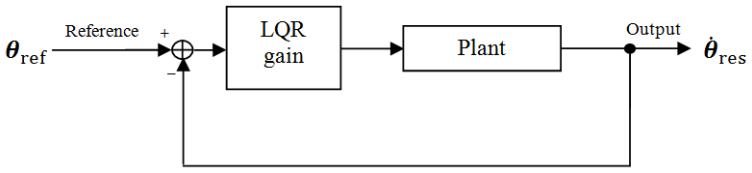

Figure A.5: Linear Quadratic Regulator control block diagram

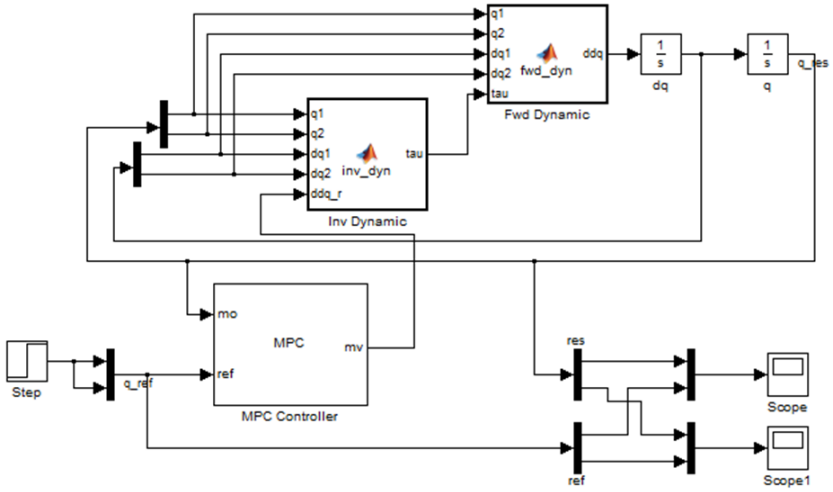

Figure A.6: Simulation block diagram of the system with MPC Controller

performance of MPC. Figure A.5 shows the block diagram of LQR that implemented in the 2-link manipulator system.

The concept of LQR is it will generate the suiTable gain value that will be used to determine the feedback control law of the state-space plant model. It will use the same state-space formulation as in internal modelling of MPC.

A.4 Simulation

The simulation for the system is conducted using MATLAB R2012b software and its diagram can be referred to Figure A.6. For the MPC technique, the diagram is devided into four parts which are input, controller, plant and output.

• Input - There are two types of input for the simulation. At first, the step input is given to the system (at t=1s). Then, the step input is changed to the sin(t) wave input and the output of both inputs are recorded for further analysis.

• Controller - The simulation uses the MPC controller that is developed using the MPC Toolbox. It contains two inputs (reference input and manipulated output from the plant) and one output which is manipulated variable. The control horizon, prediction horizon, sampling time and weighting matrices can be set inside the controller setting.

• Plant - The plant consists of two blocks which are Inv_Dynamic and Fwd_Dynamic. The Inv_Dynamic block calculates the produced torques based on the given input. The Fwd_Dynamic block calculates the resulted joint accelerations based on the given torques.

• Output - The output part consists of two scopes to measure the resulted position responses and position references for respective links of the robot.

The simulations for MPC method are conducted in 5s with the sampling time of 10ms. However, the simulations for LQR methods are conducted in 10s with the same sampling time of 10ms. Since its calculations are for the discrete model, thus the sampling will be determined in number of step (1000 step). Table A.1 described the parameters used in the simulation of the manipulator system. The simulations are devided into two cases which use differents value for its weighting factors. For the MPC method, each cases will be compared together with the different prediction horizon value but with the same values for the Control Horizon (intervals) = 3 and the Control Interval (time units) = 0.01.

In Case 1, the symmetric weighting matrix value for the output Q is set at 1.00 while for the control input R is also set at 1.00. This settings are considered to generate a good controller setting for the specific MPC controller [181]. However, in Case 2, the weighting matrix value Q is set to 10 times higher from the value in the Case 1, while R maintain the same value. Table A.2 described the parameters for each cases. The variation of weighting factors value for Q and R, the prediction horizon and its produced responses will be used for the simulation and its result will be evaluated. The condition of the reference trajectory are subject to $\boldsymbol{\theta}(0) = \theta_0$, $\boldsymbol{\theta}(\mathrm{T}) = \theta_T$ and $\dot{\boldsymbol{\theta}}(0) = \dot{\boldsymbol{\theta}}(\mathrm{T})$ where, θ_0 is the initial state $\big(\theta_1(0), \theta_2(0)\big)$ and θ_T is the final state $\big(\theta_1(\mathrm{T}), \theta_2(\mathrm{T})\big)$.

Table A.1: Parameters for the simulated system

Parameters	**Discription**	**Values**
m_1	Mass of link 1	1.00 kg
m_2	Mass of link 2	1.00 kg
l_1	Length of link 1	1.00 m
l_2	Length of link 2	1.00 m
s_1	Position of COM at link 1	0.50 m
s_2	Position of COM at link 2	0.50 m
I_1	Inertia tensor of link 1	0.083 kgm^2
I_2	Inertia tensor of link 2	0.083 kgm^2
g	Gravity	9.81 m/s^{-2}

A.4.1 Simulation results

Figure A.7 and Figure A.8 shows the simulation results of the manipulator system for the MPC's prediction horizon of 10, 15 and 30, with step input. While Figure A.9 and Figure A.10 shows the simulation results of the system for the LQR's method with step input. As depicted in Figure A.7 and Figure A.11, it shows that the manipulator gave a good response when the parameters of Case 1 are considered for MPC method. The manipulator can converge to the given reference trajectory in a short period (0.15 seconds) of simulation time with a small error. Conversely, by the LQR method, the response can only converge to the reference trajectory in almost 7 seconds of simulation time, as shown in Figure A.9. For the sin(t) input signals, the error for the LQR system were also bigger comparing to the MPC system, as depicted in Figure A.13.

However, when the values of Case 2 are considered, the MPC system generates almost the same result as in Case 1 eventhough the Q gain value has increased to 10, as shown in Figure A.8. Eventually, the LQR system still shown the big delay response and error as shown in Figure A.10 for step input and Figure A.14. Anyway, the results were seen much better compared to the value used in Case 1 of LQR system.

Table A.2: Parameters for the MPC and LQR controller

Case	Q	R	Prediction Horizon
1	1.00	1.00	10, 15, 30
2	10.0	1.00	10, 15, 30

A.4.2 Discussion

The simulations result for Case 1 and Case 2 shows that the variation of weighting factor had generated the different effect for the system especially in LQR method. For the MPC method, by the setting parameters used in the simulations, as the prediction horizon values increase, the response converging time also getting increase. Moreover, for the LQR method, as the values of Q gain increased, the responses converging times decreased and the errors became smaller.

A.5 Conclusion

This paper presented a trajectory generation method of 2-link manipulator system using the nonlinear optimal control approach. The Model Predictive Control (MPC) method is chosen as the optimal control approach as it consist of an optimizer (cost function) procedure. The MPC controller were designed using the MPC Toolbox in MATLAB R2012b software. The control methodologies for the proposed technique and its simulation results were presented. The variation of response was realized by considering the setting parameters used in the system. Thus, the optimal dynamic performance can be utilized. The effectiveness of the implemented method had been examined and discussed by comparing with the LQR method. The simulations result confirmed the capability of the proposed method.

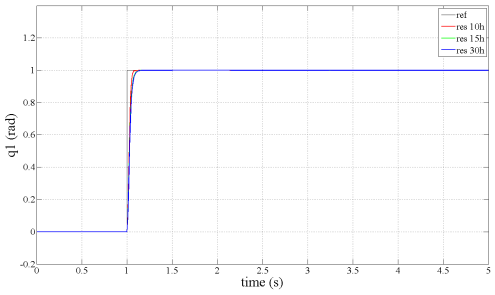

(a) Trajectory for θ_1 of link 1

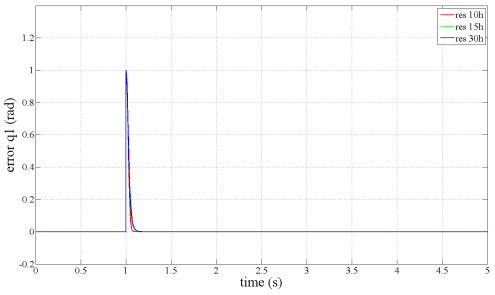

(b) Error results for θ_1 of link 1

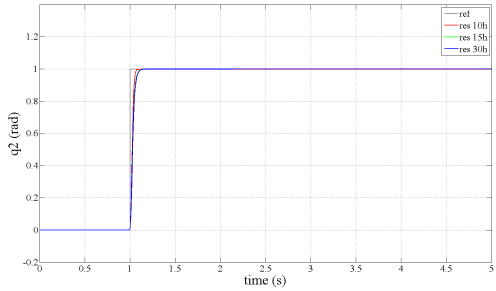

(c) Trajectory for θ_2 of link 2

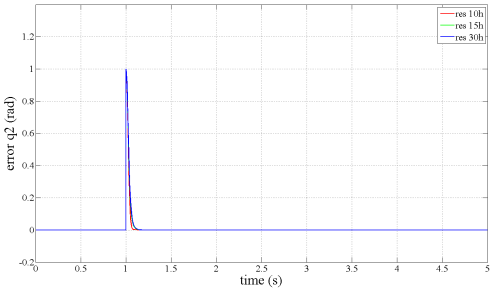

(d) Error results for θ_2 of link 2

Figure A.7: The trajectory generation responses for θ_1 and θ_2 of Case 1 with Step input (MPC method).

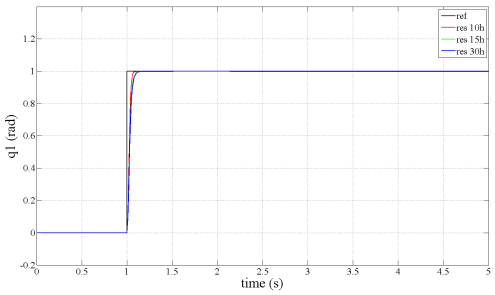

(a) Trajectory for θ_1 of link 1

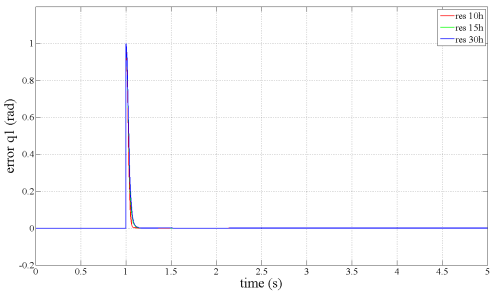

(b) Error results for θ_1 of link 1

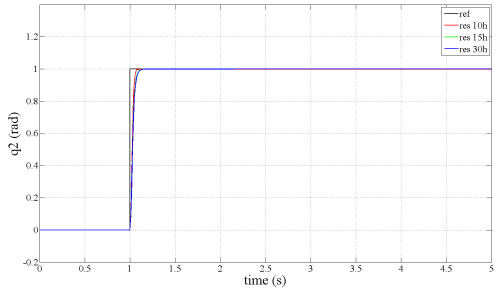

(c) Trajectory for θ_2 of link 2

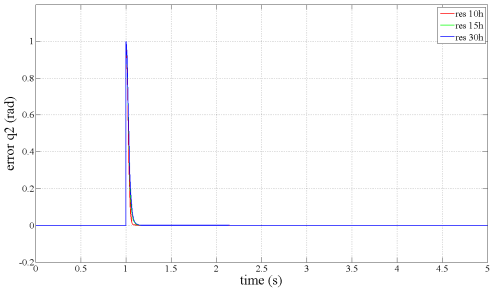

(d) Error results for θ_2 of link 2

Figure A.8: The trajectory generation responses for θ_1 and θ_2 of Case 2 with Step input (MPC method).

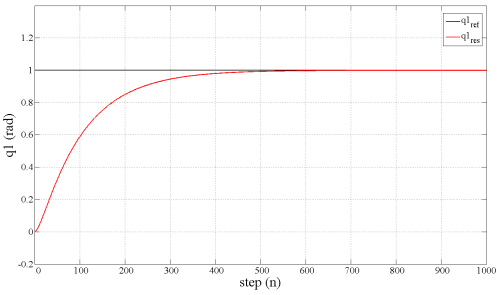

(a) Trajectory for θ_1 of link 1

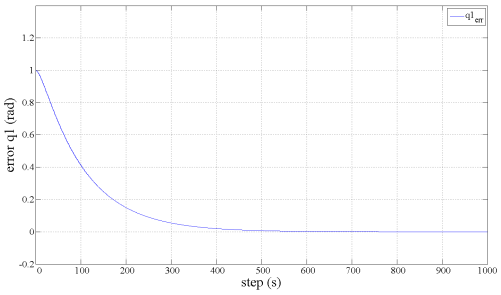

(b) Error results for θ_1 of link 1

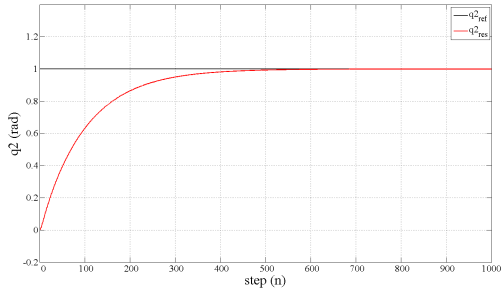

(c) Trajectory for θ_2 of link 2

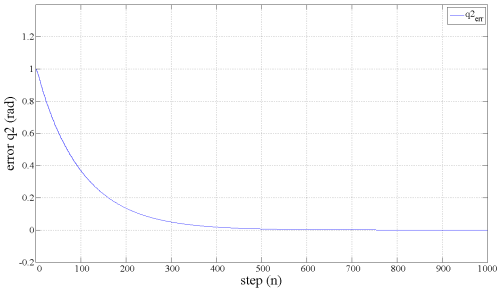

(d) Error results for θ_2 of link 2

Figure A.9: The trajectory generation responses for θ_1 and θ_2 of Case 1 with Step input (LQR method).

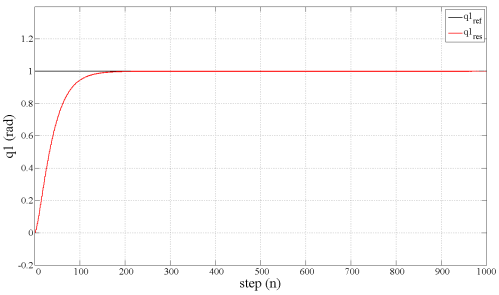

(a) Trajectory for θ_1 of link 1

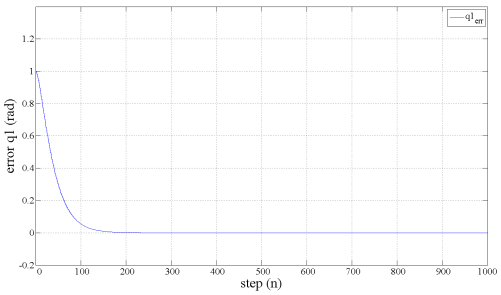

(b) Error results for θ_1 of link 1

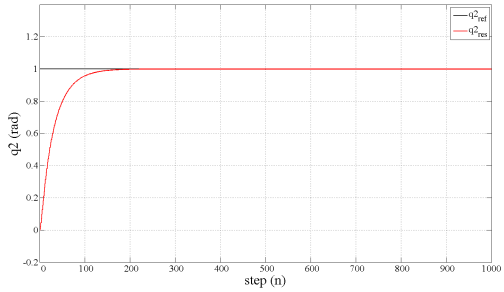

(c) Trajectory for θ_2 of link 2

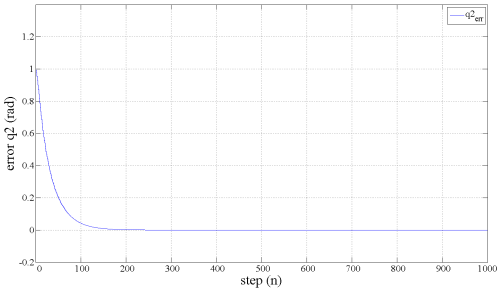

(d) Error results for θ_2 of link 2

Figure A.10: The trajectory generation responses for θ_1 and θ_2 of Case 2 with Step input (LQR method).

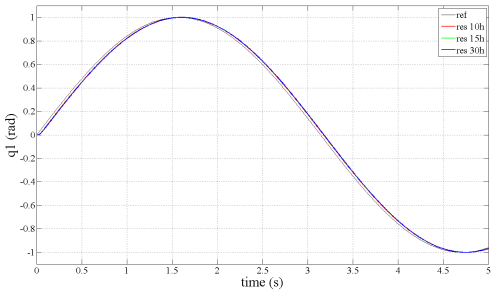

(a) Trajectory for θ_1 of link 1

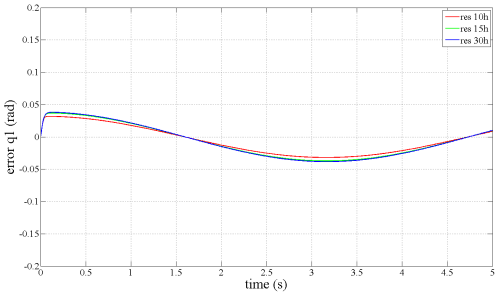

(b) Error results for θ_1 of link 1

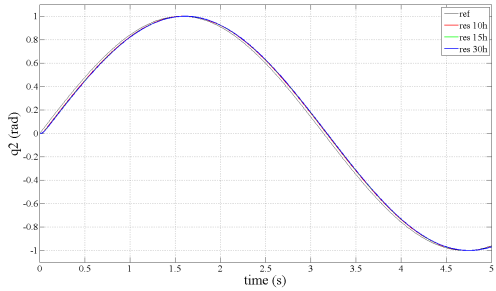

(c) Trajectory for θ_2 of link 2

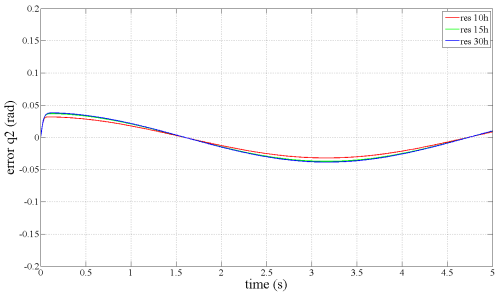

(d) Error results for θ_2 of link 2

Figure A.11: The trajectory generation responses for θ_1 and θ_2 of Case 1 with Sin(t) input (MPC method).

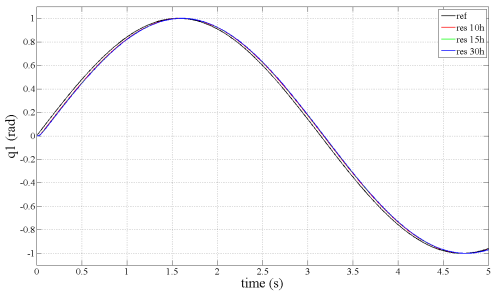

(a) Trajectory for θ_1 of link 1

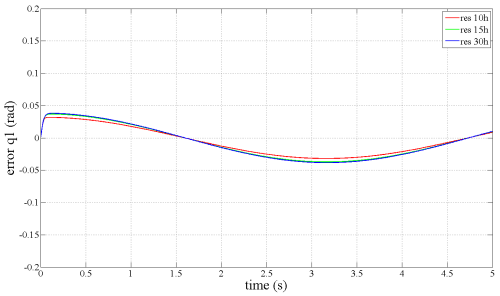

(b) Error results for θ_1 of link 1

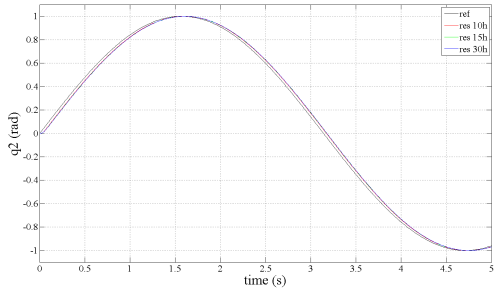

(c) Trajectory for θ_2 of link 2

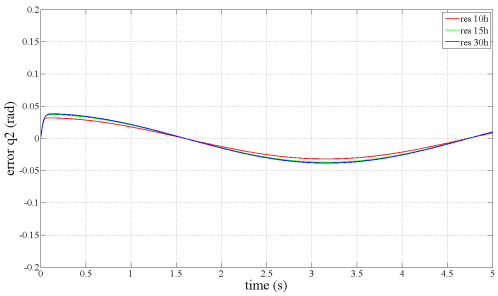

(d) Error results for θ_2 of link 2

Figure A.12: The trajectory generation responses for θ_1 and θ_2 of Case 2 with Sin(t) input (MPC method).

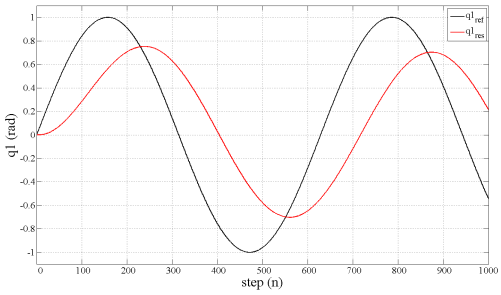

(a) Trajectory for θ_1 of link 1

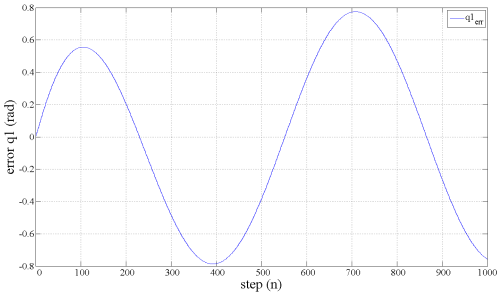

(b) Error results for θ_1 of link 1

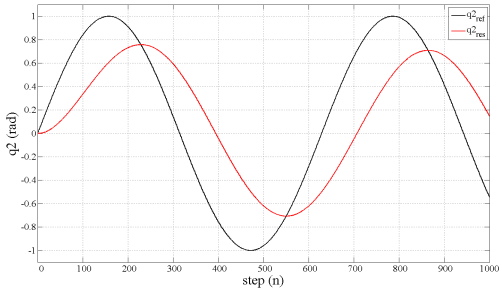

(c) Trajectory for θ_2 of link 2

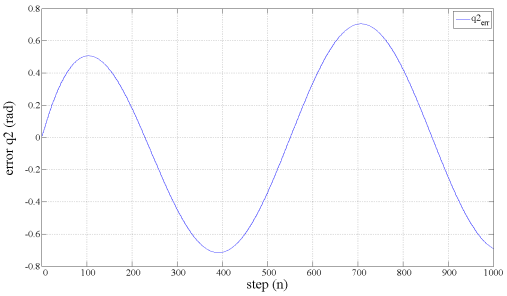

(d) Error results for θ_2 of link 2

Figure A.13: The trajectory generation responses for θ_1 and θ_2 of Case 1 with Sin(t) input (LQR method).

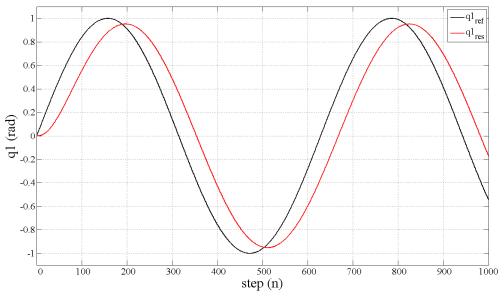

(a) Trajectory for θ_1 of link 1

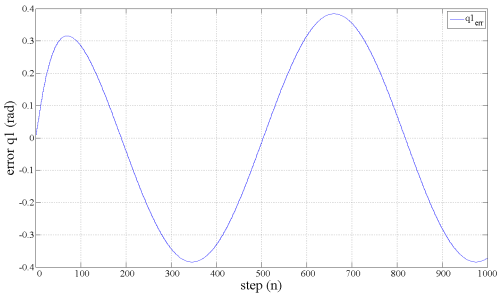

(b) Error results for θ_1 of link 1

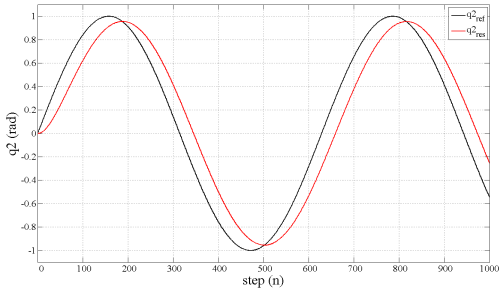

(c) Trajectory for θ_2 of link 2

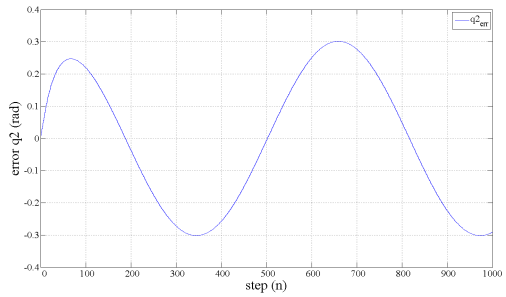

(d) Error results for θ_2 of link 2

Figure A.14: The trajectory generation responses for θ_1 and θ_2 of Case 2 with Sin(t) input (LQR method).

Appendix B

Publications

B.1 Journal Papers

M. H. Jamaluddin, T. Shimono and N. Motoi, "Force-Based Compliance Controller Utilizing Visual Information for Motion Navigation in Haptic Bilateral Control System," *IEEJ Journal of Industry Applications*, Vol. 3, No. 3, pp. 227-235, 2014.

B.2 International Conferences

M. H. Jamaluddin, T. Shimono and N. Motoi, "Haptic Bilateral Control System with Visual Force Compliance Controller," in *Proceedings of The* 22^{nd} *IEEE International Symposium on Industrial Electronics*, pp. 1-6, 2013.

M. H. Jamaluddin, T. Shimono and N. Motoi, "An Integration Method between Vision-based Disturbance Observer and Bilateral Haptic System for Robust Tracking of Target Object," in *Proceedings of The* 13^{th} *IEEE International Workshop on Advanced Motion Control*, pp. 723-728, 2014.

M. H. Jamaluddin, T. Shimono and N. Motoi, "Motion Navigation in Haptic Bilateral System Based on Vision-based Force Compliance Controller Taking Object Coordinate into Account,"

in *Proceedings of The* 23^{rd} *IEEE International Symposium on Industrial Electronics*, pp. 2234-2239, 2014.

B.3 Domestic Conferences

M. H. Jamaluddin, T. Shimono and N. Motoi, "A Scaling Effect of Visual Force in Haptic Bilateral Control System," in *IEEJ Joint Technical Meeting on Industrial Instrumentation and Control (IIC) and Mechatronics Control (MEC)*, pp. 37-42, 2013.

T. Shimono, M. H. Jamaluddin and N. Motoi, "Object Follow-up Control Based on Visual Feedback in Remote Control System," in *IEEJ Joint Technical Meeting on Industrial Instrumentation and Control (IIC)*, pp. 45-46, 2013.

Appendix C

Awards

C.1 Best Paper Presentation Award

IEEJ Technical Committee on Mechatronics Control, January 10^{th}, 2014.

C.2 Best Paper Presentation Award

IEEJ Industry Applications Society, March 31^{st}, 2014.

表　彰　状

メカトロニクス制御技術委員会

優秀論文発表賞

横浜国立大学

Jamaluddin Muhammad Herman　殿

MEC－１３－１４１　A Scaling Effect of Visual Force in Haptic Bilateral Control System

平成２５年メカトロニクス制御研究会におけるあなたの標記研究発表はメカトロニクス制御の発展に貢献する優秀なものと認められます
ここにその努力と功績をたたえ表彰致します

平成２６年１月１０日

一般社団法人電気学会 産業応用部門
メカトロニクス制御技術委員会

委員長　島田　明

表彰状

部門優秀論文発表賞

MUHAMMAD HERMAN BIN JAMALUDDIN 殿

発表題名

「A Scaling Effect of Visual Force in Haptic Bilateral Control System」

平成 25 年電気学会産業応用部門研究会における優秀論文発表の功績を顕彰するため産業応用部門表彰規程に基づき部門優秀論文発表賞を贈呈致します

平成 26 年 3 月 31 日

一般社団法人 電気学会産業応用部門

部門長 清水 敏久